Image Quality and Dosimetry of a Dual Source Computed Tomography Scanner with Special Emphasis on Radiation Dose of Lung in a Chest Examination

Dissertation

for attaining the PhD degree

of Natural Sciences

submitted to the Faculty of Physics

of the Johann Wolfgang Goethe -University

in Frankfurt am Main

by

Jijo Paul

from Cochin, India

Frankfurt, 2011

(D 30)

Accepted by the Faculty of Physics (13)

Johann Wolfgang Goethe- University as a Dissertation

Dean	: Prof. Dr. Michael Huth
Expert assessor	: Prof. Dr. Werner Maentele, Prof. Dr. Thomas J.Vogl
Date of the disputation	: 14.07.2011.

My Special thanks to

Prof. Dr. Thomas J.Vogl, MD, Prof. Dr. Werner Mäntele, PhD

Dr. Ralf W.Bauer, MD

For their support, motivation and appreciation

(For my Family with Love and Gratitude)

Index of Contents:

Chapter: 1

Chapter: 2

Index of Contents:

List of Abbreviations:

AEC	: Automatic Exposure Control
CECT	: Contrast Enhanced Computed Tomography
CT	: Computed Tomography
CTDIvol.	: Volume Computed Tomography Dose Index
DE	: Dual-Energy
DLP	: Dose-Length-Product
DSCT	: Dual Source Computed Tomography
E	: Effective Dose
EDLP	: Effective dose calculated by DLP method
FOV	: Field of View
HU	: Hounsfield Unit
ICRP	: International Commission on Radiological Protection
kV.	: kilo-Voltage
mAs	: milli-Ampere second
MDCT	: Multi-detector Computed Tomography
MSCT	: Multi Slice Computed Tomography
NECT	: Non-contrast Enhanced Computed Tomography
PACS	: Picture Archiving and Communication System
SNR	: Signal-Noise-Ratio
TLD	: Thermo luminescent dosimeter
WT	: Tissue weighting factor

Chapter-1

1.1 Abstract (English)

1.1.1 PURPOSE

The purpose of the current study was to evaluate the Dual Source Computed Tomography scanner in terms of Image quality and dosimetry with special emphasis of radiation dose of lung in a Chest examination.

1.1.2 MATERIALS AND METHODS

Study 1: Examinations were performed on a dual-source CT system (Somatom Definition Flash, Siemens). Four scan protocols were investigated: (1) single-source 120 kV, (2) single-source 100 kV, (3) high-pitch 120 kV, and (4) dual-energy with 100/Sn140 kV with equivalent CTDIvol and no automated tube current modulation. E was then determined following recommendations of ICRP publication 103 and 60 and specific k values were derived.

Study 2: 126 adult patients that received a non-contrast-enhanced (NCCT) and a contrast-enhanced CT (CECT) scan of the chest in one session were enrolled in this study. Each 42 patients were examined on a 16- (Sensation 16, Siemens), 64- (Definition, Siemens) and 128-slice (Definition Flash, Siemens) CT scanner with the same examination protocol: 120 kV, 110 mAs, pitch of 1.2, inspiratory breathe hold.

Study 3: The chest of an anthropomorphic phantom was scanned on a DSCT scanner (Siemens Somatom Definition flash) using different clinical protocols, including single- and dual-energy modes. Four scan protocols were investigated: 1) single-source 120 kV, 110mAs 2) single-source 100 kV, 180mAs 3) high-pitch 120 kV, 130mAs 4) dual-energy with 100/Sn140 kV, eff.mAs 89, 76.

The Automatic Exposure Control was switched off for all the scans and the CTDIvol selected was in between 7.12 and 7.37 mGy. The raw data reconstructed using the reconstruction kernels B31f, B80f and B70f, and slice thicknesses were 1.0 mm and 5.0 mm. Finally, the same parameters and procedures were used for the scanning of water phantom. Friedman test and Wilcoxon-Matched-Pair test were used for statistical analysis.

Study 4: Forty patients underwent a CT neck with dual energy mode (DECT under a Somatom Definition flash Dual Source CT scanner (Siemens, Forchheim, Germany)). Tube voltage: 80-kV and Sn140-kV; tube current: 110 and 290 mAs; collimation-2X32X0.6mm. Raw data were reconstructed using a soft convolution kernel (D30f). Fused images were calculated using a spectrum of weighting factors (0.0, 0.3, 0.6 0.8 and 1.0) generating different ratios between the 80- and Sn140-kV images (e.g. factor 0.6 corresponds to 60% of their information from the 80-kV image, and 40% from the Sn140-kV image). CT values and SNRs measured in the ascending aorta, thyroid gland, fat, muscle, CSF, spinal cord, bone marrow and brain. In addition, CNR values calculated for aorta, thyroid, muscle and brain. Subjective image quality evaluated using a 5-point grading scale. Results compared using paired *t*-tests and nonparametric-paired Wilcoxon-Wilcox-test.

1.1.3 *RESULTS*

DLP-based estimates differed by 4.5-16.56% and 5.2-15.8% relatively to ICRP 60 and 103, respectively. The derived k factors calculated from TLD measurements were 0.0148, 0.015, 0.0166, and 0.0148 for protocol 1, 2, 3 and 4, respectively. Effective dose estimations by ICRP 103 and 60 for single-energy and dual-energy protocols show a difference of less than 0.04 mSv.

Image noise was significantly lower in the most recent scanner generation for both NECT and CECT. Dose parameters were significantly lower in 128- and 64-slice group compared to the 16-slice group: for CECT, DLP increased by 34.1% in the 16-slice group, by 8.1% in the 64-slice group. For all groups, there was a significant increase in dose with an inverse relation of image noise between NECT and CECT.

The DLP based on the given CTDIvol values showed significantly lower exposure for the Dual Energy 140-kV, 100-kV protocol when compared to standard 120-kV (percent difference 5.18%), standard 100-kV (percent diff. 4.51%), and Flash 120-kV (percent diff. 8.81%). The highest change in Hounsfield Units observed with DE Sn140-kV (Hounsfield unit 15.18) compared to standard 100-kV protocol (24.35 HU). The differences in noise between the different clinical protocol data sets were statistically significant [Flash 120kV versus DE 100-kV ($p<0.01$) and Flash 120-kV versus DE Sn140-kV ($p<0.01$) protocols]. The DE Sn140-kV protocol shows the highest image noise (14.5 HU for 5.0 mm slice (B31f) and 162 HU for 1.0 mm slice (B70f) thickness). The difference between reconstruction kernel B31f and B80f images made using 5.0mm reconstruction thickness were statistically significant ($p<0.0312$) and 1.0mm slice thickness shows the significance of $p<0.0312$ between B31f and B70f reconstructions. In both cases, the lowest image noise obtained from B31f reconstructed images. Again the slice thickness is significantly affects image noise ($p<0.03$) and the noise was higher at 1.0 mm compared to 5.0 mm slice thickness.

Statistically significant increases in mean CT values noted in anatomic structures when increasing weighting factors used (all $P \leq 0.001$). For example, mean CT values derived from the contrast enhanced aorta were 149.2+/-12.8 HU

(Hounsfield unit), 204.8+/-14.4 HU, 267.5+/-18.6 HU, 311.9+/-22.3 HU, and 347.3+/-24.7 HU, when the weighting factors 0.0, 0.3, 0.6, 0.8 and 1.0 were used. The highest SNR and CNR values were found in materials when the weighting factor 0.6 used. The difference CNR between the weighting factors 0.6 and 0.3 was statistically significant in the contrast enhanced aorta and thyroid gland (P = 0.012 and P = 0.016, respectively). Visual image assessment for image quality showed the highest score for the data reconstructed using the weighting factor 0.6.

1.1.4 CONCLUSION:

Estimates of E based on DLP work equally well for single-energy, high-pitch and dual-energy CT examinations. The tube potential definitely affects effective dose in a substantial way. Effective dose estimations by ICRP 103 and 60 for both single-energy and dual-energy examinations differ not more than 0.04 mSv.

This study demonstrates that with AEC patient dose will be significantly different between NECT and CECT chest examinations for three generations of CT machines. However, technological developments lead to a significant reduction of dose and image noise with the latest CT generation.

The clinical protocol, reconstruction kernel, slice thickness and phantom diameter or the density of material it contains directly affects the image quality. Dual Energy protocol shows the lowest Dose-Length-Product compared to all other protocols examined, the fused image shows excellent image quality and the noise is same as that of single or high-pitch mode protocol images. Advanced CT technology improves image quality and considerably reduces radiation dose.

Different fusion factors used to create images in DECT cause statistically significant differences in CT value, SNR, CNR and image quality. Best results obtained using the weighting factor 0.6 for all anatomic structures used in this study.

1.2 ZUSAMMENFASSUNG (Deutsch)

Zielsetzung der Studie war die Evaluation eines Dual-Source-Computertomographen (Somatom Definition Flash der Firma Siemens) hinsichtlich Bildqualität und Dosimetrie mit speziellem Fokus auf der Lungendosis in Thoraxuntersuchungen. In insgesamt vier Teilstudien wurden hierbei verschiedene Teilaspekte in einem Alderson Rando-Phantom sowie im klinischen Einsatz untersucht. Im ersten Teilversuch insgesamt vier klinisch verwendete CT-Protokolle (Single-source 120 kV, Single-source 100 kV, High-pitch 120 kV und Dual-energy) mit CTDIvol-äquivalenten Einstellungen hinsichtlich ihrer effektiven Dosis (E) im Phantomversuch mit Thermolumineszenzdosimetern verglichen, spezifische Konversionsfaktoren k für die Berechnung von E aus dem Dosislängenprodukt bestimmt und mit den Empfehlungen der ICRP-Publikationen 103 und 60 verglichen. In einer zweiten Teilstudie wurde für drei verschieden CT-Generationen (16-, 64- und 128-Zeiler) der Effekt von intravenösem Kontrastmittel auf die Bildqualität und Dosisparameter CTDIvol und DLP im Vergleich zu nativen Thorax-CT-Untersuchungen in denselben Patienten und die Rolle der automatischen Röhrenstrommodulation untersucht. In einem dritten Teilversuch wurde wieder im Phantomversuch der Einfluss des Untersuchungsprotokolls, der rekonstruierten Schichtdicke und des Rekonstruktionskerns auf die Bildqualität (Rauschen) untersucht. In einem vierten Teilversuch wurde der Einfluss von verschiedenen Mischverhältnissen der Daten der hohen und niedrigen Röhrenspannung bei Patienten, die eine Dual-energy-CT des Halses erhalten hatten, auf die Bildqualität und den Kontrast in verschiedenen Geweben untersucht.

Als Ergebnisse lassen sich daraus zusammenfassen: (1) die DLP-basierten Berechnungen anhand der ICRP-103 und 60-Empfehlungen unterscheiden sich teils substantiell von den TLD-basierten Messungen, weichen jedoch untereinander kaum voneinander differieren; die abgeleideten k-Faktoren lagen zw. 0.0128-0.0166; (2) das Bildrauschen war mit der neusten CT-Generation sowohl für die kontrastmittelverstärkten als auch die nativen Aufnahmen signifikant geringer. Ebenfalls lagen die Dosisparameter in der 128- und 64-Zeilengruppe signifikant unter denen der 16-Zeilergruppe (8,1-34,1%) bei identischen Untersuchungsparametern; (3) Eine klare Abhängigkeit des Bildrauschens von der Schichtdicke und vom Rekonstruktionskern wurde für alle vier Protokolle festgestellt.; (4) Die CT-Dichtewerte der Zielstrukturen zeigten sich stetig steigend mit zunehmendem Anteil der Bildinformation aus dem Niedrigspannungsdatensatz. Das höchste Signal-Rausch- und Kontrast-Rausch-Verhältnis sowie die beste subjektive Bildqualität konnte bei einem Mischverhältnis von 60% niedrige kV mit 40% hohe kV dokumentiert werden. Schlussfolgernd lässt sich feststellen, dass die Ableitung von E aus dem DLP für die untersuchten Protokolle gleichermaßen gut für den klinischen Einsatz funktioniert und Unterschiede zwischen ICRP 103 und 60 im männlichen Thorax zu vernachlässigen sind. Bei der kontrastmittelverstärkten Thorax-CT mit automatischer Röhrenstromanpassung wurden durch technische Weiterentwicklungen signifikante Dosiseinsparungen und Bildqualitätsverbesserungen in der neusten CT-Generation erzielt. Für alle untersuchten Protokolle lies sich im Dual-Source-CT der neusten Generation auch eine deutliche Abhängigkeit der Bildqualitätsparameter von der rekonstruierten Schichtdicke und dem Rekonstruktionskern nachweisen.

In kontrastmittelverstärkten Dual-energy-Untersuchungen scheint dabei ein Mischverhältnis mit 60% Anteil aus der niedrigen Röhrenspannung (entsprechend einem virtuellen 100 kV-Bild) die optimale Bildqualität hinsichtlich der Weichteilbeurteilung zu liefern.

1.3 Detaillierte deutsche Version

1.3.1 Zielsetzung

Zielsetzung der Studie war die Evaluation eines Dual-Source-Computertomographen hinsichtlich Bildqualität und Dosimetrie mit speziellem Fokus auf der Lungendosis in Thoraxuntersuchungen.

1.3.2. Materialien und Methoden

Studie-1: Vier CTDIvol-äquivalente Thoraxuntersuchungsprotokolle wurden hinsichtlich ihrer effektiven Dosis (E) an einem anthropomorphen Alderson Rando Phantom, welches mit Thermolumineszenzdosimetern bestückt war, in einem Dual-Source-CT (Somatom Definition Flash, Siemens) untersucht: 1) single-source 120 kV, 2) single source 100 kV, 3) dual-source high-pitch mit 120 kV und 4) dual-energy mit 100/Sn 140 kV. Eine automatische Dosismodulation wurde nicht benutzt. E wurde anhand der Empfehlungen der ICRP-Publikaitonen 103 und 60 berechnet und spezifische k-Faktoren wurden berechnet.

Studie-2: Die Dosiswerte CTDIvol und DLP sowie das Bildrauschen von insgesamt 126 Patienten, welche eine klinisch indizierte native und kontrastmittelverstärkte Thorax-CT-Untersuchung mit automatischer Dosismoduliern (CAREdose 4D, Siemens) hatten, wurden zwischen drei CT-Geräten und zwischen nativer und kontrastmittelverstärkter Verglichen. Je 42 Patienten erhielten ihre Untersuchung an einem 16-Zeilen- (Sensation 16, Siemens), einem 64-Zeilen- (Definition, Siemens) und einem 128-Zeilen-CT-Gerät (Definition Flash, Siemens) mit den gleichen Protokolleinstellungen: 120 kV, 110 mAs, pitch 1,2, Inspiration.

Studie-3: Der Thorax des Alderson Rando Phantoms wurde an einem Dual-Source-CT untersucht (Definition Flash, Siemens) mit vier verschiedenen Protokollen wie oben (Studie 1) untersucht. Die Rohdaten wurden mit drei verschiedenen Kernen (B31f, B70f und B80f) in zwei verschiedenen Schichtdicken (1,0 mm und 5,0 mm) rekonstruiert. Mit denselben Untersuchungsprotokollen wurde anschließend ein homogenes Wasserphantom untersucht. Das Bildrauschen wurde verglichen und in Abhängigkeit von Untersuchungsprotokoll und Rekonstruktionsparametern dargestellt.

Studie-4: An 40 Patienten wurde aus klinischer Indikation heraus ein CT-Hals im Dual-energy-Modus mit folgendem Untersuchungsprotokoll durchgeführt (Definition Flash, Siemens): Röhrenspannung Röhre A 80 kV, Röhre B Sn140 kV mit einem Röhrenstrom von 290 mAs und 110 mAs bei einer Kollimierung von 32 x 0,6 mm. Die Rohdaten wurden mit einem mittelweichen Kern rekonstruiert (D30f). Die Rohdaten der hohen und niedrigen Röhrenspannung wurden in unterschiedlichen Mischverhältnissen rekonstruiert (30%, 60% und 80% der niedrigen kV). Die CT-Dichte sowie das Signal-Rausch- und Kontrast-Rausch-Verhältnis wurden für die Unterschiedlichen Mischverhältnisse sowie die reinen 80-kV- und Sn140kV-Daten gemessen und berechnet. Die Messungen erfolgten in der Aorta ascendens, der Schilddrüse, Fettgewebe, Muskulatur, Liquor, Rückenmark, Gehirn und Knochenmark. Die subjective Bildqualität wurde anhand einer 5-Punkte-Skala bewertet.

1.3.3 Ergebnisse

Studie-1: DLP-basierte Berechnungen anhand der ICRP-60- und 103-Konversionsfaktoren unterschieden sich von den TLD-basierten Messungen um 4,5-16,6% bzw. 5,2-15,8%. Die davon abgeleideten k-Konversionsfaktoren berechneten sich auf 0.0148, 0.015, 0.0166 und auf 0.0148 für Protokoll 1, 2, 3 und 4. Die absolute Differenz von E lag zwischen der ICRP 103 und 60 Methode bei 0.04 mSv.

Studie-2: Das Bildrauschen war mit der neusten CT-Generation sowohl für die kontrastmittelverstärkten als auch die nativen Aufnahmen signifikant geringer. Ebenfalls lagen die Dosisparameter in der 128- und 64-Zeilengruppe signifikant unter denen der 16-Zeilergruppe: im Vergleich zur 128-Zeilengruppe war bei den kontrastmittelverstärkten Aufnahmen der DLP in der 16-Zeilengruppe um 34,1%, in der 64-Zeilengruppe um 8,1% höher.

Studie-3: Das DLP war signifikant geringer beim Dual-energy-Protokoll verglichen mit dem 120 kV- (-5,18%), dem 100 kV- (-4,51%) und dem High-pitch-Protokoll (-8,81%). Das Dual-energy-Protokoll hatte die höchsten Rauschwerte (14,5 HU bei B31f 5 mm und 162 HU bei B70f 1 mm). Sowohl für die dicken als auch die dünnen Schichtdicken war das Rauschen für den B31f-Kern signifikant geringer als mit den kantenbetonten Kernen B70f und B80f. Weiterhin hat die Schichtdicke signifikanten Einfluss auf das Bildrausen und war in den 5 mm-Schichten signifikant geringer ($p < 0,03$).

Studie-4: Die CT-Dichtewerte zeigten sich stetig steigend mit zunehmendem Anteil der Bildinformation aus dem Niedrigspannungsdatensatz für alle gemessenen anatomischen Landmarken. Beispielsweise lag die mittlere Dichte in der Aorta bei 149,2 HU, 204,8 HU, 167,5 HU, 311,9 HU und 347,3 HU bei reinen SN140 kV,

Mischfaktor 0,3, 0,6, 0,8 und reinen 100 kV. Das höchste Signal-Rausch-Verhältnis und Kontrast-Rausch-Verhältnis konnte bei einem Mischverhältnis von 60% niedrige kV mit 40% hohe kV (0,6) gemessen werden. Die subjektive Bildqualitätsanalyse lieferte ebenfalls bei diesem Mischverhältnis die besten Ergebnisse.

1.3.4 Schlussfolgerung

Studie-1: Berechnung von E basierend auf dem DLP funktionieren mit annähernd gleicher Genauigkeit für Single-energy-, High-pitch- und Dual-energy-Thoraxprotokolle wobei die Abweichungen in der Gesamteffektivdosis nach den Berechnungsmethoden der ICRP 103 und 60 Empfehlungen nur geringfügig abweichen (0,04 mSv). Studie-2: Bei Thorax-CT-Untersuchungen mit automatischer Röhrenstrommodulation sind die applizierten Dosen zwischen nativer und kontrastmittelverstärkter Untersuchung für alle drei Generationen von CT-Geräten signifikant unterschiedlich bei gleichbleibend guter Bildqualität. Technische Weiterentwicklungen führten jedoch zu einer signifikanten Dosisersparnis mit der modernsten Generation (128-Zeilen-Gerät). Studie-3: Das Untersuchungsprotokoll, der Rekonstruktionskern und die Schichtdicke beeinflussen in diesem Phantomversuch direkt die Bildqualität. Das Dual-energy-Protkoll zeigte dabei bei vergleichbarer Bildqualität das geringste DLP. Studie-4: Verschiede Mischrelationen der Bilddaten bei hoher und niedriger Röhrenspannung führen zu signifikant unterschiedlichen CT-Werten und Bildqualitätsparametern. Ein Mischverhältnis von 0.6 zeigte dabei die besten Ergebnisse.

Chapter- 2

2.1 Introduction

2.1.1 REVIEW OF LITERATURE

Computed Tomography (CT) is a medical imaging procedure employing tomography produced by computer processing. A three-dimensional image is created by digital geometry processing from a large series of two-dimensional X-ray images of the inside of a physical object captured around a single axis of rotation [1]. An Italian radiologist Alessandro Vallebona suggested a technique to describe a single slice of body on the radiographic film in early 1900. This method is known as tomography and this procedure had been one of the pillars of radiological imaging until the late 1970s. Sir Godfrey Hounsfield fabricated a commercially viable CT scanner in Hayes United Kingdom in 1967 [2], at EMI Central Research Laboratories using X-rays. The first EMI-Scanner was established in Atkinson Morley Hospital in Wimbledon, England, and the first patient brain scan was performed on 1 October 1971[3]. The scanner was worked with Translate/Rotate principle and it had a single photomultiplier detector [3]. Since CTs introduction in the 1970s, it becomes a primary instrument in medical diagnosis. Helical CT technology [4, 5] and more recently multi-slice helical CT [6, 7] have produced dramatic improvements in scanner ability and image quality. However, according to the sudden development of this technology the radiation dose delivered to the patient is higher during helical CT examinations [7-10]. The generation of 64 slices CT systems introduced in 2004 and clinical experience with 64-slice CT system indicates that many of the issues of previous scanner generations are resolved. Some of the challenges in clinical routine still exist; for example, obese patient remains an issue because of the limited tube power.

In addition, for chest (cardiac) examination motion artifacts often compromise image quality. CT manufactures recently introduced a dual-source CT (DSCT) system to solve the clinical constraints of 64-slice CT. This scanner is characterized by two x-ray tubes and two corresponding detectors established an angular offset of 90° into the rotating gantry [11].

2.1.2 REFERENCE

1. Herman, G. T., Fundamentals of computerized tomography: Image reconstruction from projection, 2nd edition, Springer, 2009.

2. "Obituary—Sir Godfrey Hounsfield". BMJ 2004; 329: 687 doi: 10.1136/ bmj.329.7467.687 (Published 16 September 2004).

3. Beckmann E. C, CT scanning the early days , The British Journal of Radiology, 79 (2006), 5–8 (January 2006).

4. Kalender WA, Seissler W, Klotz E, Vock P, Spiral volumetric CT with single-breath-hold technique, continuous transport, and continuous scanner rotation. Radiology 1990; 76:181–183.

5. Crawford CR, King KF, Computed tomography scanning with simultaneous patient translation, Med Phys. 1990 Nov-Dec;17(6):967-82.

6. Hu H. Multi-slice helical CT: scan and reconstruction. Med Phys 1999;26:5–18

7. Clarke J, Cranley K, Robinson J, Smith PH, Workman A. Application of draft European Commission reference levels to a regional CT dose survey. Br J Radiol. 2000 Jan;73(865):43-50.

8. David J. Brenner, Carl D. Elliston, Eric J. Hall**,** Walter E. Berdon, Estimated Risks of Radiation-Induced Fatal Cancer from Pediatric CT, *AJR* 2001; 176:289-296.

9. Hidajat N, Wolf M, Nunnemann A, Liersch P, Gebauer B, Teichgräber U, et.al, Survey of conventional and spiral ct doses, Radiology. 2001 Feb;218(2):395-401.

10. Paterson A, Frush DP, Donnelly LF, Helical CT of the body: are settings adjusted for pediatric patients? AJR 2001;176:297–301.

11. Flohr TG, McCollough CH, Bruder H, Petersilka M, Gruber K, Süss C et.al, First performance evaluation of a dual-source CT (DSCT) system, Eur Radiol (2006) 16: 256–268, DOI 10.1007/s00330-005-2919-2.

2.2 Theoretical background

2.2.1 Computed Tomography

2.2.1.1 Dual Source Computed Tomography (Somatom Definition)

To solve the clinical constraints of 64-slice CT system, Siemens Medical Solutions introduced a Dual Source CT (DSCT) system-the Somatom Definition-in 2005. This CT system is furnished with two x-ray tubes, two corresponding detectors and the two data acquisition systems fixed on a rotating gantry with a 90-degree angular offset (*Fig. 2.1*) [1].

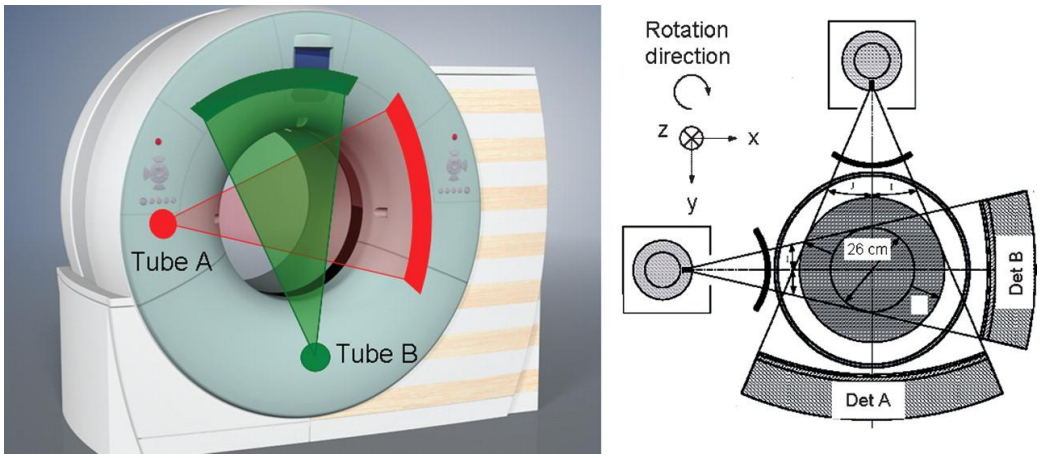

Figure- 2.1: show the Definition Dual Source CT scanner and its tube-detector configuration.

The first detector covers the full scan field of view (50 cm diameter), while due to the space restriction of the gantry the second is confined to a smaller, central (26 cm in diameter), field of view (FOV). Each detector comprises 40 detector rows, where the central 32 ones have a 0.6 mm collimated slice width and the outer rows (on both sides) a 1.2 mm collimated slice width. The total coverage in the z-axis of each detector is 28.8 mm at the isocenter. Using the z-flying focal spot technique (2, 3), two succeeded 32-slice readings with 0.6 mm collimated slice width are combined to one 64-slice projection with a sampling distance of 0.3 mm at the isocenter. By this way, each detector acquires 64 overlapping 0.6 mm slice per rotation.

The gantry rotation time is 0.33sec. although the system can also perform larger rotations times of 0.5 s and 0.1 s. Both the Siemens STRATON X-ray tubes [4] allows up to 80 kW peak power from the two on-board generators, so each tube can be operated independently with regard to their kilovolt and milliampere configurations. The detector using this system is Ultra Fast Ceramic (UFC™) detectors. This highly efficient detector needs only the smallest possible amount of radiation dose to obtain good image quality – even at low mA settings. The Definition DSCT system can be used both as single-source and dual-source mode. When this is suitably configured in dual-energy mode, computer system develops three image data sets: one for each tube (which was set at a certain kilovolt) and an additional mixed image that comprises features from both sources. The presence of a second tube produces scatter radiation in the first detector and vice versa. Anti-scatter grids cannot able to suppress fully these additional photons. Therefore, to avoid image distortion and to bring back image contrast a dedicated scattered-radiation correction algorithm is provided [5].

In Definition scanner the data is simultaneously acquired from 90 degree angle (from both detectors) thus temporal resolution equivalent to one quarter of the gantry rotation time (t. rot=0.33sec), and the temporal resolution is t.rot/4 equal to 83ms. Going from a single segment reconstruction to multi segment reconstruction only slightly improve the image quality (single source CT has multi segment reconstruction). There is an increase of significant diagnostic value, when the temporal resolution increases to 83 ms. The main distinguishing mark of dual source CT is the flexibility it offers with respect to modes of operation and the opportunity to combine the resulting acquisition image data. Dual source acquisition data can be used in a variety of ways and detector B data with a smaller scan field (FOV) are extrapolated to a full-size detector, using detector A data at the same projection angle [6].

2.2.1.2 Dual Source Computed Tomography (Somatom Definition Flash)

The new CT characterizes a well-established concept of Dual Source acquisition but ameliorate it in a multitude of ways. Not only can the patient table travel at more than 43 cm/sec, the Somatom Definition Flash is equipped with two 38.4 mm detectors that each acquire 128x2 slices of image data [7]. Gantry rotation time has dropped to 0.28 s, which translates into a temporal resolution of just 75 ms. X-ray tube power has been increased to 2 x 100 kW (total 200kW) to accommodate even the most obese patients. The photograph of Definition flash CT scanner shows in *figure 2.2*.

Figure- 2.2: show the photograph of Siemens Somatom Definition flash Dual Source CT scanner.

The size of the gantry aperture is 78cm thus the maximum FOV is 78cm. The minimum reconstruction slice width is 0.4mm and freely selectable scan pitch of 0.2-3.2. A complete thoracic scan with the Somatom Definition Flash takes about 0.6 seconds that means, for the first time, patients not required to hold their breath during scanning.

2.2.1.3 REFERENCE

1. Flohr TG, McCollough CH, Bruder H, Petersilka M, Gruber K, Süss C et.al, First performance evaluation of a dual-source CT (DSCT) system, Eur Radiol (2006) 16: 256–268, DOI 10.1007/s00330-005-2919-2.

2. Flohr T, Stierstorfer K, Raupach R, Ulzheimer S, Bruder H, Performance evaluation of a 64-slice CT system with *z*-flying focal spot, Rofo. 2004 Dec;176(12):1803-10.

3. T. Flohr, K. Stierstorfer, S. Ulzheimer, H. Bruder, A. Prinak, C McCollough. Image reconstruction and image quality evaluation for a 64-slice CT scanner with *z*-flying focal spot, Med. Phys. 32, 2536 (2005); doi:10.118/1.1949787.

4. Bruder H, Stierstorfer K, McCullough C, Raupach R, Petersilka M, Grasruck M, et.al, Design considerations in cardiac CT, Medical Imaging 2006: Physics of Medical Imaging. Edited by Flynn, Michael J.; Hsieh, Jiang. Proceedings of the SPIE, Volume 6142, pp. 151-163 (2006).

5**.** Martin Petersilka, Herbert Bruder**,** B Krauss, Karl Stierstorfer, Thomas G. Flohr. Technical principles of dual source CT. Euro Journal of Radiol 68 (2008) 362–368.

6. Peter Schardt, Josef Deuringer, Jörg Freudenberger, Erich Hell, Wolfgang Knüpfer, Detlef Mattern, et.al, New X-ray tube performance in computed tomography by introducing the rotating envelope tube technology. Med. Phys. 31**,** 2699 (2004); doi:10.1118/1.1783552.

7. Media Relations: Marion Bludszuweit, Siemens AG, Erlangen, November 24, 2008, Information number: HIM200811.012 efp.

2.2.2 BASICS OF RADIATION DOSE

2.2.2.1 Literature Review

Definition of effective dose is the weighted sum of organ doses resulting from the computed tomography examination [1], where the radiosensitive organs defined along with their tissue-weighting factors. As a fact, it is very difficult to confirm exactly the radiation dose to an individual organ from a CT scan although above definition appears straightforward to estimate effective dose. This is even harder to comprehend when an effort to estimate the effective dose for each patient, each one has its own unique characteristics of height, weight, age, gender, and composition. Still several different methods developed for estimating effective dose.

First attempt was based on Monte Carlo simulations carried out at several years ago [2-5]. Dose estimation experiment was performed by members of the United Kingdom's National Radiological Protection Board (NRPB), used Monte Carlo methods to simulate CT scanning around a early created mathematical patient model (MIRD V) [6]. In an independent approach Zankl et al [7] from the Gesellschaft für Strahlen- und Umweltforschung (GSF) demonstrated simulations on two different mathematical sex-specific phantoms "Adam" and "Eva" [8]. This work was performed according to the ICRP data on reference man, that is similar to the MIRD V phantom. Another effort was that assess the energy imparted, established by Atherton and Huda [9-13]. The measure of the deposited total ionizing energy in a patient through out the duration of CT examination is energy imparted. On the base of simulation data of Jones and Shrimpton [4, 5], the energy imparted was calculated for a mathematical anthropomorphic phantom [5].

An another method used to estimate the effective dose is described by the European Guidelines on Quality Criteria for Computed Tomography [14] using conversion factors, which were based on the work of Jessen et al [15].

A.M Groves et al. [16] estimated CT radiation dose on a 16-detector unit directly employed an anthropomorphic phantom and thermo luminescent dosimeters (TLDs). They found that the radiation dose calculated directly with TLD was 18% higher than the computer simulated dosimetry (Monte-carlo), in keeping with the previously accepted underestimation by computer simulation method compared with TLD measurements.

2.2.2.2 Factors Influence radiation dose

In general, there are some elements that are directly determine radiation dose such as x-ray beam energy (kilo-volt peak), tube current (in milli-amperes), rotation or exposure time (in second), section thickness (mm), object thickness or attenuation, pitch and/or spacing, dose reduction techniques such as tube current variation or modulation, and distance from the x-ray tube to isocenter. Except these factors some other parameters that have an indirect effect on radiation dose—those factors that determine image quality but no direct effect on radiation dose, for example, the reconstruction filter. All parameters mentioned above are affects the radiation dose directly or indirectly. Choices of these factors may depend on an operator, the change of settings that do directly change radiation dose.

The single scan dose (D_S) changes with tube potential (kVp), beam filtration, tube-current –time product (mAs), source-to-skin distance (SSD), and patient attenuation factors [17]:

$$D_S \alpha . kVp^c . mAs . \frac{B}{SSD^2} \quad (2.1)$$

where the exponent c $\approx$3 varies with type and shape of filtration and B is the patient transmission. Dose in the center of the patient, however, is mainly determined by transmission. Measurements with CT dosimetry phantoms indicate that patient transmission and SSD have opposing effects on surface dose in normal practice, i.e., larger patients have smaller SSD's but reduced transmission, while smaller patients have greater transmission but larger SSD's [17].

a) Beam Energy- The energy of the x-ray beam has a straight influence on patient radiation dose and can be observed from equation 1. However, radiation dose also determined by the choice of filter selected for the scanning.

b) Photon Fluence- The photon fluence is determined by the tube current–time product (milli-ampere-seconds) and indicates a direct influence on patient dose. There is an issue with modern scanners, the user inputs a parameter labeled "mAs," but that mAs is normally the effective milli-ampere-seconds value, which is (milli-amperage x time)/pitch. When pitch is changed in these scanners, the milli-ampere-seconds value would be change in a corresponding fashion to maintain the effective milli-ampere-seconds value in a constant manner [18].

c) Helical Pitch- The pitch parameter in a spiral scans (table distance traveled in one 360° rotation/total collimated width of the x-ray beam) has directly depends on patient radiation dose. This is essential because as pitch increases the time that any one point in space spends in the x-ray beam decreased.

d) X-ray Beam Collimation: The current experiments show that the effects of beam collimation were large with multi-detector scanners than a single-detector scanner. However, early reports from early versions of multi-detector scanners giving a significant dependence on x-ray beam collimation [19].

e) Effects of object (patient) size- When the x-ray tube moves around the patient the tissues are exposed with both entrances (as the tube positioned directly over the tissue) as well as exit radiation (as the tube moves to the other side of the patient). The entrance radiation is closer as exit radiation dose if the patient size is smaller; this will give a uniform dose distribution (nearly equal at all locations in a 16-cm-diameter phantom). The exit radiation dose is much less degree for the larger patients due to its attenuation through more tissue. For a normal adult person, in the scan plane the higher radiation dose values occurring near the periphery of the slice (entrance exposure is highest).

f) Other parameters reduce scan dose- In addition to the technical parameters discussed earlier manufacturers have recently provided additional facilities to users to reduce patient dose. One of these is an option to make changes in tube current based on the calculated attenuation of the patient at a certain location (Automatic Exposure Control). For this the mA programmed to a maximum value and can be reduced according to the information of location along the patient is expected

to be less attenuating than the most attenuating location to be imaged. This is determined by using both antero-posterior and lateral planning projection views. According to the length of the patient, the tube current programmed to vary by location along and even as the tube is rotating around the patient. The exact details of the option vary by manufacturer.

g) Indirect effects- In addition to the direct effects, that collimation has, as described earlier; there is some other indirect effects, fore example the effect of reconstruction algorithm on dose. The other factor is reconstruction thickness. When thinner reconstructed slice thickness was used for imaging with all other factors held constant, there will be more noise in the images (noise is defined as the standard deviation of the CT number). The image noise is typically increases with $1/\sqrt{T}$, where T is the nominal section thickness. Therefore, a 10-mm-thick slice section can expect to have 3.2 times less noise compared with a 1-mm-thick section. Usually the kilovolt peak or milliampere-seconds value or both are increase to reduce the noise due to narrower sections. Certain reconstruction algorithms that enhance higher spatial frequencies and improve spatial resolution (such as required for lung or skeletal imaging) also increase the noise in the image. The kV or milliampere-seconds value or both of them may be increased to avoid these increases in noise. The radiation dose may increase because of increase in kilovolt peak or milliampere-seconds values. Therefore, the change of algorithm or slice thickness may not have a direct effect on radiation dose; the selection of scan factors depends on the resulting increase in image noise may result in an increase in radiation dose.

2.2.2.3 BASICS OF CT DOSE MEASUREMENTS

A) Dose-Length-Product method

The basic CT dose descriptors have been in existence for many years and continue to be redefined as multi-detector CT (MDCT) evolves. The primary measured value is known as the CT Dose Index (CTDI) and represents the integrated dose along the z-axis from one axial CT-scan (one rotation of the x-ray tube) [16, 18]. All other CT dose descriptors derived from this CTDI primary measured value. It is great significant to note that the CTDI is always calculated in the axial scan mode and that doses for spiral scan modes are calculated from the axial information systems involving shaped or bow-tie beam filters generate lower surface doses for the same operating factors due to reduced beam intensity toward the fan edges. SSD varies greatly from one scanner to the next scanner design. To convert exposure to dose in air $CTDI_{100}$ calculation uses the *f* factor and other tissues have different *f* factors. The *f* factor (in units of rads per roentgen) determined by the ratio of the mass energy absorption coefficient of a tissue to that of air [20]:

$$f = 0.87 * [(\mu_t/\rho_t)/ (\mu_a/\rho_a)] \quad (2.2)$$

Where μ_t/ρ_t is the mass energy absorption coefficient of the tissue (eg, bone, lung, soft tissue) and μ_a/ρ_a is the mass energy absorption coefficient of air. The mass energy absorption coefficient strongly depends on tissue and energy of the photons, particularly in the range of energy used in CT. Therefore, the $CTDI_{100}$ measurement presents a very simplified condition for calculating radiation dose. At 70 keV effective energy, *f* factor is defined to be 0.87 (air is assumed) for $CTDI_{100}$.

a) Computed Tomography Dose Index FDA ($CTDI_{FDA}$) - The Code of Federal Regulations, 21 CFR 1020.33, section (h) (1) defines CTDI as ‘‘the integral of dose profile along a line perpendicular to the tomographic plane divided by the product of the nominal tomographic section thickness and the number of tomograms produced in the single scan”; [21].

$$CTDI_{FDA} = \frac{1}{nT}\int_{-7T}^{+7T} D(z)dz \qquad (2.3)$$

where *z* is the position along a line perpendicular to the tomographic plane, *D*(*z*) is dose at position *z*, *T* is the nominal tomographic section thickness, and *n* is number of tomograms produced in a single scan.

b) Computed Tomography Dose Index 100($CTDI_{100}$) - Theoretically, the CTDI should be measured from plus to minus infinity. Since in practice the ion chamber used for the measurement of CTDI is typically 100 mm long, the IEC (International Electro-technical Commission) has specifically defined the CTDI measured with such a method as $CTDI_{100}$. In general, the $CTDI_{100}$ is different from $CTDI_{FDA}$.

$CTDI_{100}$ (cGy)= [Rdg$\times C_{tp} \times K_{el} \times N_x \times f_{med}$x100 (mm)]/Total nominal beam width (mm) (2.4)

Where Rdg is electrometer reading, C_{tp} is the temperature and pressure correction factor, K_{el} is the electrometer calibration factor (C/Rdg) and f_{med} is F factor which is used to convert exposure in air to absorbed dose in medium (0.94 cGy for muscle and acrylic).

c) Weighted CTDI ($CTDI_W$) - CT dosimetry includes evaluation of CTDI dependence on the measurement point position in the field-of-view. For example, for body CT imaging, the CTDI is typically a factor or two higher at the surface than at the center of the field-of-view. The average CTDI across the field-of-view is given by the weighted CTDI ($CTDI_w$),

$$CTDI_w = 2/3\ CTDI\ (surface) + 1/3\ CTDI\ (center) \quad (2.5)$$

d) CTDI Volume ($CTDI_{Vol}$) - Using the $CTDI_{100}$ definition, the IEC has defined the term CTDI Volume ($CTDI_{vol}$).

$$CTDI_{vol} = \frac{N.T}{I} .CTDI_W \quad (2.6)$$

Where *N* is the number of simultaneous axial scans per x-ray source rotation, *T* is the thickness of one axial scan (mm), and *I* is the table increment per axial scan (mm).

e) Spiral CT- $CTDI_{Vol}$- In spiral CT, the ratio of the table travel per rotation (*I*) to the total nominal beam width (*N*.*T*) referred to as pitch (8). Therefore,

$$CTDI_{vol} = \frac{1}{Pitch} . CTDI_w \quad (2.7)$$

The $CTDI_w$ symbolize the average radiation dose over the *x* and *y* directions and the $CTDI_{vol}$ stands for the average radiation dose over the *x*, *y*, and *z* directions. $CTDI_{vol}$ consider into account protocol specific information such as pitch that is why it is a important indicator of the dose for a specific clinical exam protocol.

f) Dose-Length Product (DLP) - Dose-Length Product is used to define the total energy absorbed by a scanned volume from a given protocol. DLP represents integrated dose along the scan length,

$$\text{DLP (mGy.cm)} = \text{CTDI}_{vol} \text{ (mGy) X scan length (cm).} \quad (2.8)$$

The radiation risk for a 20 mm scan length entirely differs from that of a 200 mm scan length, in spite of each having the identical $CTDI_{vol}$ value. The dose-length product clearly provides an indication of the energy imparted for a particular clinical scan. While two scan protocols may have the same $CTDI_{vol}$, their DLP value may be substantially different due to difference in scanned volume length. Now a days most of the CT manufacturers include DLP information on the scanner control console for programmed scan protocols and scan lengths.

g) Effective Dose (mSv)

A reasonable estimate of effective dose can be obtained by using of the following below:

$$\text{Effective dose (mSv)} = k.\ DLP \quad (2.9)$$

Where k (mSv.mGy-1.cm-1) is dependent upon body region and given in the European Guidelines on Quality Criteria for Computed Tomography (EUR 16262 EN, May 1999) [14]. The chest conversion factors based on Monte Carlo simulations modeling single section scanners were 0.017 mSv/mGycm in the European Commission guidelines- 2000 [22] and 0.014 mSv/mGycm in the 2004 European Commission guidelines [23]. The latest 2004 recommendation was used to calculate effective dose in our study.

B) Thermo luminescence dosimetry (TLD)

Some materials absorb radiation energy and retain a part of energy absorbed in metastable states. When this energy is subsequently released in the form of ultraviolet, visible or infrared light, the phenomenon is called luminescence. There are two types of luminescence: fluorescence and phosphorescence. Fluorescence is the process that happen with a time delays of between 10^{-10} to 10^{-8} second and phosphorescence with a time delay exceeding 10^{-8} seconds. The phosphorescence process can be progress with a suitable excitation in the form of heat (temperature) or light. If the emission of light by the application of heat, the phenomenon is called thermo-luminescence and the material is called thermo-luminescent (TL) material. The most commonly used TL dosimeter is LiF:Mg,Ti (TLD-100) in medical applications because of their tissue equivalence.

The emitted TL intensity is a function of the applied temperature T. Keeping the heating rate constant makes the temperature T proportional to time t and so the TL intensity can be plotted as a function of time. This will give a curve and this curve is called as TLD glow curve (*Fig. 2.3*). The peaks in the glow curve may be useful to correlate with trap depths responsible for TL emission.

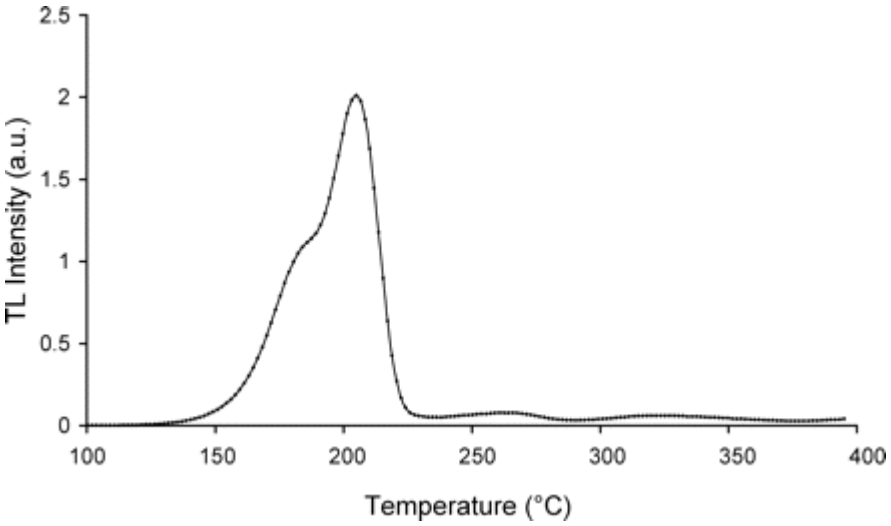

Figure- 2.3: shows a Typical glow-curve of LiF:Mg,Ti measured with a TLD reader at a low heating rate.

The major dosimetric peak of the LiF:Mg,Ti glow curve between 180° and 260°C of temperature is important for dosimetric purpose. The total TL signals emitted, the part under the appropriate area of the glow curve can be used to determine radiation dose through proper calibration. TL dosimeters should calibrate before they used for dosimetric purpose (thus, they serve as relative dosimeters). It is required to apply some particular correction factors (the corrections such as energy, fading and dose-response non-linearity corrections) for the derivation of radiation dose absorbed by TL dosimeters.

2.2.2.4 REFERENCE

1. International Council on Radiation Protection. 1990 recommendations of the International Commission on Radiological Protection Publication 60, Annals of the ICRP 1991; 21. Oxford, England: Pergamon, 1991.

2. Shrimpton PC, Jones DG, Hillier MC, Wall BF, Le Heron JC, Faulkner K. Survey of CT practice in the UK Part 2: Dosimetric aspects. NRPB R249. Chilton, England: National Radiological Protection Board, 1991.

3. Jones DG, Shrimpton PC. Survey of CT practice in the UK Part 3: Normalised organ doses calculated using Monte Carlo techniques. NRPB R-250. Chilton, England: National Radiological Protection Board, 1992.

4. Jones DG, Shrimpton PC. Normalised organ doses for x-ray computed tomography calculated using Monte Carlo techniques NRPB SR-250. Chilton, England: National Radiological Protection Board, 1992.

5. Shrimpton PC, Jones DG. Normalised organ doses for x-ray computed tomography calculated using Monte Carlo techniques and a mathematical anthropomorphic phantom. Radiat Prot Dosimetry (1993) 49 (1-3): 241-243.

6. Cristy M. Mathematical phantoms representing children of various ages for use in estimates of internal dose NUREG/CR-1159 ORNL/NUREG/TM-367. Oak Ridge, Tenn: Oak Ridge National Laboratory, 1980.

7. Zankl M, Panzer W, Drexler G. The calculation of dose from external photon exposures using reference human phantoms and Monte Carlo methods Part VI: Organ doses from computed tomographic examinations. GSF-Bericht 30/91. Neuherberg, Germany: Gesellschaft für Strahlen- und Umweltforschung, 1991.

8. Kramer R, Zankl M, Williams G, Drexler G. The calculation of dose from external photon exposures using reference human phantoms and Monte Carlo methods Part I: The male (Adam) and female (Eva) adult mathematical phantoms. GSF-Bericht S-885. Munich, Germany: Gesellschaft für Strahlen- und Umweltforschung, 1982.

9. Huda W, Atherton JV. Energy imparted in computed tomography. Med. Phys. 22, 1263 (1995); doi:10.1118/1.597564.

10. Atherton JV, Huda W, Energy imparted and effective doses in computed tomography, Med Phys. 1996 May;23(5):735-41.

11. Huda W, Scalzetti EM, Roskopf M, Effective doses to patients undergoing thoracic computed tomography examinations Med Phys. 2000 May;27(5):838-44.

12. Dan E. Ware, MD, Walter Huda, PhD, Patricia J. Mergo, MD, Anthony L. Litwiller, RT(R)(CT), Radiation Effective Doses to Patients Undergoing Abdominal CT Examinations, March 1999 Radiology, 210, 645-650

13. International Council on Radiation Protection. Recommendations of the International Commission on Radiological Protection, 1977 Publication 26, Annals of the ICRP 1(3) (reprinted with additions in 1987). Oxford, England: Pergamon, 1977; [superseded by ICRP Publication 60].

14. European Guidelines on Quality Criteria for Computed Tomography (EUR 16262 EN, May 1999). Available at: www.drs.dk/guidelines/ct/quality/index.htm 2002; Accessed July.

15. Jessen KA, Shrimpton PC, Geleijns J, Panzer W, Tosi G, Dosimetry for optimisation of patient protection in computed tomography. Appl Radiat Isot. 1999 Jan;50(1):165-72.

16. A.M Groves, K. E Owen et.al., 16-detector multislice CT: dosimetry estimation by TLD measurement compared with Monte Carlo simulation, The British Journal of Radiology, 77 (2004), 662–665.

17. Specification and acceptance testing of computed tomographic scanners. AAPM report no. 39.

18. H.D. Nagel, Radiation Exposure in Computed Tomography, (COCIR, Frankfurt, 2000).

19. AAPM, Report No. 31, Standardized Methods for Measuring Diagnostic X-ray Exposures (American Institute of Physics, New York, 1990).

20. Michael F. McNitt-Gray, AAPM/RSNA Physics tutorial for residents: topics in CT, Radiation dose in CT, doi: 10.1148/rg.226025128. November 2002 Radiographics, 22, 1541-1553.

21. Diagnostic x-ray systems and their major components; amendments to performance standard--FDA. Final rule, Fed Regist. 1984 Aug 31;49(171):34698-714.

22. Bongartz G, Golding SJ, Jurik AG, et. al., European Guidelines on Quality Criteria for Computed Tomography. EUR 16262. The European Commission's Study Group on Development of Quality Criteria for Computed Tomography. Luxembourg, Luxembourg: European Commission, 2000.

23. Bongartz G, Golding SJ, Jurik AG, et al. 2004 CT quality criteria. Luxembourg, Luxembourg: European Commission, March 2004.

2.2.3 IMAGE QUALITY

2.2.3.1 Physics behind image quality

Attenuation can be defined as the combination of absorption and scattering of radiation by the material under investigation. The two main mechanisms responsible for these effects in the photon energy range used in CT are the Compton scatter and the photoelectric effect. The contribution of these two processes to the attenuation of different materials varies and depends on the energy of the X-ray photons. Inside the energy range considered the total cross section of the Compton effect is almost independent of photon energy, whereas the total cross section of the photo electric effect is strongly energy-dependent. For soft tissues, CT numbers do not vary much with beam energy but for high z materials it change dramatically. Therefore, it is possible to differentiate materials further by applying different X-ray spectra and can be analyze the differences in attenuation [1]. This works especially well in materials with high atomic numbers because of the photoelectric effect (*Fig. 2.4*) [2, 3]. One of these materials is iodine, which commonly used in CT as a contrast material and generally known to have stronger enhancement at low tube voltage settings [4]. This behavior makes it beneficial to use clinically the spectral information to separate iodine from other materials that do not exhibit this effect.

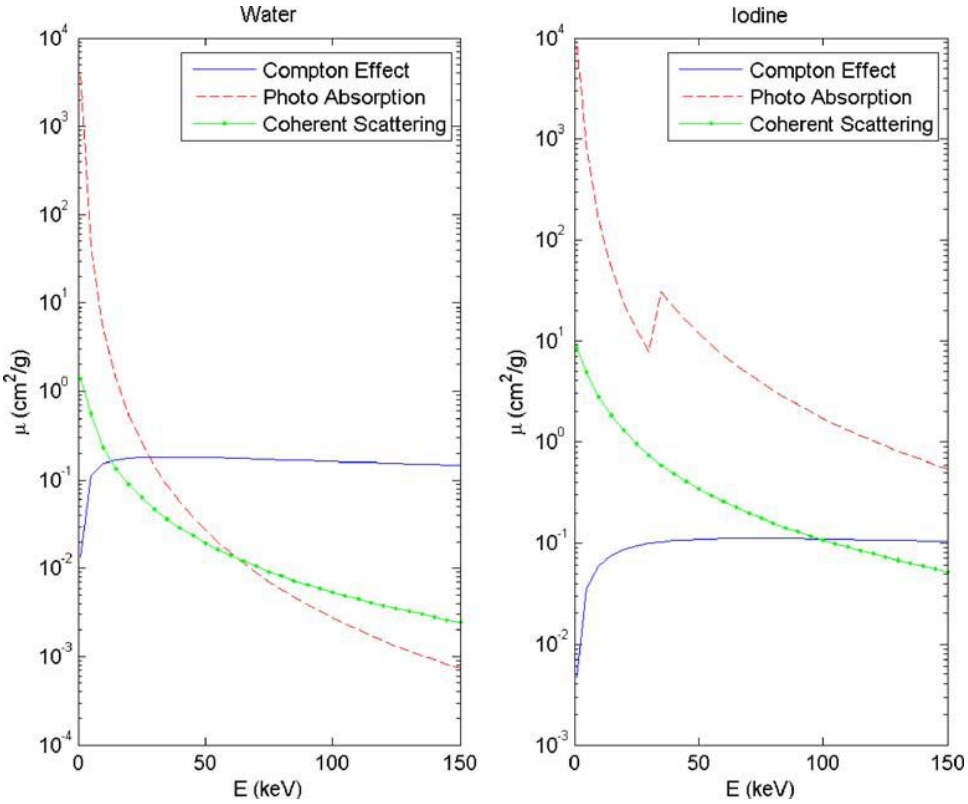

Figure- 2.4: shows attenuation in water and iodine at different photon energies with the components Compton Effect, photoelectric effect, and coherent scatter. Note the obvious difference in photo absorption at the k-edge, which is, however, below the presently used range of the energy spectrum.(Data courtesy of XCOM Photon Cross Sections Database [5])

2.2.3.2 Quantitative CT (CT Number Accuracy)

In quantitative CT (QCT), CT numbers are used directly for tissue characterization [6]. The information obtained from CT images can be used for the calculation of density to CT number conversion. This relationship is typically scanner dependent. Each CT image is a two-dimensional matrix of CT numbers corresponding to mean linear attenuation coefficients of the material in each voxel [7]. Scanner software has tools, which will report the mean CT numbers for the region of interest in a CT image.

The measured mean CT number for a given material should correspond to a value calculated based on the mean linear attenuation coefficient for the given material and water at specific beam energy.

2.2.3.3 Random Uncertainty in pixel value (Image Noise)

Ideally, a CT-scan of a uniform phantom would have uniform pixel values (CT numbers) throughout the phantom image. The Hounsfield Unit of an image of a homogenous phantom is not uniform in reality. The variation of CT numbers in pixel intensities consists of random and systematic components. The random component of image non-uniformity is noise. Its effect on the image is to place a lower limit on the level of subject contrast that can be distinguished by the observer. The most of the soft tissue details are in low contrast in nature therefore the pixel noise is a critical limiting factor in CT imaging. Assuming that digitization error is insignificant in modem scanners (6), total random pixel noises (Np) given by:

$$Np \approx \sqrt{Ne^2 + Nq^2} \tag{2.10}$$

Electronic noise (Ne) arises as random variation in detector signal prior to digitization; quantum noise (Nq) is due to random variation in numbers of detected x-ray quanta [8]. Quantum noise (Nq) arises from statistical uncertainty in the finite number of transmitted x-ray photons (n) collected in forming the image [9], i.e.:

$$Nq \alpha n^{-1/2} \tag{2.11}$$

The noise can be expressed in terms of standard deviation (SD) of the CT numbers in Hounsfield units (HU). Alternatively, as a percent of the linear attenuation coefficient of water (μw) and corrected for the scanner contrast scale [10].

$$Noise = \delta .CS. 100\% / (\mu w) \tag{2.12}$$

where δ is the standard deviation of CT numbers within the region of interest; CS is the contrast scale defined as CS =(μm- μw /CTm-CTw), where μm and μw are the linear attenuation coefficients for the subject material and water, respectively, and CTm and CTw are the measured CT numbers for the subject material and water, respectively [8]. Theoretically, minimal noise images should increase normal structure accuracy.

Signal-Noise-Ratio- SNR is the mean density of the object in a circular region of interest (ROI) divided by standard deviation (SD) from the mean pixel values in Hounsfield units (HU) within the ROI.

SNR = Object density/image noise (2.13)

Contrast-Noise-Ratio

CNR = (Objective density- Background density)/Image noise (2.14)

Thus, a CNR of 1.0 obtained when the contrast (ie, the difference in attenuation) between an object and its background was equal to the image noise measured by the SD.

2.2.3.4 REFERENCE

1. Avrin DE, Macovski A, Zatz LE, Clinical application of Compton and photo-electric reconstruction in computed tomography: preliminary results, Invest Radiol. 1978 May-Jun;13(3):217-22.

2. Kruger RA, Riederer SJ, Mistretta CA, Relative properties of tomography, K-edge imaging, and K-edge tomography. Med Phys. 1977 May-Jun;4(3):244-9.

3. Riederer SJ, Mistretta CA (1977) Selective iodine imaging using K-edge energies in computerized x-ray tomography. Med Phys. 1977 Nov-Dec;4(6):474-81.

4. Nakayama Y, Awai K, Funama Y, Hatemura M, Imuta M, Nakaura T, Ryu D, Morishita S, Sultana S, Sato N, Yamashita Y (2005) Abdominal CT with low tube voltage: preliminary observations about radiation dose, contrast enhancement, image quality, and noise. Radiology 237:945–951

5. Berger MJ, Hubbell JH, Seltzer SM, Chang J, Coursey JS, Sukumar R, Zucker DS (2005) XCOM: Photon Cross Sections Database, NIST Standard Reference Database 8 (XGAM). http://www.physicsnistgov/xcom

6. Specification and acceptance testing of Computed Tomography scanners, AAPM Report no. 39, May 1993.

7. Cann CE and Genant HK: “Cross-Sectional Studies of Vertebral Mineral Using Quantitative Computed Tomography”, J. Comput. Assist. Tomogr., 6:216 (1982).

8. Quality assurance for computed-tomography simulators and the computed tomography- simulation process: Report of the AAPM Radiation Therapy Committee Task Group No. 66, Sept.2003

9. Cohen G and DiBianca FA: “The Use of Contrast Detail Dose Evaluation of Image Quality in a Computed Tomographic Scanner,” J Comput Assist Tomogr. 1979 Apr;3(2):189-95.

10. AAPM, Report No. 39. Specification and Acceptance Testing of Computed Tomography Scanners (American Institute of Physics, New York, 1993).

Chapter-3

Estimation and Comparison of Effective Dose (E) in Standard Chest CT by Organ Dose Measurements and Dose-Length-Product Methods and Assessment of the Influence of CT Tube Potential (Energy Dependency) on Effective Dose in a Dual-Source CT

3.1 ABSTRACT

Purpose: To determine effective dose (E) during standard chest CT using an organ dose-based and a dose-length-product-based (DLP) approach for four different scan protocols including high-pitch and dual-energy in a dual-source CT scanner of the second generation.

Material and Methods: Organ doses were measured with thermo luminescence dosimeters (TLD) in an anthropomorphic male adult phantom. Further, DLP-based dose estimates were performed by using the standard 0.014 mSv/mGycm conversion coefficient k. Examinations were performed on a dual-source CT system (Somatom Definition Flash, Siemens). Four scan protocols were investigated: (1) single-source 120 kV, (2) single-source 100 kV, (3) high-pitch 120 kV, and (4) dual-energy with 100/Sn140 kV with equivalent CTDIvol and no automated tube current modulation. E was then determined following recommendations of ICRP publication 103 and 60 and specific k values were derived.

Results: DLP-based estimates differed by 4.5-16.56% and 5.2-15.8% relatively to ICRP 60 and 103, respectively. The derived k factors calculated from TLD measurements were 0.0148, 0.015, 0.0166, and 0.0148 for protocol 1, 2, 3 and 4, respectively. Effective dose estimations by ICRP 103 and 60 for single-energy and dual-energy protocols show a difference of less than 0.04 mSv.

Conclusion: Estimates of E based on DLP work equally well for single-energy, high-pitch and dual-energy CT examinations. The tube potential definitely affects effective dose in a substantial way. Effective dose estimations by ICRP 103 and 60 for both single-energy and dual-energy examinations differ not more than 0.04 mSv.

3.2.1 INTRODUCTION

Radiation doses delivered to patients undergoing CT examinations are relatively high in comparison with doses associated with other types of diagnostic radiological procedures [1]. A single parameter reflects the relative risk from exposure to ionizing radiation is effective dose (E). It shows the risk of detrimental biologic effects from a non-uniform, partial-body exposure in terms of a whole-body exposure [2, 3]. For calculating effective dose, the risk coefficients used had been derived from a cohort that included all ages and both sexes and depended primarily on the excess risk observed in Japanese atomic bombing survivors. Therefore, it is useful for comparing and optimizing different CT procedures, particularly when comparing examinations from different CT techniques and effective dose is not applicable to any single adult individual. An anthropomorphic phantom is a realistic description of the human body (*Figure 3.1*).

Two common methods used in this study to estimate effective dose for a CT examination were compared: first, the classical method that explicitly use tissue-weighting factors as specified by the International Commission on Radiological Protection (ICRP) [7, 8] based on organ dose estimates. Second method is based on the dose-length-product (DLP) and “k-factor” that depends on the anatomic region examined.

Tissue-weighting factors derived primarily from the Japanese atomic bomb survivors [4-7], it represent the relative radiation sensitivity of each type of body tissue as determined from population averages over age and sex.

Effective dose is the weighted summation of the absorbed dose to each specified organ and tissue multiplied by the ICRP-defined tissue-weighting factor for that same organ or tissue for partial body irradiation [8].

If a number of organs are considered, their radiation sensitivity and the severity of damage and its treatability are different. To consider the risk factor depending on age and sex, the equivalent dose (is the product of average absorbed dose to tissue and radiation weighting factor) is not sufficient. So a term called tissue weighting factor (w_T) is assigned to each tissue/organ.

$$HE = \sum_{T,R}(D_{T,R}.w_R.w_T), \qquad \text{Unit: mSv}$$

Where HE is the effective dose, w_T is the tissue-weighting factor, w_R is the radiation-weighting coefficient, $D_{T,R}$ is the average absorbed dose to tissue T, T is the subscript for each radiosensitive tissue, and R is the subscript for each type of radiation. Three different sets of tissue weighting factors have defined in publications by the ICRP and these revisions intended to reflect advances in knowledge about the radiation sensitivity of various organs and tissues. The publications are ICRP 26, published in 1977 [3]; ICRP 60, in 1991 [7]; and ICRP 103, in 2007 [8]. From ICRP 26 the name of the summed quantity “effective dose equivalent” changed to “effective dose” in ICRP 60 in addition changes of tissue-weighting factors. Although for several primary organs ICRP 103 assigns different tissue-weighting factors, it retains the name “effective dose.” In addition, the three ICRP recommendations differ somewhat in calculation methodology. For example, in ICRP 60 the mean organ dose is to be used but in ICRP 26 organ doses defined by a single-point dose in the organ of interest. With each publication, the trend has been to specify

weighting factors for an increasing number of organs and tissues, which decreased the weighting of “remainder tissues” (*Table 3.1*). An example is the brain, it is listed as a primary organ in ICRP 103 but ICRP 26 and ICRP 60 treated as one of the “remainder” organs. According to time, the specific tissues weighting factor also changed. For example, gonads weighting factor decreased in each subsequent publication. Nevertheless, for the breast, weighting decreased in ICRP 60 but then increased in ICRP 103. Depending on which ICRP report used, the estimates of effective dose for the exact same CT examination can differ substantially because of these changes. Here we used the latest ICRP Publication 103 for the organ and thorax dose calculation and ICRP 60 used for comparison purpose.

Method 2: DLP can be defined as the product of the volume CTDI and the irradiated scan length.

$$DLP = CTDIvol \times irradiated\ length,$$

where CTDIvol is the volume CTDI [9, 10], dose-length-product (DLP), defined according to International Electro-technical Commission standards [8], recorded for each scan from the scanner console. The “*k* factor,” or conversion factor relating DLP to effective dose, was determined by dividing effective dose by DLP. The effective dose determined by using TLD measurements also compared with that estimated by using DLP multiplied by European Commission chest conversion factors. These factors based on Monte Carlo simulations modeling single section scanners were 0.017 mSv/mGycm in the European Commission guidelines- 2000 [11] and 0.014 mSv/mGycm in the 2004 European Commission guidelines [12]. The latest 2004 recommendation was used to calculate effective dose in our study.

The effective dose of ± 15% deviation were reported using this method relative to the organ dose-based technique for CT scans obtained at 120 kV [13]. In helical CT, this calculation method is apt to underestimate effective dose when DLP calculated with only the CTDIvol and the prescribed scan range because the irradiated length typically exceeds the prescribed scan length [14, 15, and 16]. Most manufacturers of CT scanners now compute and display DLP taking into account the entire irradiated length rather than the lesser-prescribed scan length because of the wide spread use of this method [16].

Effective dose is widely used by the academic, clinical, and manufacturing communities in spite of these sources of variation in the calculation of effective dose [16]. Therefore, the purpose of this investigation was to determine how well estimates of effective dose calculated using DLP agree with calculations based on organ dose estimates after adopting the revised tissue weighting factors of ICRP 103 or when using tube potential values other than 120 kV, including high-pitch and dual-energy CT protocols. In spiral CT, both dose and noise depend on pitch, but not in the same way. If mAs instead of effective mAs are used, the dose is always inversely proportional to pitch. The behavior of noise as a function of pitch depends on the scanner type (single vs. multi-detector row) and reconstruction mode (ECG-gated vs. non-gated). In non-ECG-gated spiral multi-detector row CT, noise depends on pitch, which results in comparable noise when the ratio of tube current-time-product to pitch is held constant.

3.2.2 MATERIALS & METHODS

Computed Tomography Device

All phantom examinations were performed on a dual-source CT device of the second generation (Somatom Definition Flash, Siemens Healthcare, Forchheim, Germany). This scanner houses two tube-detector systems mounted at an angular off-set of 95° within the same gantry that simultaneously revolve around the patient's body. Each detector is capable of acquiring 128 x 0.6 mm slices with one rotation. A gantry rotation time of 0.28 s results in a maximal temporal resolution of 75 ms. The scanner can be used in three different scan modes: 1) as a regular single-source 128-slice device with a tube potential of 80, 100, 120 or 140 kV; 2) as a dual-source device in high-pitch mode with a 128-slice configuration on both detectors with a tube potential range between 80 and 140 kV up to maximum pitch of 3.0 (in the latest software version up to 3.2, in ECG-gated mode up to 3.4); 3) in dual-energy mode as a 64-slice device with a tube potential combination of tube A and B of either 80/140 kV, 80/140 kV + tin filter or 100/140 kV + tin filter, where the latter is the configuration of choice because of the good tissue penetration of both the 100 kV and the hardened 140 kV spectrum. As dose reduction technologies, the manufacturer implemented an asymmetric collimator at the side of the x-ray tubes (so called adaptive dose shield) which dynamically blocks irrelevant pre- and post-spiral x-ray quanta that do not contribute to the actual image but cause the “over radiation” phenomenon. Further, for dual-energy data acquisition, a tin filter was applied to the 140 kV tube that blocks low energy quanta and thus reduces energy overlap of the high and low kV spectrum (so called selective photon shield).

Third, the real-time tube current modulation software (CAREDose 4D) in a new version is also implemented in the scanner software. However, for this phantom trial, this feature was not turned on.

Phantom

An anthropomorphic male phantom (Alderson Rando, The Phantom Laboratory, Salem, NY, USA) was used for organ-based dose measurements in this study. The phantom corresponds to a 175 cm tall and 73.5 kg heavy male person without arms and legs (*Figure 3.1 and figure 3.2A*). The phantom is constructed with a natural human skeleton which is cast inside soft tissue-simulating material. The phantom's soft tissue is manufactured with a proprietary urethane formulation. The material has an effective atomic number and mass density simulating muscular tissue with randomly distributed fat. The lung material has the same effective atomic number as the soft tissue material with a density that simulates human lungs in a median respiratory state. The phantom is sliced at 2.5 cm intervals and has several drilled holes for the placement of thermo-luminescence dosimeters.

Thermo-luminescence Dosimeters (TLD)

The thermo-luminescence dosimeters used for this study (TLD 100, Harshaw Chemical Company, Solon, Ohio, USA) had a diameter of 1 mm and a length of 6 mm (*figure 3.2B*). All TLDs were processed using standard handling and processing techniques. Specific corrections or conversions for fading, linearity, energy, and absorbed dose had been applied to all TLD data in a consistent manner. There were totally 132 TLDs used for a single scan. 126/132 TLDs were inserted in the suitable pre-determined positions within the Alderson phantom; Six TLDs were used for measurement of background radiation levels.

All TLD measurements were read with a standard TLD reader (UD 505 A, National, Japan) (*figure 3.2C*). Before irradiation, the TLDs were heated according to the seven segment-annealing program in an annealing oven *(figure 3.2D*). During the heating cycle, the hot air stream circulated by a built-in fan to ensure equal temperature distribution throughout the oven volume. Also the cooling phase was temperature controlled. A digital display showed the actual temperature, and built-in lamps indicate the program progress. The standard oven was supplied with an RS232 interface. TLDs considered representing the most appropriate way for organ dose measurements. The TLD measurements in this project reflect point dose measurements that are assumed to be representative of the dose to the whole organ [17]. Total thorax effective dose (mSv) from the CT examinations was calculated by summing the absorbed doses (mGy) of individual organs weighted for their radiation sensitivity [7].

Examination Protocols

Totallly four different scan protocols were investigated: (1) single-source with 120 kV, 110 eff.mAs, rotation time of 0.5s, pitch 1.2, collimation of 128 x 0.6 mm, (2) single-source with 100 kV, 180 eff.mAs, rotation time of 0.5 s, pitch 1.2, collimation of 128 x 0.6 mm, (3) high-pitch mode with 120 kV and 130 eff.mAs on each one of the both tubes, rotation time of 0.28 s, pitch 3.0, collimation of 2 x 128 x 0.6 mm, and (4) dual-energy mode with 100 kV/Sn140 kV and eff.mAs 89/76 on tube A and B, rotation time of 0.28 s, pitch of 0.55 and a collimation of 2 x 64 x 0.6 mm (*Table 3.2*). Protocols were designed CTDIvol-equivalent compared to the standard 120 kV/110 mAs protocol, which represents the manufacturer's recommendation for standard

chest CT examinations. The default CTDIvol was 7.25 +/- 0.15 mGy. No tube current modulation was used.

Examinations

First, an anterio-posterior topogram of the chest of the Alderson phantom was obtained. The total scan length was planned as 49 cm, which was starting from 2 cm above the first rib up to the lower end of the body of the L1 vertebra. The reconstructed field of view (FOV) was kept constant at 400 x 400 mm for all protocols except protocol 3 (high-pitch mode), because here 332 mm is the maximum achievable FOV as detector B is smaller due to restrictions of space in the gantry . For each protocol the phantom with the referring set of TLDs was scanned totally six times to bring enough energy to the TLDs for sufficient and reliable measurements. Accordingly, to obtain the dose of a single scan, the total dose measured with the TLDs was divided by six after each set of measurements for each of the four protocols.

Energy Dependency of Effective Dose

The DLP and k values (*Table 3.4*,) computed for each examination were energy independent and the organ dose based tissue-weighting factors are energy dependent. The values for EDLP, E60, and E103 at each tube potential were first normalized to CTDIvol (EDLP/CTDIvol, E60/CTDIvol and E103/CTDIvol, respectively) (*Table 4*) to assess the influence of CT tube potential (energy dependency) on estimations of effective dose. From the normalized effective dose values (E60/CTDIvol or E103/CTDIvol) we computed the coefficient of variation as a function of energy [coefficient of variation = (standard deviation/mean) x 100%].

Any energy dependence of the organ dose calculations can be quantified by using these coefficients of variations.

3.2.3 RESULT

Organ Dose According to TLD Measurements

The absolute TLD dose measurements of different radiosensitive organs calculated according to ICRP 103 recommendations are summarized in *Table 3.3* and *Figure 3.3*. In the four of the investigated chest CT protocols, the maximum single organ dose was noted for the lungs with 13.73 mGy in the high-pitch mode, followed by 13.3 mGy in dual-energy mode, 13.24 mGy with the single-source 100 kV protocol and 12.75 mGy for the standard 120 kV protocol.

Comparison of Effective Dose Based on ICRP 103, ICRP 60 and DLP

The effective dose measured with TLDs utilizing tissue weighting factors as recommended by ICRP publication 103 were 5.33 mSv, 5.44 mSv, 6.22 mSv, and 5.09 mSv, respectively, for the single-source 120 kV, single-source 100 kV, high-pitch, and dual-energy protocol. *Figure 3.4* gives an overview on the obtained results comparing effective dose estimates by ICRP 103, 60 and as calculated by using DLP method.

The differences of absolute dose values were the largest when comparing E_{DLP} to E103 for (*Table 3.4*) protocol 1 (120 kV) with 0.28 mSv, protocol 2 (100 kV) with 0.42 mSv, and protocol 4 (dual-energy) with 0.3 mSv, respectively. When we look at the high-pitch protocol (third protocol), the largest absolute difference in effective dose

was 1.04 mSv when comparing E_{DLP} to E60. Correspondingly, relative differences were 5.3% (120 kV), 7.7% (100kV), 16.7% (high-pitch) and 5.9% (dual-energy) between E_{DLP} and E103 respectively.

When changing from ICRP 60 to 103 tissue weighting factors, effective dose estimates were almost unaffected for the single-source 100 kV protocol (0.02 mSv corresponding to a 0.37% increase) and the dual-energy protocol (0.07 mSv corresponding to a 1.39% increase). An interesting point noted in this study was the dual-energy protocol delivered the least effective dose for chest CT independent of the way E was calculated (4.79 mSv, 5.02 mSv, and 5.09 mSv for E_{DLP}, E60, and E103, respectively).

Effective Dose Calculated from DLP and Derived k Factors

E_{DLP} (*Table 3.4*) underestimated effective dose for all investigated scan protocols relative to the TLD-based, organ-based calculations. The percentage differences between E_{DLP} and E103 [100% × (E_{DLP} – E103) / ½ (E_{DLP}+E103)] were 5.5%, 8.2%, 17.1% and 6.1% for protocol 1, 2, 3, and 4. The referring k factors (k = TLD-measured dose/DLP) were calculated to be 0.0148, 0.015, 0.0166, and 0.0148, respectively, for the single-source 120 kV, single-source 100 kV, high-pitch, and dual-energy protocol.

Energy Dependency of Effective Dose

Each of the input parameters (CTDIvol, DLP, k factors) used to compute E_{DLP} were fixed and energy independent (tube potential). The normalized values for E_{DLP} per CTDIvol (*Table 3.4*) were 0.685 mSv/mGy (120kV), 0.686 mSv/mGy (100kV), 0.735

mSv/mGy (high-pitch) and 0.6535 (dual-energy). These values must be seen as energy independent organ dose calculations and the coefficient of variation for E_{DLP} was 4.3%. For each examination type, the coefficients of variation for E60 and E103 values, which are based on energy-dependent organ dose calculations, were within 1% of each other and were approximately 9-10% for the investigated chest CT protocols when looking at effective dose (*Table 3.4*). Thus for the same total CTDIvol, definitely tube potential has an effect on estimates of effective dose.

Single- or Dual-Energy effective dose Protocols- A comparison

Tissue-Weighting factor based effective dose estimations by ICRP 103 and 60, single-energy and dual-energy examinations with an observed difference of no more than 0.4 mSv. With ICRP103 calculation, the percent difference obtained for Standard 120kV was 4.7% and 6.9% (Standard 100kV) from Dual Energy. Further 5.4%, 8% respectively for standard 120 and standard 100kV with ICRP60.

3.2.4 TABLES AND FIGURES

Body Tissue or Organ	Publication ICRP 26	ICRP 60	ICRP103
Lung	0.12	0.12	0.12
Colon		0.12	0.12
Stomach		0.12	0.12
Breast	0.15	0.05	0.12
Bladder		0.05	0.04
Liver		0.05	0.04
Esophagus		0.05	0.04
Thyroid	0.03	0.05	0.04
Skin		0.01	0.01
Bone surface	0.03	0.01	0.01
Brain			0.01
Salivary glands			0.01
Gonads	0.25	0.20	0.08
Red bone marrow	0.12	0.12	0.12
Remainder	0.30	0.05	0.12
Total	1.00	1.00	1.00

Table- 3.1: Tissue weighting factors from International Commission on Radiological Protection (ICRP) publications 26, 60 and 103.

Scan parameters	**Protocol 1**	**Protocol 2**	**Protocol 3**	**Protocol 4**
Scan mode	Single-source	Single-source	Dual-source Single-energy	Dual-source Dual-energy
tube potential / effective tube current time product	120 kV, 110 mAs	100 kV, 180 mAs	120 kV, 130 mAs	100/Sn140 kV, 89/76 mAs
Total scan time (s)	4.73	4.73	1.1	10.68
Rotation time (s)	0.5	0.5	0.28	0.28
Detector collimation (mm)	128 x 0.6	128 x 0.6	128 x 0.6 x 2	64 x 0.6 x 2
CTDIvol (mGy)	7.37	7.32	7.12	7.33
Pitch	1.2	1.2	3.0	0.55

Table- 3.2: This table shows the parameters for the four investigated CT examination protocols in this study.

	Organ dose (mGy) calculated from TLD measurements			
Organ	120 kV, 110 mAs,	100 kV, 180 mAs,	120 kV, 130 mAs,	100/Sn140 kV, 89/76 mAs,
	Single-source	Single-source	Dual-source	Dual-energy
Lung	12.75	13.24	13.73	13.3
Stomach	12.52	12.13	13.16	11.68
Colon	0.04	0.04	0.06	0.035
Bone marrow	2.58	3.12	3.37	2.99
Breast	0	0	0	0
Remainder	5.04	4.98	5.48	4.81
Gonads	0.09	0.07	0.09	0.07
Thyroid	10.35	11.62	21	5.29
Esophagus	13.4	13.44	15.1	13.85
Bladder	0.19	0.13	0.21	0.15
Liver	8.86	8.73	9.78	7.88
Bone surface	2.6	3.1	3.37	2.99
Skin	3	2.8	2.9	2.78
Brain	0.26	0.32	0.49	0.34
Salivary glands	0.27	0.33	0.5	0.35
Effective dose	5.3324	5.444	6.217	5.094

Table-3.3: This table shows the organ doses calculated from the TLD measurements according to International Commission on Radiological Protection (ICRP) publication 103.

	120 kV, 110 mAs, Single-source	100 kV, 180 mAs, Single-source	120 kV, 130 mAs, Dual-source	100/Sn140 kV, 89/76 mAs, Dual-energy
E103 (mSv)	5.33	5.44	6.22	5.09
E60 (mSv)	5.29	5.42	6.28	5.02
CTDIvol (mGy)	7.37	7.32	7.12	7.33
DLP (mGycm)	361	358	374	342
EDLP = k (0.014) x DLP (mSv)	5.05	5.02	5.24	4.79
k = E103/DLP (mSv/mGycm)	0.0179	0.0184	0.02	0.018
k = E60/DLP (mSv/mGycm)	0.0178	0.018	0.02	0.0178
E103-E60 (mSv)	0.04	0.02	-0.06	0.07
(E103-E60)/E60 (%)	0.7	0.4	1	1.4
EDLP-E103 (mSv)	-0.28	-0.43	-0.98	-0.3
(EDLP-E103)/E103 (%)	5.2	7.9	15.8	5.9
EDLP-E60 (mSv)	-0.24	-0.4	-1.04	-0.23
(EDLP-E60)/E60 (%)	4.5	7.4	16.56	4.6
EDLP/CTDIvol (mSv/mGy)	0.6852	0.6858	0.7359	0.6535
E60/CTDIvol (mSv/mGy)	0.7178	0.7404	0.882	0.6848
E103/CTDIvol (mSv/mGy)	0.7232	0.7432	0.8735	0.6944
Coefficient of variation E60/CTDIvol (%)		10		
Coefficient of variation E103/CTDIvol (%)		9		

Table- 3.4: TLD- and DLP-based effective patient dose (E) estimates energy dependency and comparisons for International Commission on Radiological Protection (ICRP) Publications 60 and 103.

Figure- 3.1: Photograph of the utilized Alderson Rando anthropomorphic phantom.

A) B)

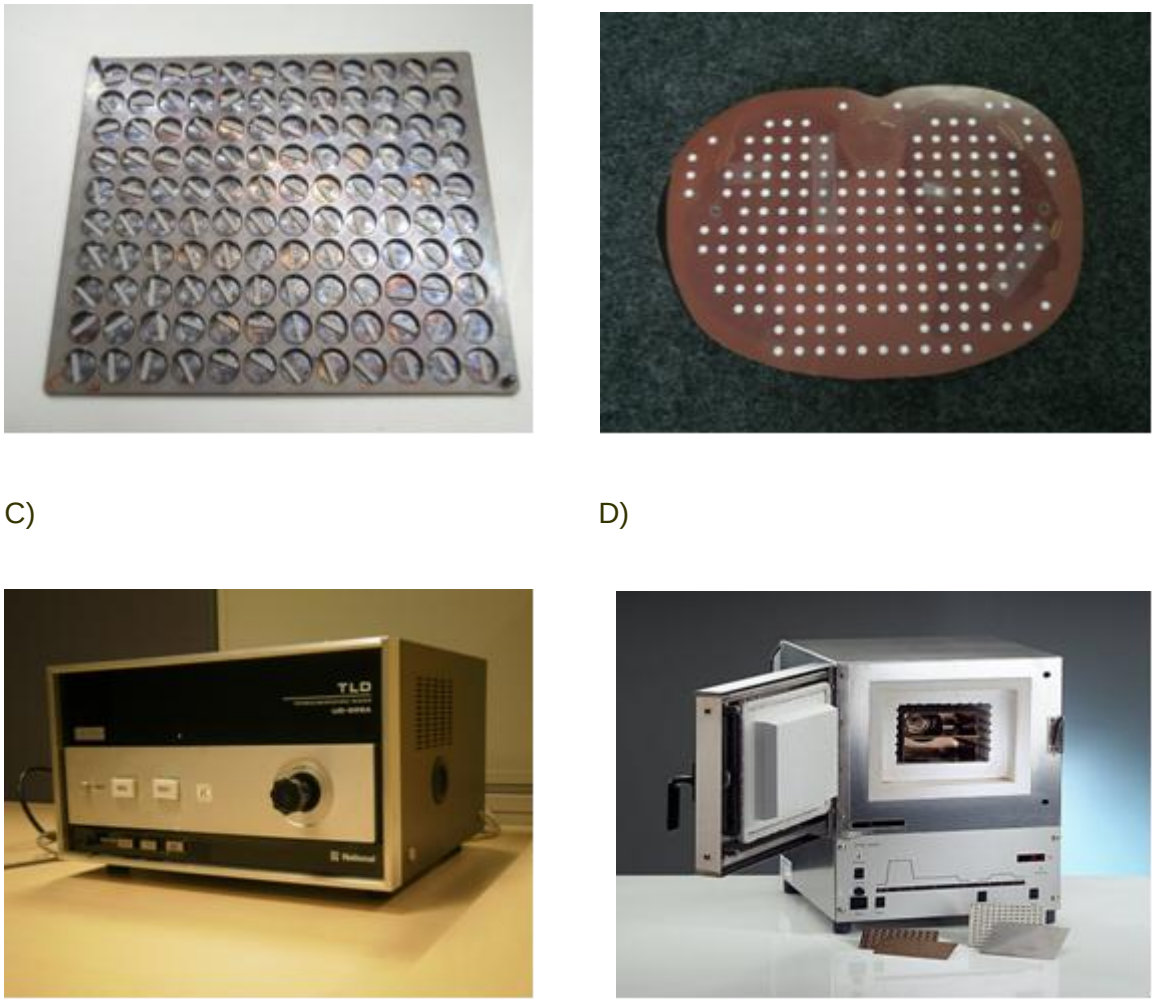

C) D)

Figure- 3.2: Photographs of A) thermo luminescent dosimeters, B) axial section of Rando phantom, C) TLD reader, and D) heating oven

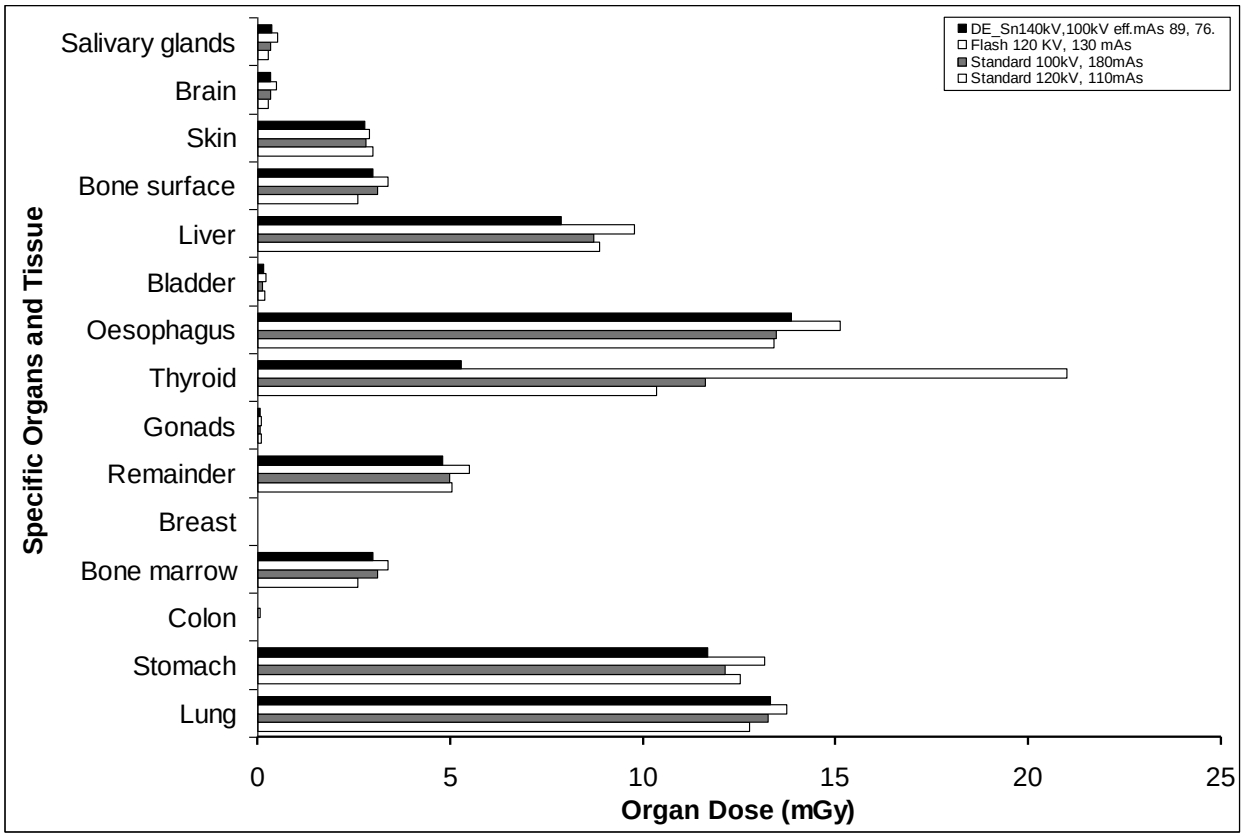

Figure- 3.3: The bar graph shows effective doses (mSv) of specific organs for the four different examination protocols.

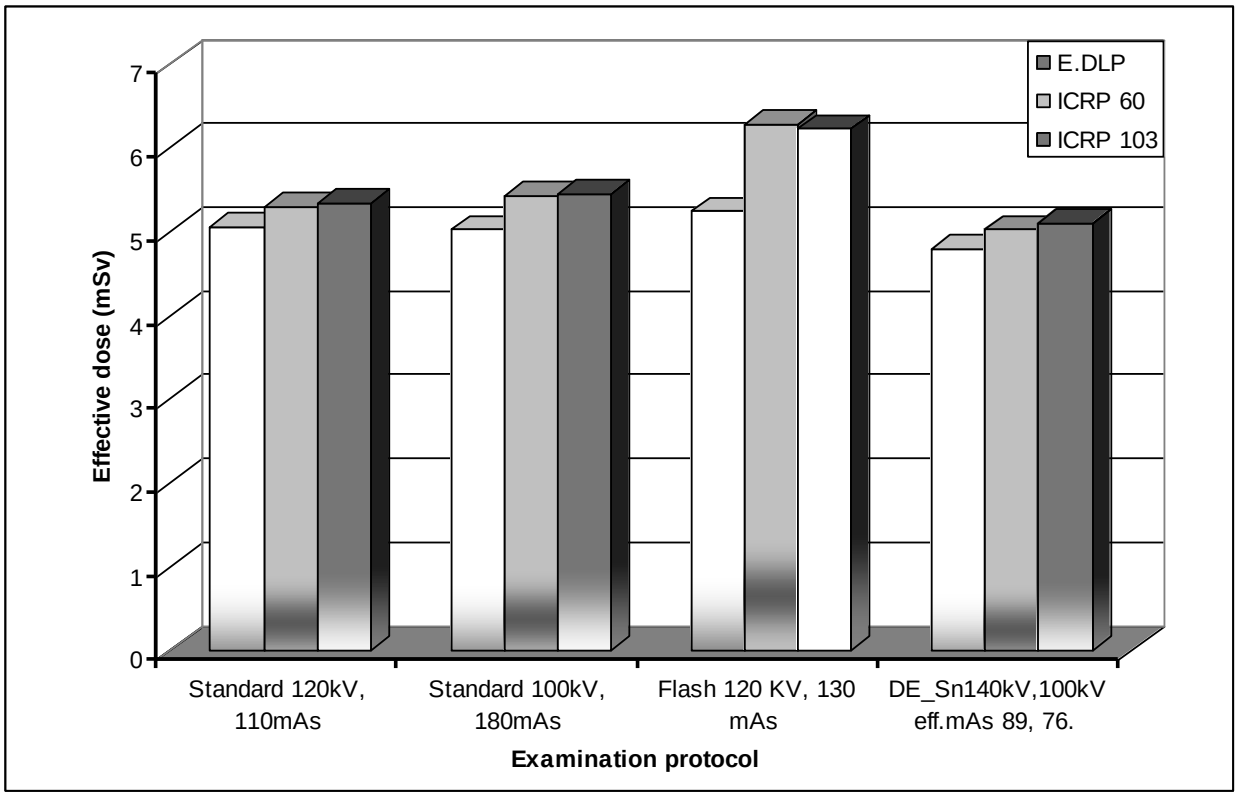

Figure- 3.4: The bar graph shows the comparison of effective patient dose (E) for the four different chest CT protocols investigated according to recommendations of International Commission on Radiological protection (ICRP) publications 103, 60 or as calculated using (DLP) and k coefficient (0.014 mSv/mGycm).

3.2.5 DISCUSSION

Results of one study [18] estimated that CT accounted for only 10% of diagnostic examinations in US hospitals in 2000, but accounted for nearly 70% of the corresponding medical dose. The International Commission on Radiological Protection (ICRP) publications provides the methods of assessing radiation dose from computed tomography. The results of this study reinforce the fact again; the effective dose is a derived parameter. Depending on which set of tissue-weighting factors are used, E values may vary substantially. Effective dose is a parameter that can estimate the relative biologic risk [11] and is not a physical parameter that can be measured. The effective dose can be determined by a variety of methods; here in the study we used TLD and DLP methods for clinical CT examination protocols of the adult chest. Latest computed E/DLP (k) coefficients [12] are used to convert values of DLP in to effective dose, the measure of patient dose currently being provided on clinical CT scanners, into a corresponding effective dose of the patient.

According to Roberts et al., the effect of the change in ICRP tissue weighting factors for examinations of the head is significant, as the dose with the 2007 factors is roughly double that as with the 1991 factors [19]. Nevertheless, our study shows that the percent difference of E is approximately equal to or less than 2% when looking at chest CT between ICRP 103 and 60 with lower values for ICRP 60. Adopting E_{DLP} instead of E60 would further increase the underestimation compared with E103 for all four protocols used. This finding is not surprising because this universal “k-value” is based on the data averaged over many scanners and models and is therefore not specific to the CT scanner investigated in this study [11].

However, the purpose of generating scanner specific k values plays an important role to validate or analyze the standard k value used for finding E from DLP. If the k values are validated, these specific coefficients can be used to compute E from DLP for this specific CT scanner. In the present study, we showed that estimating effective dose from DLP and k coefficient [11] works well for second-generation DSCT chest examinations including high-pitch and dual energy mode, and we calculated scanner specific k values from DLP and TLD measurements.

The k value used in this study is independent of energy (tube potential), because each of the energy independent parameters were used to compute E_{DLP} (CTDIvol, DLP, and the DLP to E conversion coefficient k). However, E60 and E103 values were strictly based on energy-dependent organ dose calculations (tissue weighting factors). The energy dependency that can calculate from the values obtained for E_{DLP}, E60 and E103 at each tube potential normalized to CTDIvol. The coefficient of variation was calculated from the normalized values of effective dose by using a formula (standard deviation of the normalized effective dose values of each tube potential/mean of normalized values of each tube potential) (*Table 4*). For the four investigated chest scan protocols, our study shows that the tube potential has a minimal effect on estimates of effective dose when CTDIvol is given.

It can be noted that the lowest effective dose was observed for the investigated dual-source dual-energy protocol with 100/Sn140 kV, even lower than with the standard 120 kV protocol which represents the manufacturer's recommendation. This finding was constantly present, independently of the methods how E was calculated (E60, E103, or E_{DLP}).

This is a finding of particular clinical importance since there have been major concerns about a possible increased patient dose because of the simultaneous irradiation of the same scan volume with the dual-source concept.

Another important finding is the comparatively higher effective dose of the dual-source high-pitch protocol compared to other single- or dual-energy protocols. This finding is a little bit surprising, because the high-pitch scan mode (high table feed and tube rotation speed) should not be increasing effective dose per se. It may be hypothesized that in the high-pitch mode there is still an over-beaming effect of pre- and post-scan volume despite the use of the dynamic collimation system referred to as adaptive dose shield. This theory may be supported when we look at single organ dose values: organs located in the upper abdomen and the thyroid gland show substantially higher organ dose values in the high-pitch mode compared to the three other scan modes. As a clinical consequence of that, it can be suggest that the investigated dual-source high-pitch chest protocol should be preferably used, if there is a substantial benefit of the extremely short examination time. This may be justified as for example in emergency cases, restless patients or pediatric examinations when sedation or anesthesia with their inherent risk profiles can be avoided.

A limitation of this work is that we used only a single male adult-sized anthropomorphic phantom for this study. For dose assessment in pediatric patients a further study is required with referring phantoms. Another point to mention is the continuously increasing number of over-weighted and obese patients. These patients will show absorption characteristics different from the Alderson Rando phantom due to their altered geometry and chemical composition, thus being likely to result in different organ dose distributions.

3.2.6 CONCLUSION

In conclusion, the use of organ-based dose estimates in place of DLP-based estimates with a fixed k coefficient of 0.014 mSv/mGycm will result in an increased effective patient dose for chest CT examinations for the evaluated dual-source CT scanner and protocols by 4.5-16.56% when using ICRP 60 and by 5.2-15.8% when using ICRP 103 tissue weighting factors. These results are essentially independent of tube potential, suggesting that estimates of effective dose based on DLP work equally well for single-energy and dual-energy CT examinations. Only for the dual-source high-pitch mode, a substantial difference observed and a conversion coefficient of 0.0166 mSv/mGycm should used for DLP-based calculation of E. Further, effective dose estimations by ICRP 103 and 60 for both single-energy and dual-energy examinations did not differ by more than 0.04 mSv.

3.2.7 REFERENCE

1. Ravenel JG, Scalzetti EM et.al. Radiation Exposure and Image Quality in Chest CT Examinations, AJR 2001;177:279–284.

2. Jacobi W. The concept of effective dose: a proposal for the combination of organ doses. Radiat. Environ Biophys 1975; 12:101–109

3. International Commission on Radiological Protection. Recommendations of the International Commission on Radiological Protection. Oxford, UK: Pergamon Press, 1977:ICRP publication no. 26

4. McCollough CH, Schueler BA. Calculation of effective dose. Med Phys 2000; 27:828–837

5. Martin CJ. Effective dose: how should it be applied to medical exposures? Br J Radiol 2007; 80:639–647

6. American Association of Physicists in Medicine (AAPM). The measurement, reporting and management of radiation dose in CT: report of AAPM Task Group 23 of the Diagnostic Imaging Council CT Committee. College Park, MD: AAPM, 2007: report no. 96

7. International Commission on Radiological Protection. 1990 recommendations of the International Commission on Radiological Protection. Ann ICRP 1991; 21: publication no. 60

8. International Commission on Radiological Protection. 2007 recommendations of the International Commission on Radiological Protection. Ann ICRP 2007; 37: publication no. 103

9. Jessen KA, Shrimpton PC, Geleijns J, Panzer W, Tosi G. Dosimetry for optimisation of patient protection in computed tomography. Appl Radiat Isot 1999; 50:165–172

10. Jessen KA, Panzer W, Shrimpton PC, et al. European Guidelines on quality criteria for computed tomography. Brussels, Belgium: European Commission, 2000:EUR 16262

11. Bongartz G, Golding SJ, Jurik AG, et. al., European Guidelines on Quality Criteria for Computed Tomography. EUR 16262. The European Commission's Study Group on Development of Quality Criteria for Computed Tomography. Luxembourg, Luxembourg: European Commission, 2000.

12. Bongartz G, Golding SJ, Jurik AG, et al. 2004 CT quality criteria. Luxembourg, Luxembourg: European Commission, March 2004.

13. McCollough CH. Patient dose in cardiac computed tomography. Herz 2003; 28:1–6

14. Crawford CR, King KF. Computed tomography scanning with simultaneous patient translation. Med Phys 1990; 17:967–982

15. Nicholson R, Fetherston S. Primary radiation outside the imaged volume of a multislice helical CT scan. Br J Radiol 2002; 75:518–522

16. Christner JA, Kofler JM, McCollough. Estimating Effective dose for CT using Dose-Length Product compared with using organ doses consequences of adopting international commission on Radiological Protection 103 or dual energy scanning. AJR2010; 194:881-889.

17. McDermotta A. Pediatric organ dose measurements in axial and helical multislice CT. Med Phys 2009 May; 36(5): 1494–1499.

18. Mettler FA, Wiest PW, Locken JA, Kelsey CA. CT scanning: patterns of use and dose. J Radiol Prot 2000; 20:353–359.

19. Roberts JA, Drage NA, Davies F et al., Effective dose from cone beam CT examinations in dentistry, British Journal of Radiology 2009; 82: 35-40.

Chapter 4

Effect of Contrast Medium on Image Noise and Radiation Dose in Adult Chest Computed Tomography Using Automatic Exposure Control: A Comparative Study between 16-, 64- and 128-slice CT

4.1 ABSTRACT

Objective: The purpose of this study was to determine the difference in radiation dose between a non-enhanced and contrast-enhanced chest CT examination contributed by contrast material with different scanner generations with automatic exposure control (AEC).

Materials and Methods: 126 adult patients that received a non-contrast-enhanced (NCCT) and a contrast-enhanced CT (CECT) scan of the chest in one session were enrolled in this study. Each 42 patients were examined on a 16- (Sensation 16, Siemens), 64- (Definition, Siemens) and 128-slice (Definition Flash, Siemens) CT scanner with the same examination protocol: 120 kV, 110 mAs, pitch of 1.2, inspiratory breathe hold. However, the AEC technology (Care Dose 4D, Siemens) underwent technical changes in each of the three scanner generations. Dose length product (DLP) and CT dose index volume (CTDIvol) were recorded. Image noise was measured in the ascending aorta using a region of interest tool.

Results: Image noise was significantly lower in the most recent scanner generation for both NECT and CECT. Dose parameters were significantly lower in the 128- and 64-slice group compared to the 16-slice group: for CECT, DLP was increased by 34.1% in the 16-slice group, by 8.1% in the 64-slice group. For all groups, there was a significant increase in dose and image noise between NECT and CECT.

Conclusion: This study demonstrates that with AEC patient dose will be significantly different between NECT and CECT chest examinations for three generations of CT machines. However, technological developments lead to a significant reduction of dose and image noise with the latest CT generation.

4.2.1 INTRODUCTION

Although computed tomography accounts for only the minority of radiological procedures, it accounts for more than two thirds the radiation exposure of the population in Western societies [1, 2]. Radiation dose in CT is mainly influenced by protocol design and the type of CT scanner. With multi-detector CT (MDCT) the basic determinants are x-ray energy (i.e. tube voltage), tube current-time-product (mAs), maximum tube output capacity, tube rotation time and pitch [3]. The effect of mAs on radiation dose is well known to show a linear correlation. Further, x-ray absorption will increase with the diameter of an object, which will lead to an increase of image noise. This represents a major issue in clinical routine as patients´ body habitus significantly varies. If tube current-time-product settings are kept constant independent of patient size, image quality will deteriorate in big patients. On the other hand side, slim patients will receive an unnecessarily high dose exposure. To avoid these problems, all CT manufacturers have meanwhile introduced online tube current output modulation systems, also known as automatic exposure control (AEC) [4, 5, 6], that are capable of modulating the tube current output in x-, y- and z-direction to maintain a certain predefined image noise level [7]. However, besides object diameter also the effective atomic number and physical density of a material will influence x-ray absorption. In contrast-enhanced CT examinations, this is mainly iodinated contrast material. Thus, to maintain constant image quality, AEC systems will have to increase tube output compared to a non-contrast-enhanced scan.

The focus of our research was to determine the effect of iodinate contrast material on dose exposure in chest CT examinations using AEC when all other examination parameters are kept constant. We retrospectively looked at data from three different CT generations (16-, 64- and 128-slice devices) from the same manufacturer (Siemens Healthcare) on which AEC had undergone upgrades from generation to generation. While several studies looked at image quality and dose reduction using these AEC systems, to the best of our knowledge there is no information available on the effect of the presence of iodinated contrast material on radiation dose.

4.2.2 MATERIALS & METHODS

Patients and Image Acquisition

Data from totally 126 adult patients (> 18 years in age) who underwent a dual-phase CT examination of the chest for clinical purpose were retrospectively analyzed. Patients first underwent a non-contrast-enhanced scan followed by a contrast-enhanced scan within the same examination. Each 42 patients were examined on a 16-slice (Sensation 16), 64-slice (Definition) and 128-slice (Definition Flash, all from Siemens Healthcare) CT device. Contrast enhancement was achieved by injecting 60 ml of iodinated contrast material (400 mgI/ml; Imeron 400, Bracco Imaging) followed by a 30 ml NaCl bolus in a peripheral arm vein at a flow rate of 3 ml/s using an automated double-syringe power injector (Injektron CT2, Medtron). Scan delay was set to 50 s after start of injection. Besides that, all CT examination parameters were kept constant between non-enhanced and contrast-enhanced scan and also for all three types of CT devices: tube potential 120 kV, quality reference tube current-time-product 110 mAs, rotation time 0.5 s, pitch 1.2, inspiratory breathe hold, cranio-caudal scan direction. Collimation was 16 x 1.5 mm for the 16-slice, 64 x 0.6 mm for the 64-slice and 128 x 0.6 mm for the 128-slice machine. Scan range was the same for non-enhanced and contrast-enhanced scans. Images were reconstructed at a slice thickness of 5 mm with an increment of 5 mm using a medium-soft convolution kernel (B30f) and a soft tissue window (width: 450 HU, center: 50 HU). Automatic exposure control (AEC) was used for all scans. The automatic dose modulation software provided by the manufacturer (Care Dose 4D, Siemens Healthcare),

adjusts tube current output in x-, y- and z-direction in a real-time manner to maintain image noise at a predefined level as described earlier [8, 9]. Tube current values are calculated and adapted to the patient size and attenuation changes based on his attenuation profile. This information is obtained from the topogram, where the patient's attenuation profile in z-axis direction in the plane of projection (normally anterior-posterior) is measured. Tube output demand in the perpendicular direction (angular modulation in x-y projection) is adjusted online using real-time x-ray-flux measurements on the detector side [10]. The user can choose from three different pre-sets with weak, average or strong tube current modulation. In our routine use and for this study, we use the average mode as default. However, these AEC algorithms have undergone upgrades between each of the three scanner generations.

Dose Estimates and Image Noise Assessment

CT dose index volume (CTDIvol) and dose length product (DLP) as measure of patient dose were recorded from the patient protocol which is automatically generated by the scanner software after the end of an examination and stored in our PACS system. CTDIvol and, as a function of that, DLP were considered to be appropriate as protocol-specific factors such as pitch and collimation are already included in these determinants and, thus, they are suitable to compare examination protocols between different scanners. Image noise was measured centrally in the scan volume in the ascending aorta by utilizing a circle region of interest tool (ROI) on a standard PACS workstation (Centricity 4.2, General Electric Healthcare).

The ROI was drawn as large as possible, but inclusion of extra-vascular structures, vessel wall calcifications or thrombus, artifacts, and partial volume effects was carefully avoided. Image noise was defined as the standard deviation (SD) from the mean CT density expressed in Hounsfield Units (HU) within the ROI. Measurements were performed in axial slices. Largest thorax diameters as measure of body habitus in anterior-posterior as well as in lateral direction were measured on axial slices.

Statistical Analysis

Statistical analysis was performed computer-based using dedicated software (BIAS, Epsilon-Verlag, Frankfurt, Germany). A p-value of ≤ 0.05 considered to indicate statistically significant differences for all used tests. As data was not distributed normally, the Wilcoxon-Mann-Whitney-U test was utilized to compare continuous variables. Numerical variables were compared using Fisher´s exact test.

4.2.3 RESULTS

All patients underwent both CT scan successfully without any complications. All examinations were diagnostic. There were no significant differences between the three patient groups regarding age, gender distribution, thorax diameter or attenuation of the ascending aorta (see *Table 4.1*).

Image Noise

Image noise was significantly lower with the latest generation of CT (NECT: 9.9±1.0 HU, CECT: 10.4±1.1 HU) compared to the 64-slice (NECT: 11.0±1.6 HU, CECT: 12.1±1.6 HU) and the 16-slice device (NECT: 11.3±0.9 HU, CECT: 12.7±1.0 HU). The differences between the 64-slice and 16-slice group did not reach statistical significance. Data is summarized in *Table 4.2*. When comparing NECT and CECT between each group, image noise was significantly lower in the non-enhanced scan in all three groups ($p < 0.0001$ for all groups).

Dose Parameters

CTDIvol and DLP for the NECT scan were significantly lower in the 128-slice compared to the 64-slice and the 16-slice group, further lower in the 64-slice group compared to the 16-slice group. Dose parameters for the CECT scan were significantly lower in the 128-slice group compared to the 16-slice group, however, no such differences were observed compared to the 64-slice group. Data is summarized in *Table 4.2*. For NECT, the DLP in the 16-slice group was higher by 42.7%, in the 64-slice group by 12.9% compared to the 128-slice group.

When looking at CECT, the DLP in the 16-slice group was higher by 34.1%, in the 64-slice group by 8.1% compared to the 128-slice group (*figure 4.1*).

The percentage increase of the DLP between NECT and CECT was 1.2%, 3.1% and 7.7% for the 16-slice, 64-slice and 128-slice group, respectively. Although impressively larger with the more recent scanner generations, these differences in radiation dose received by patient without and with contrast material were statistically significant for all three types of scanners ($p < 0.0001$ for all groups) (*table 4.3*).

4.2.4 TABLES AND FIGURES

Patient characteristics:

Variable	Group 1 16-slice	Group 2 64-slice	Group 3 128-slice	p-value
Age (years)	46.3±17.3	49.4±18.6	49.4±18.1	1 vs 2: 0.42 1 vs 3: 0.43 2 vs 3: 0.92
Gender (male:female ratio)	30:12	21:21	26:16	1 vs 2: 0.07 1 vs 3: 0.49 2 vs 3: 0.38
Thorax diameter NECT (mm)	333±74	336±57	330±74	1 vs 2: 0.72 1 vs 3: 0.62 2 vs 3: 0.83
Thorax diameter CECT (mm)	347±31	343±31	344±32	1 vs 2: 0.58 1 vs 3: 0.61 2 vs 3: 0.98
Attenuation AA NECT (HU)	37±7	39±4	38±6	1 vs 2: 0.61 1 vs 3: 0.87 2 vs 3: 0.32
Attenuation AA CECT (HU)	141±19	146±27	148±23	1 vs 2: 0.15 1 vs 3: 0.26 2 vs 3: 0.68

Table- 4.1: No significant differences observed regarding patient age, gender distribution, thorax diameter and attenuation in the ascending aorta (AA) for the non-enhanced (NECT) and contrast-enhanced (CECT) scan.

Variable	Group 1 16-slice	Group 2 64-slice	Group 3 128-slice	p-value
Image noise NECT (HU)	11.3±0.9	11.0±1.6	9.9±1.0	1 vs 2: 0.47 1 vs 3: <0.0001 2 vs 3: 0.0004
Image noise CECT (HU)	12.7±1.0	12.1±1.6	10.4±1.1	1 vs 2: 0.06 1 vs 3: <0.0001 2 vs 3: <0.0001
CTDIvol NECT (mGy)	10.7±1.1	8.5±1.9	7.4±2.0	1 vs 2: <0.0001 1 vs 3: <0.0001 2 vs 3: 0.008
CTDIvol CECT (mGy)	10.9±1.1	8.8±2.0	8.1±1.9	1 vs 2: <0.0001 1 vs 3: <0.0001 2 vs 3: 0.08
DLP NECT (mGycm)	408±42	323±73	286±72	1 vs 2: <0.0001 1 vs 3: <0.0001 2 vs 3: 0.01
DLP CECT (mGycm)	413±43	333±75	308±74	1 vs 2: <0.0001 1 vs 3: <0.0001 2 vs 3: 0.08

Table- 4.2: Comparison of noise and dose parameters between the groups

Intra-group comparison of noise and dose parameters

Variable	Background noise NECT vs CECT	CTDIvol NECT vs CECT	DLP NECT vs CECT
Group 1 16-slice	$p < 0.0001$	$p < 0.0001$	$p < 0.0001$
Group 2 64-slice	$p < 0.0001$	$p < 0.0001$	$p < 0.0001$
Group 3 128-slice	$p = 0.0002$	$p < 0.0001$	$p < 0.0001$

Table- 4.3: In all three groups with different generations of automatic tube current output modulation, image noise, CTDIvol and DLP were significantly lower for the non-enhanced (NECT) compared to the contrast-enhanced (CECT) scan.

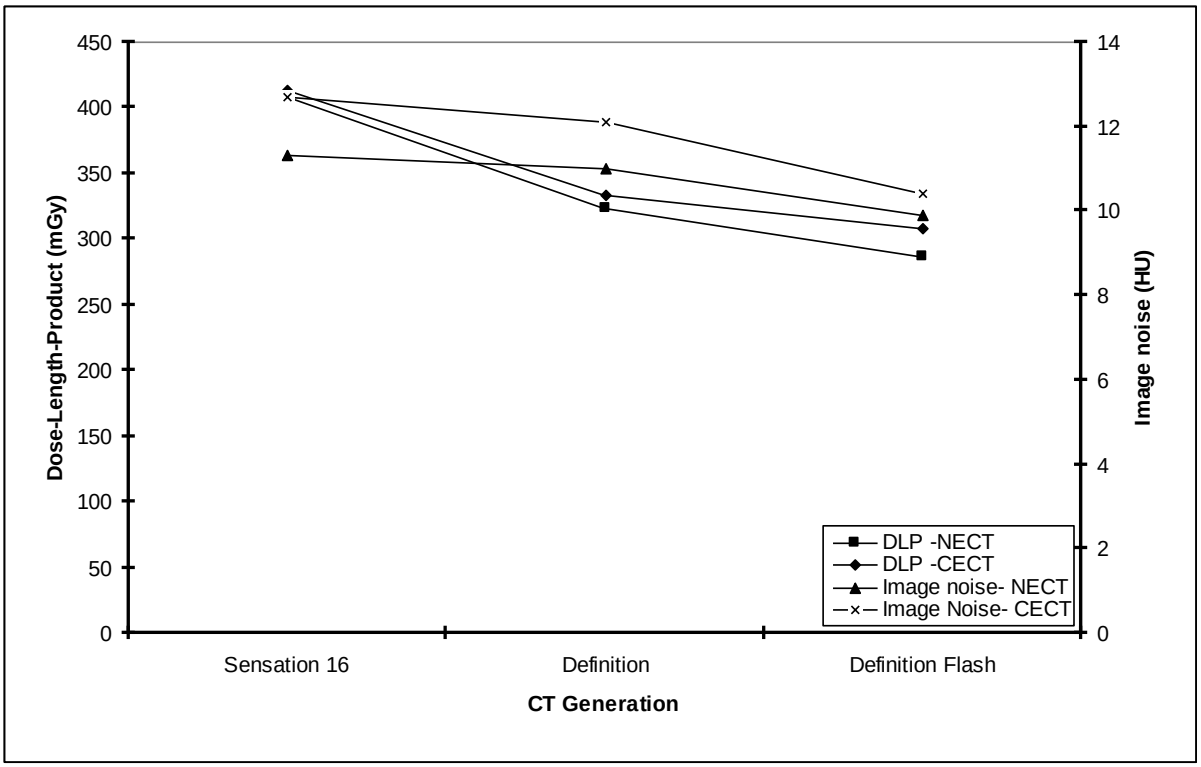

Figure- 4.1: shows the comparison of DLPs obtained (CECT and NECT) and Image noise values for different generation CT Units.

4.2.5 DISCUSSION

Radiation exposure of the population in Western societies and the disproportionate contribution of computed tomography has come more and more to awareness through the last decade, not only in radiology but in medicine in general. Hence, algorithms to modulate tube current output according to the anatomical region were introduced with the first MDCT scanners and were developed further from scanner generation to generation. Meanwhile these automatic exposure control systems are available with every manufacturer, and there is fundamental evidence that these systems effectively reduce patient dose and/or maintain image quality at a stable level compared to fixed tube current settings.

However, to the best of our knowledge there is no data available on the extra-radiation dose delivered to patients in contrast-enhanced in comparison to non-contrast-enhanced examinations with the use of AEC. Thus, the purpose of our study was to determine whether patients receive significantly different radiation doses for contrast medium examinations or not and how image quality varies. As a result, we found consistently and significantly higher values for CTDIvol and DLP for the CECT compared to the NECT examinations for all three CT generations. The reason behind this difference is, the contrast media is a high atomic number material (Iodine Z= 53, K shell BE= 33.2-KeV), the presence of contrast material in the patients absorbs much more (significantly) radiation compared to NCCT. The human anatomy changes with z-position for a given patient and the size of a patient differs strongly for various patients. Therefore, to achieve a constant image quality level the exposure has to be adapted for all z-positions and patient sizes.

The latest AEC method is very strong to maintain image quality (reduce image noise) and reduce radiation dose [11, 12]. To make the image quality (noise) stable for NCCT and CECT images, the Automatic Exposure Control in CT system act on mAs control [13] and it reduce effective mAs for NCCT than CECT. The automatic adaptation of the exposure is readily available in state-of-the-art CT scanners. Angular tube current modulation reduces the dose without affecting the image noise level, z-modulation or automatic exposure control increases/decreases the dose in order to keep a (almost) constant image noise level.

We compared the image quality parameters (noise and HU) of different generation CT units and our result shows a decrease of image noise and improves image quality according to CT generation. This effect was more pronounced in the recent scanner generation. When we look at image noise, values were also consistently and significantly higher in the CECT examinations. However absolute changes were in the dimension of 1-2 HU, which is very unlikely to be detected by a radiologist's eye, thus indicating that the aim of maintaining stable image quality between NECT and CECT examinations is fulfilled very well in the presence of iodinated contrast material by the AEC software. Although not primary goal of this study, we found a general and substantial reduction of dose parameters with more recent scanner generations. Compared to the latest 128-slice generation, DLP was 34.1-42.7% higher in the 16-slice group and 8.1-12.9% higher in the 64-slice group with the same scan parameter settings. There are many possible explanations for this finding. First, advances and further improvements in the AEC software itself may be an important contributor.

Second, scanner hardware also underwent major upgrades and technical developments on the detector material side as well as on the electronic components side. As a major contribution to dose reduction procedures, a so called “adaptive dose shield” (ADS) was introduced with the latest 128-slice CT device. According to the manufacturer’s information ADS is a dynamic collimator on the x-ray tube side blocking x-ray quanta at the beginning and end of the spiral acquisition that would not contribute to the calculation of the actual image but are known as a phenomenon called “over-radiation”. With wider detectors, this problem gained importance in MDCT as larger and larger volumes would be unnecessarily exposed for half a rotation to radiation. Inherent differences in the scanners themselves, including design, manufacture, and proprietary method of automated tube current modulation are contribute to the range of doses for CT [14].

As a limitation of this study, it needs to be mentioned, that we compared different CT generations from a single manufacturer only. A comparison of different CT generation from different vendors may be of interest, especially with regards to the over-radiation-phenomenon.

4.2.6 CONCLUSION

In conclusion, this study demonstrated that dose parameters and image noise are significantly lower in NECT than CECT in all investigated CT scanners with AEC. Again, with AEC patient dose will be significantly different between NECT and CECT chest examinations for three generations of CT machines. However, technological developments lead to a significant reduction of dose and image noise with the latest CT generation.

4.2.7 REFERENCE

1. Mukundan S Jr, Wang PI, Frush DP, et al. MOSFET dosimetry for radiation dose assessment of bismuth shielding of the eye in children. *AJR* 2007; 188: 1648–1650

2. Task Group on Control of Radiation Dose in Computed Tomography. Managing patient dose in computed tomography: a report of the International Commission on Radiological Protection. *Ann ICRP* 2000; 30:7–45

3. McNitt-Gray MF. AAPM/RSNA Physics tutorial for residents: topics in CT—radiation dose in CT. RadioGraphics 2002; 22:1541-1553.

4. Shuai Leng, Lifeng Yu, Cynthia H. McCollough et.al., Radiation Dose Reduction at CT Enterography: How Low Can We Go While Preserving Diagnostic Accuracy?, AJR 2010; 195:76-77.

5. Kibaek Lee, Wonho Lee, Junhyup Lee, et.al., Dose reduction and image quality assessment in MDCT using AEC (D-DOM & Z-DOM) and in-plane bismuth shielding, Radiat Prot Dosimetry (2010) doi: 10.1093/rpd/ncq159.

6. Chang Hyun Lee, Jin Mo Goo, Hyun Ju Ye, et.al., Radiation Dose Modulation Techniques in the Multidetector CT Era: From Basics to Practice, RadioGraphics, 28, 1451-1459.

7. Boone JM, Geraghty EM, Seibert JA, J. Anthony Seibert, et al. Dose reduction in pediatric CT: a rational approach. Radiology 2003; 228:352-360.

8. Graser A, Wintersperger BJ, C. Suess et.al., Dose reduction and image quality in MDCT colonography using tube current modulation. AJR Am J Roentgenol. 2006 Sep;187(3):695-701.

9. Brian C. Allen, Mark E. Baker, David M. Einstein, et.al., Effect of Altering Automatic Exposure Control Settings and Quality Reference mAs on Radiation Dose, Image Quality, and Diagnostic Efficacy in MDCT Enterography of Active Inflammatory Crohn's Disease. *AJR* 2010; 195:89-100.

10. Rizzo S, Kalra M, Schmidt B et al. Comparison of Angular and Combined Automatic Tube Current Modulation Techniques with Constant Tube Current CT of the Abdomen and Pelvis, *AJR* 2006; 186:673-679.

11. Marcus Söderberg, Mikael Gunnarsson. Automatic exposure control in computed tomography – an evaluation of systems from different manufacturers. DOI 10.3109/02841851003698206 © 2010. Informa UK Ltd. (Informa Healthcare, Taylor & Francis AS)

12. Erin Angel, Nazanin Yaghmai, Cecilia Matilda Jude, et.al., Dose to Radiosensitive Organs During Routine Chest CT: Effects of Tube Current Modulation. *AJR Am J Roentgenol*. 2009 November ; 193(5): 1340–1345. doi:10.2214/AJR.09.2886.

13. Kalender WA, Wolf H, Suess C. Dose reduction in CT by anatomically adapted tube current modulation. II. Phantom measurements. Med Phys. 1999. Nov;26(11): 2248-53.

14. Koller CJ, Eatough JP, Bettridge A. Variations in radiation dose between the same model of multislice CT scanner at different hospitals. Br J Radiol 2003; 76:798–802.

Chapter- 5

Relationships of Clinical Protocols and Reconstruction Kernels with Image Quality and Radiation Dose in a 128-slice CT Scanner: Study with an Anthropomorphic and Water Phantom

5.1 ABSTRACT

***Purpose*:** The aim of this study was to explore the relationship of scanning parameters (clinical protocols), reconstruction kernels and slice thickness with image quality and radiation dose in a DSCT.

Materials and methods: The chest of an anthropomorphic phantom was scanned on a DSCT scanner (Siemens Somatom Definition flash) using different clinical protocols, including single- and dual-energy modes. Four scan protocols were investigated: 1) single-source 120 kV, 110mAs 2) single-source 100 kV, 180mAs 3) high-pitch 120 kV, 130mAs 4) dual-energy with 100/Sn140 kV, eff.mAs 89, 76. The Automatic Exposure Control was switched off for all the scans and the CTDIvol selected was in between 7.12 and 7.37 mGy. The raw data reconstructed using the reconstruction kernels B31f, B80f and B70f, and slice thicknesses were 1.0 mm and 5.0 mm. Finally, the same parameters and procedures were used for the scanning of water phantom. Friedman test and Wilcoxon-Matched-Pair test were used for statistical analysis.

***Results*:** The DLP based on the given CTDIvol values showed significantly lower exposure for protocol 4, when compared to protocol 1 (percent difference 5.18%), protocol 2 (percent diff. 4.51%), and protocol 3 (percent diff. 8.81%). The highest change in Hounsfield Units was observed with dual-energy Sn140-kV (Hounsfield unit 15.18) compared to protocol 2 (24.35 HU). The differences in noise between the different clinical protocol data sets were statistically significant [protocol 3 vs. dual-energy 100-kV ($p<0.01$) and protocol 3 vs. dual-energy Sn140-kV ($p<0.01$)].

The dual-energy Sn140-kV protocol shows the highest image noise (14.5 HU for 5.0 mm slice (B31f) and 162 HU for 1.0 mm slice (B70f) thickness).

The difference between reconstruction kernel B31f and B80f images made using 5.0mm reconstruction thickness was statistically significant ($p<0.0312$) and 1.0mm slice thickness shows the significance of $p<0.0312$ between B31f and B70f reconstructions. In both cases, the lowest image noise was obtained from B31f reconstructed images. Again the slice thickness is significantly affects image noise ($p<0.03$) and the noise was higher at 1.0 mm compared to that at 5.0 mm slice thickness.

***Conclusion*:** The clinical protocol, reconstruction kernel, slice thickness and phantom diameter or the density of material it contains directly affects the image quality. Dual Energy protocol shows the lowest Dose-Length-Product compared to all other protocols examined, the fused image shows excellent image quality and the noise is same as that of single or high-pitch mode protocol images. Advanced CT technology improves image quality and considerably reduces radiation dose.

5.2.1 INTRODUCTION

The rapid advance in computed tomography continuously improves image quality and diagnosis accuracy. The robustness and speed of the modality entail a wide and growing spectrum of clinical indications. During the past years, multi-detector row CT (MDCT) has evolved in to clinical practice with a rapid increase in the number of detector slices. Today's 128 slice CT systems (DSCT) allow whole-body examinations with sub millimeter resolution in short scan times [1, 2]. The second-generation dual-source CT (128-slice CT) houses two tube-detector systems mounted at an angular off-set of 95° within the same gantry that simultaneously revolve around the patient's body. Each detector is capable of acquiring 128 x 0.6 mm slices with one rotation. The main characteristic feature of dual source CT is the flexibility it offers with respect to modes of operation and the possibility to combine the resulting acquisition data.

Images suitable for their intended diagnostic purpose are required, therefore low noise, high contrast resolution, sharpness of the image and the absence of artifacts would be the ideal cases. However, this is not an easy task, since patient dose and scan time have to be taken into consideration. In addition, reconstruction parameters – convolution kernels, reconstruction increments, effective slice width, *z*-interpolation algorithms, pitch– all affect the image quality and all vary depending on the manufacturer and the scanner model. In general, noise in CT depends on the number of x-ray photons reaching the detector (quantum noise), the electronic noise of the detecting system, and the reconstruction kernel (sharper kernels give noisier images).

Since x-ray photon statistics obey the Poisson distribution, the corresponding image noise is approximately proportional to $1/\sqrt{N}$, where *N* is the number of photons that have contributed to the raw image. Since the number of photons reaching the detector depends on the object attenuation, which in turn depends on photon energies, *N* is strongly dependent on tube potential. In addition, *N* is proportional to section width, tube current, and the amount of time necessary to acquire all the projection data needed for the reconstruction. In sequential mode, this time equals to the “x-ray on” time per rotation, so image noise is approximately proportional to $1/\sqrt{mAs}$ [3]. In spiral mode, however, the interpolation algorithm, which transforms the projection data acquired at various z-axis locations into projection data at one specific z-axis location, must be taken into account. Because the spiral interpolation algorithm is inherently different for multi– detector row CT compared to single detector row CT [4], the relationship between noise and pitch in spiral CT depends on the scanner type (single vs. multi– detector row CT). In addition, because cardiac spiral reconstructions are optimized to decrease motion artifact [5, 6] (ie, provide the best possible temporal resolution), the relationship between noise and pitch also depends on the multi– detector row CT reconstruction mode (cardiac vs. non-cardiac).

It is possible to use a variety of clinical protocols and reconstruction kernels for the imaging of patients with DSCT. There are some clinical patient studies published with single energy [7], high pitch protocols [8, 9], or dual energy [10, 11] with image quality. According to our knowledge, there is no study published yet comparing single-source, dual-source and high-pitch protocol with image quality for a given CTDIvol.

Dual-energy protocol has a number of decisive advantages, for example material differentiation, cardio pulmonary imaging etc, so it is important to determine the quality of the image and the radiation dose accumulating the patient for various protocols. By dual-energy examination, it is possible to generate fusion-weighted images (this is a part of information obtained from detectors A and B according to weighting) without any additional scanning. This may reduce radiation dose and this technique can be used for further clinical information. Because of these important functions, assessments of the quality of fused images are essential. Finally, with high-pitch mode, the patient scanning time can reduce considerably and this is essentially advantageous for restless patients. This is achieved by fast table feed and high tube rotation speed, in this case there is a probability of reduces image quality. Because of these reasons, we firmly believe that this study plays certainly an important role.

5.2.2 MATERIALS AND METHODS

CT scanner and scan protocols

The second-generation Dual source CT scanner from Siemens healthcare solution was used for this study (Somatom Definition flash). Definition flash is equipped with two 38.4 mm detectors that each acquires 128 slices of image data and provides a temporal resolution of 75-ms. Four scan protocols were investigated: 1) single-source 120-kV, 110mAs, 2) single-source 100-kV, 180mAs, 3) high-pitch 120-kV, 130mAs, and 4) dual energy with 100-kV, Sn140-kV, eff.mAs 89, 76. Selection of these protocols was based on the fact that the CTDIvol was 7.25 +/- 0.15 mGy. The total scan length was selected as “37 cm”; it started at 2cm above the first rib and went down to the lower end of L1 vertebra. The Automatic Exposure Control (AEC) was switched off for all the scans. The Field of view (FOV) was 400 mm for all protocols except for the high-pitch mode, for which 332 mm is the maximum achievable FOV. The raw data obtained from each scan were reconstructed with three different reconstruction kernels (B31f, B80f, and B70f), this includes 1.0 mm and 5.0 mm reconstructed slice thicknesses (*Table 5.1*). At first, before starting the presented study the Hounsfield unit was checked with water phantom and confirmed it at an appreciated level.

Alderson anthropomorphic Phantom

The anthropomorphic phantom used for this study was Rando-Alderson-anthropomorphic male Phantom (The Phantom Laboratory, Salem, NY, USA).

The phantom has 175 cm (5’9”) height, 73.5 kg weight, and male figure without arms or legs. The phantom was constructed with a natural human skeleton, which cast inside soft tissue-simulating material. Lungs were molded to fit the contours of the natural rib cage and the air space of the head, neck and stem bronchi duplicated. The phantom was sliced at 2.5 cm intervals. The phantom’s soft tissue was manufactured with a proprietary urethane formulation and the material has an effective atomic number and mass density, which simulates muscle tissue with randomly distributed fat. Lung material has the same effective atomic number as the soft tissue material with a density, which simulates lungs in a median respiratory state. The molded lungs are hand-shaped and fitted in rib cage and the skeletons are natural human skeletons.

Water Phantom

Standard water phantom, which is used for the quality assurance of Computed Tomography scanner was used for this study. The phantom is cylindrical in shape, completely closed and filled with water having the inner diameter of 18.5 cm and outer 20 cm. 18.5 cm is the water section and the rest 1.5 cm is the PMMA box.

Image Quality measurements

Images were reconstructed from every acquisition using three different reconstruction kernels including 5.0 mm and 1.0 mm of slice thickness. The first image quality parameter assessed was the consistency of Hounsfield Unit (HU).

We selected four regions of interest (ROI) in a homogenous area of heart for the measurement of HU and the mean standard deviations of pixels in the same region of interest (ROI) were taken as image noise. The mean HU and standard deviation (noise) were calculated from four Regions of Interest (ROI) in a slice (*figure 5.1*) and such types of 10 readings were taken from different z-axis positions (different slices). All samples were collected from the homogenous area of heart at the levels of Thoracic vertebra 8, 9, and 10. The same position and standard 1.5 cm diameter circle used for repeated measurements. We calculated Signal-to-noise Ratio from the result of HU and noise obtained from the anthropomorphic phantom.

SNR= Hounsfield Unit / image noise

Dose-Length-Product

A fixed scan length of 37cm was used for all examinations. CTDIvol and the Dose-Length-Product (DLP) from the CT scanner recorded and used the Dose-Length-Product for reporting scanner dose performance.

***Statistics*:** Comparative analyses of results were performed using Friedman Test for categorical data. Wilcoxon-Matched-Pair test used to compare results among these images regarding noise as a function of the reconstruction kernel or the slice thickness. All statistical analysis performed with commercially available software (BiAS for windows, Verson 8, epsilon-verlag, 1989-2008) [12]. *P* values less than 0.05 was considered as statistically significant.

5.2.3 RESULTS

***Change of DLP with kV*:** The absolute values of DLP (mGy.cm) obtained for protocol 1, 2, 3, and 4 are 297, 295, 308, and 282 respectively. The DLP based on the given CTDIvol values showed significantly lower exposure for the protocol 4 when compared to protocol 1 (percent difference 5.18%), protocol 2 (percent diff. 4.51%), and protocol 3 (percent diff. 8.81%).

Image quality: The highest change of Hounsfield Unit was observed with dual-energy Sn140-kV (Hounsfield unit 15.18) followed by dual-energy M.0.6 (fusion-weighted image- factor 0.6 corresponds to 60% of their information from the 100-kV image, and 40% from the 140-kV image) compared to protocol 2 (24.35 HU) (*Figure 5.2*). Differences in CT values between the different protocol data sets were statistically significant [protocol 2 vs. dual-energy Sn140-kV ($p<0.01$), protocol 2 vs. M.0.6 ($p<0.05$) and dual-energy 100-kV vs. dual-energy Sn140-kV ($p<0.05$)]. The result of SNR shows the highest image quality obtained from protocol 2 with B31f kernel (5.0mm slice thickness) reconstruction (*Figure 5.3*). The same result repeated and was more accurate and consistent with water phantom.

Effects of clinical protocol on image quality: The differences in noise between the different clinical protocol data sets were statistically significant [protocol 3 vs. dual-energy 100-kV ($p<0.01$) and protocol 3 vs. dual-energy Sn140-kV ($p<0.01$) protocols], further the dual-energy Sn140-kV shows the highest followed by dual-energy 100-kV protocol (*Table 5.2*).

Effects of reconstruction kernel on image quality: The difference in reconstruction kernel B31f and B80f images made using 5.0 mm reconstruction thickness was statistically significant ($p<0.0312$) and for 1.0 mm thickness $p<0.0312$ was obtained for B31f and B70f reconstruction kernel. In both cases, the lowest image noise was obtained from B31f reconstructed images.

Effects of slice thickness on image quality: Our study shows that the reconstruction thickness is significantly affects image noise ($p<0.03$) and the noise was higher at 1.0 mm reconstruction compared to 5.0mm for the same reconstruction kernel (B31f).

5.2.4 TABLES AND FIGURES

Scan parameters	**Protocol 1**	**Protocol 2**	**Protocol 3**	**Protocol 4**
Scan mode	Single-source	Single-source	Dual-source Single-energy	Dual-source Dual-energy
tube potential / effective tube current time product	120 kV, 110 mAs	100 kV, 180 mAs	120 kV, 130 mAs	100/Sn140 kV, 89/76 mAs
Total scan time (s)	4.73	4.73	1.1	10.68
Rotation time (s)	0.5	0.5	0.28	0.28
Detector collimation (mm)	128 x 0.6	128 x 0.6	128 x 0.6 x 2	64 x 0.6 x 2
CTDIvol (mGy)	7.37	7.32	7.12	7.33
Pitch	1.2	1.2	3.0	0.55

Table-5.1: shows the scan parameters.

	Reconstruction thickness and kernel			
Clinical Protocol	slice thickness 5.0, kernel B31f	slice thickness 5.0, kernel B80f	slice thickness 1.0, kernel B31f	slice thickness 1.0, kernel B70f
Single-source 120kV	10.38	57.37	22.82	118.83
Single-source 100kV	11.29	56.12	23.59	124.82
High-pitch 120kV	9.52	56.09	21.38	111.11
DE.A. 100kV	14.32	79.64	30.13	156.14
DE.B.Sn140kV	14.49	79.88	30.71	161.94
Dual Energy M.0.6	10.82	59.35	24.12	120.77

Table- 5.2: shows the mean measured image noise values of Rando-Alderson anthropomorphic phantom.

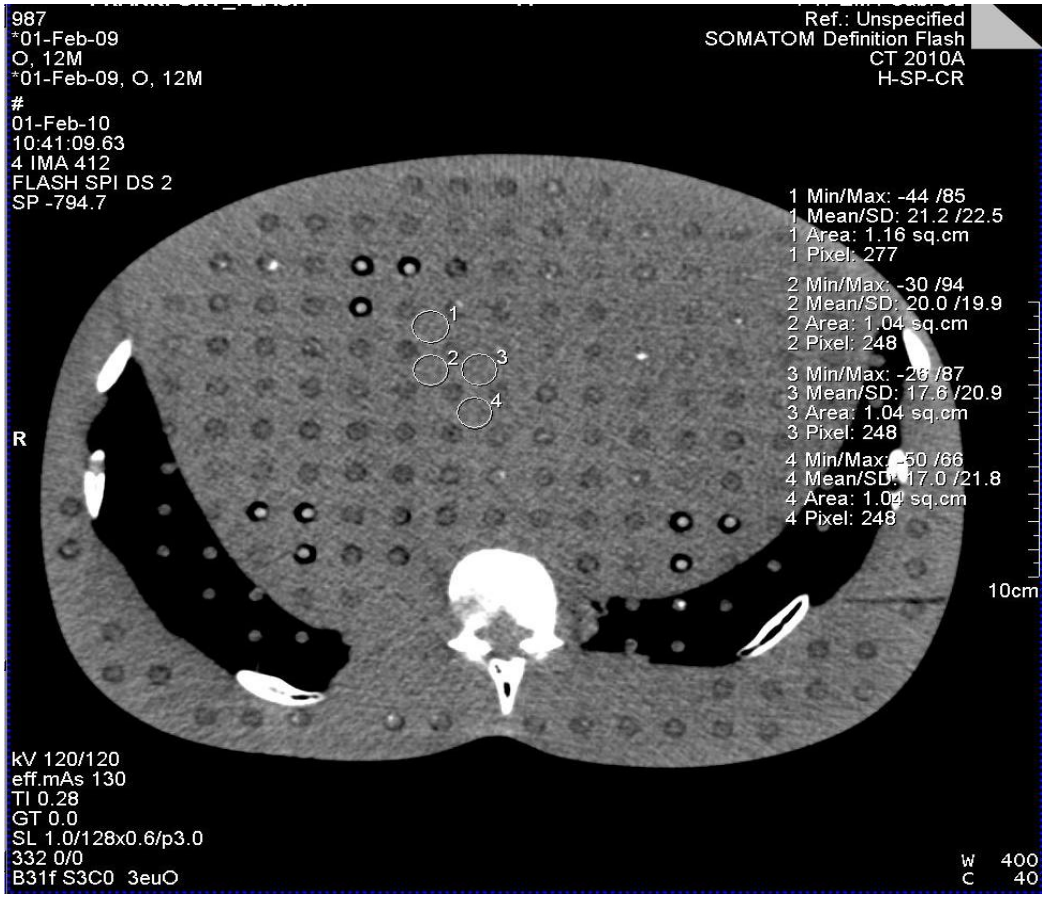

Figure-5.1: shows the Hounsfield Unit and noise measurement locations of an axial slice of an Alderson-anthropomorphic phantom.

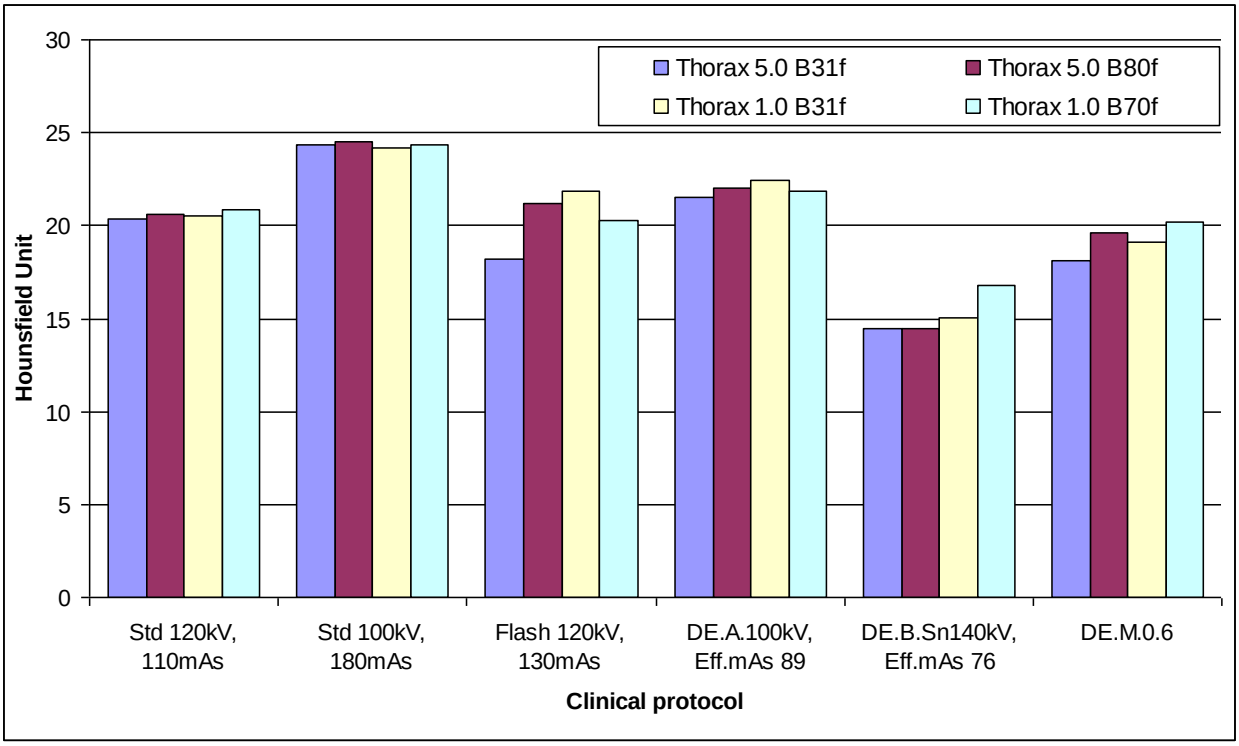

Figure- 5.2: Bar graph shows the relationship of CT number (HU) with clinical protocol and reconstruction kernel.

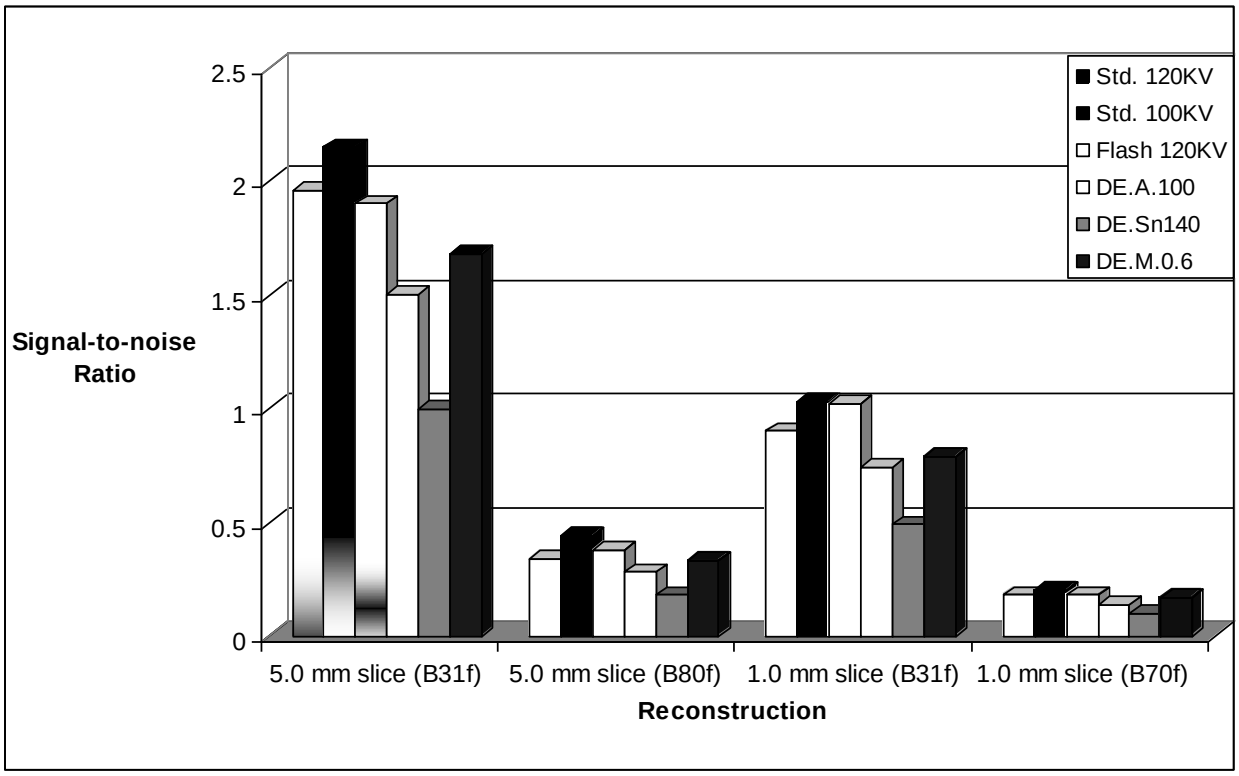

Figure-5.3: Bar graph shows the relationship of Signal-to-noise Ratio with clinical protocol and reconstruction kernel.

5.2.5 DISCUSSION

The latest generation CT scanners offer some decisive advantages, especially regarding examinations of moving structures, such as the thorax and the heart. It is also possible to perform whole-body scans extremely fast now a day: For example, a person with a height of 198 cm can be scanned in less than 5 seconds. Until now, such whole-body examinations were taking more than 10 minutes to be performed from patient preparation to diagnosis. Several studies have meanwhile shown the benefits of this dual energy new imaging technique in clinical routine with several different applications [13, 14, 15, and 16]. In a normal way increasing tube voltage (kV), tube current (mA) and slice scan time (s) will reduce image noise. The second and mA improve image noise by $1/\sqrt{mAs}$, which, since *N* is linearly related to mA and s, is predicted by theory [17]. The relationship of kV to image noise is more complex as it affects the production of photons in the x-ray tube, via radiative stopping power, and photon attenuation in the phantom, via linear attenuation coefficient. Kilo-Voltage is measured to reduce noise by ~ $(kV)^{-1.3}$. In our study, it is possible to observe that there is a difference in noise by different clinical protocols with same reconstruction kernel. Dual energy imaging has some decisive advantages in this concern because from the single scan itself, it is able to produce two sets of image data, and it can generate fused images without further processing. Even though the image noise is higher for Sn140kV or 100kV dual energy, the fused image (M.0.6) shows excellent image quality and the noise is almost same as

single or high-pitch mode. As per dose concern, dual energy imaging is contributing the least radiation dose compared to other protocols examined.

CT reconstruction algorithm differs principally in the choice of the reconstruction kernel. That providing freedom to design kernels that suppress or enhance specific ranges of spatial frequencies to affect the visual properties of the reconstructed images with the ultimate choice of reconstruction kernel affecting performance for lesion-detection tasks and noise. The result of this study shows that noise is strongly depends on reconstruction kernel and it can be suggested that the selection of kernel for an examination should be careful and according to clinical interest. Clinical applications studied by Judy and Swensson [18] showed that the detect ability of small high-contrast lesions improved as the reconstruction kernel became smoother. Prevrhal et al. [19] showed that the accuracy of evaluating thin structures improved with the use of high-resolution kernels. Ulrich Baum et al. [20] reported that, there was a significant (P<0.05) reduction in mean pixel noise in the reconstructions using MAF (Multidimensional Adaptive Filtering technique) in comparison to the standard reconstructions.

The collimation applied at dual-energy Sn140-kV/100-kV protocol was 128X0.6 mm, which makes it possible to reconstruct thin slices of 0.6 mm thickness at the price of an increased background noise. It was generated by the detector itself and the subsequent data processing, for example, dual-energy Sn 140-kV, eff.mAs 76 protocol, the noise value for the 5.0 mm reconstruction was 14.49 and 1.0 mm reconstruction was 30.71 with same reconstruction filter in this study and it states that the reconstruction slice thickness will greatly affected by the image noise.

Further, image noise is again greatly affecting by the diameter (size) and the density of the materials contained in the phantom. This is because of increased photon attenuation in the phantom.

Tube potential (voltage) determines the energy of incident X-ray beam, and variation in tube potential causes a substantial change in CT radiation dose. An important outcome that may be associated with decreased tube voltage is a notable increase in image noise. This occurs if the patient is too large or the tube current is not appropriately increased to compensate for the lower tube voltage. The dose change is approximately proportional to the square of the tube voltage change (ie, square of the ratio of final and initial peak voltage) [21], and the noise change is approximately inversely proportional to the tube voltage change [22]. For very large patients, a higher tube voltage is generally more appropriate. There is a need for further research on the use of lower tube voltage for dose advantages, because of the complex relationship between tissue contrast, image noise, and radiation dose that depends on patient size. According to preliminary results reported by Lieberman et al [23] head CT performed in children at a substantially reduced tube-voltage (if performed with increased tube current) may result in the lowest possible patient dose with no decrease in image contrast-to-noise ratio. However, further studies should precede such a reduction in the tube voltage used to acquire CT scans. Image quality ramifications of a decrease in tube voltage to reduce radiation exposure must be carefully examined before this strategy is implemented. The dual-energy Sn140kV and 100kV shows higher noise compaired with other single-or high-pitch protocols examined.

Even though the image noise is higher for Sn140kV and 100kV dual energy, the fused image shows excellent image quality and the noise is same as single or high pitch mode. Another important finding is the comparatively higher DLP of the dual-source high-pitch protocol compared to other single- or dual-energy protocols. This finding is a little bit surprising, because the high-pitch scan mode (high table feed and tube rotation speed) should not be increasing dose per se. It may be hypothesized that in the high-pitch mode there is still an over-beaming effect of pre- and post-scan volume despite the use of the dynamic collimation system referred to as adaptive dose shield. An another surprising result obtained from Dual Source CT is that dual-energy protocol shows the lowest DLP compared to all other examined protocols. The possible explanation for this improvement is that advanced CT technology (eg. Adaptive dose shielding and IRIS Iterative algorithm) is playing a crucial role to reduce the radiation dose and improve image quality.

5.2.6 CONCLUSION

The clinical protocol, reconstruction kernel, slice thickness and phantom diameter or the density of material it contains directly affects the image quality. Appropriate choices of scan technique, reconstruction algorithm and patient (phantom) size as well as use of image averaging and digital image filtering can dramatically reduce image noise. Dual Energy protocol shows the lowest DLP compared to all other protocols examined. Dual-energy Sn140kV and 100kV shows higher noise compared with other single-or high-pitch protocols examined. Even though the image noise is higher for Sn140kV and 100kV dual energy image sets, the fused images show excellent image quality and the noise is same as single or high-pitch mode protocol images. Advanced CT technology improves image quality and considerably reduce radiation dose.

5.2.7 REFERENCE

1. Flohr TG, Leng S, Yu L, et al, Dual-source spiral CT with pitch up to 3.2 and 75 ms temporal resolution: image reconstruction and assessment of image quality, Med Phys. 2009 Dec; 36 (12):5641-53.

2. Primak, A.N, J.C Ramirez Giraldo, X. Liu, et al., Improved dual energy material discrimination for dual source CT by means of additional spectral filtration. Med. Phys., 2009. 36(4): p.1359-69.

3). Andrew N. Primak, PhD, et al, Relationship between Noise, Dose, and Pitch in Cardiac Multi Detector Row CT, RadioGraphics 2006; 26:1785–1794 [Published online 10.1148/rg.266065063].

4. Flohr TG, Schaller S, Stierstorfer K, Bruder H, Ohnesorge BM, Schoepf UJ. Multi-detector row CT systems and image-reconstruction techniques. Radiology 2005; 235: 756–773.

5. Ohnesorge BM, Becker CR, Flohr TG, Reiser MF. Multi-slice CT in cardiac imaging: technical principles, clinical application, and future developments. Berlin, Germany: Springer, 2002.

6. Hsieh J. Computed tomography: principles, design, artifacts, and recent advances. Bellingham, Wash: SPIE Press, 2003; 348–357.

7. J. Matthias Kerl & Ralf W. Bauer et.al., Dose levels at coronary CT angiography—a comparison of Dual Energy-, Dual Source- and 16-slice CT. Eur Radiol. DOI 10.1007/s00330-010-1954-9

8. Bamberg F, Marcus R, et.al., Diagnostic image quality of a comprehensive high-pitch dual-spiral cardiothoracic CT protocol in patients with undifferentiated acute chest pain. Eur J Radiol. 2010 Dec 31. [Epub ahead of print].

9. Wieland H. Sommer, Edda Albrecht, et.al., Feasibility and Radiation Dose of High-Pitch Acquisition Protocols in Patients Undergoing Dual-Source Cardiac CT. AJR 2010; 195:1306–1312

10. Graser, Anno MD*; Becker, Christoph R. MD, et.al., Single-Phase Dual-Energy CT Allows for Characterization of Renal Masses as Benign or Malignant. Investigative Radiology: July 2010 - Volume 45 - Issue 7 - pp 399-405

11. Wieland H. Sommer MD, Anno Graser MD et.al., Image Quality of Virtual Noncontrast Images Derived from Dual-energy CT Angiography after Endovascular Aneurysm Repair. Journal of Vascular and Interventional Radiology Volume 21, Issue 3, March 2010, Pages 315-321

12. BiAS.für Windows Programmversion 8 epsilon-verlag 1989-2008. http:/www.bias-online.de

13. Thorsten R. C. Johnson, Bernhard Krauss, Martin Sedlmair, et al., Material differentiation by dual energy CT; inital experience. Eur. Radiol. (2007) 17:1510-1517.

14. Graser A, Johnson TR, Bader M, Dual energy CT characterization of urinary calculi: initial in vitro and clinical experience. Invest Radiol. 2008 Feb;43(2):112-9.

15. Thieme S, Becker C, Hacker M. Dual energy CT for the assessment of lung perfusion—Correlation to scintigraphy, European Journal of Radiology, Volume 68, Issue 3, Pages 369-374.

16. Eun Jin Chae, MD, Joon Beom Seo, MD, PhD, Hyun Woo Goo, MD, PhD; Xenon Ventilation CT with a Dual-Energy Technique of Dual-Source CT: Initial Experience; doi: 10.1148/radiol.2482071482 August 2008 Radiology, 248, 615-624.

17. Brooks R A and Di Chiro G. Statistical limitations in x-ray reconstructive tomography. Med Phys. 1976 (July-August 3(4)) 237–40.

18. Philip F. Judy, Ph.D. and Richard G. Swensson, Ph.D**.;** Detection of small focal lesions in CT images: effects of reconstruction filters and visual display windows, British Journal of Radiology (1985) 58, 137-145; doi: 10.1259/0007-1285-58-686-137

19. Prevrhal S, Engelke K, Kalender W et.al., Accuracy limits for the determination of the cortical width and density: the influence of object size and CT imaging parameters. Phys Med Biol.1999; 44(3):751-64.

20. Ulrich Baum, Katharina Anders et al., Improvement of image quality of multislice spiral CT scans of the head and neck region using a raw data-based multidimensional adaptive filtering (MAF) technique; Eur Radiol. DOI. 10.1007/s00330-004-2403-4; ISSN 0938-7994 (Print) 1432-1084 (Online)

21. Mannudeep K. Kalra, Michael M. Maher, Thomas L. Toth et.al., Strategies for CT Radiation Dose Optimization. Radiology 2004; 230:619–628.

22. Rehani MM, Bongartz G, Kalender W, et. al. Managing x-ray dose in computed tomography: ICRP Special Task Force report. Ann ICRP 2000; 30:7–45.

23. Lieberman K, Huda W, Chang J, Roskopf M. How should x-ray techniques be modified for pediatric patients in head CT? (abstr). Radiology 2002; 225 (P):593.

Chapter 6

Image Fusion in Dual Energy Computed Tomography for Detection of Various Anatomic Structures – Effect on Contrast Enhancement, Contrast-to-Noise Ratio, Signal-to-Noise Ratio and Image Quality

6.1 ABSTRACT

***Objective*:** The purpose of this study was to evaluate Image fusion in Dual Energy Computed Tomography for detecting various anatomic structures based on the effect on Contrast Enhancement, Contrast-to-Noise Ratio, Signal-to-Noise Ratio and Image Quality.

***Material and methods*:** Forty patients underwent a CT neck with dual energy mode (DECT under a Somatom Definition flash Dual Source CT scanner (Siemens, Forchheim, Germany)). Tube voltage: 80-kV and Sn140-kV; tube current: 110 and 290 mAs; collimation-2X32X0.6mm. Raw data were reconstructed using a soft convolution kernel (D30f). Fused images were calculated using a spectrum of weighting factors (0.0, 0.3, 0.6 0.8 and 1.0) generating different ratios between the 80- and Sn140-kV images (e.g. factor 0.6 corresponds to 60% of their information from the 80-kV image, and 40% from the Sn140-kV image). CT values and SNRs measured in the ascending aorta, thyroid gland, fat, muscle, CSF, spinal cord, bone marrow and brain. In addition, CNR values calculated for aorta, thyroid, muscle and brain. Subjective image quality evaluated using a 5-point grading scale. Results compared using paired *t*-tests and nonparametric-paired Wilcoxon-Wilcox-test.

***Results*:** Statistically significant increases in mean CT values noted in anatomic structures when increasing weighting factors used (all $P \leq 0.001$). For example, mean CT values derived from the contrast enhanced aorta were 149.2+/-12.8 Hounsfield units (HU), 204.8+/-14.4 HU, 267.5+/-18.6 HU, 311.9+/-22.3 HU, 347.3+/-24.7 HU, when the weighting factors 0.0, 0.3, 0.6, 0.8 and 1.0 were used.

The highest SNR and CNR values were found in materials when the weighting factor 0.6 used. The difference CNR between the weighting factors 0.6 and 0.3 was statistically significant in the contrast enhanced aorta and thyroid gland (P = 0.012 and P = 0.016, respectively). Visual image assessment for image quality showed the highest score for the data reconstructed using the weighting factor 0.6.

***Conclusion*:** Different fusion factors used to create images in DECT cause statistically significant differences in CT value, SNR, CNR and image quality. Best results obtained using the weighting factor 0.6 for all anatomic structures used in this study.

6.2.1 INTRODUCTION

Compton scatter and the photoelectric effect are the two main mechanisms responsible for the absorption and scattering of photon energy range used in CT. Inside the energy range considered the total cross section of the Compton Effect is almost independent of photon energy, whereas the total cross section of the photoelectric effect is strongly energy-dependent. The differentiation of material in computed tomography (CT) based on their X-ray attenuation as quantified in Hounsfield Units and displayed in shades of gray at different window levels in normal CT scans [1]. A previous study [2] demonstrated that a low tube voltage (80-kV) scan can provide better contrast and conspicuity than a high voltage (140-kV) scan for the detection of hyper vascular liver tumors, as the low tube voltage scan takes advantage of the attenuation property of iodinated contrast material at 80-kV.

However, in a previous study despite the fact that 80-kV CT images showed a higher contrast-to-noise ratio (CNR) of simulated hypervascular liver lesions, the low tube voltage scan also showed increased noise compared with the high voltage tube scan. In addition, although increasing tube current is able to decrease noise of the low tube voltage scan, the CT system is not able to provide sufficient radiation dose as desired. Those factors thus limit the widespread use of an 80-kV scan in clinical practice. However, with dual-energy CT (DECT), the noise of the 80-kV data offset by the decreased noise of the 140-kV data, and therefore, the difficulty with routine use of low-kV CT because of increased noise could be minimize with this DECT technique. As the use of DECT has recently increased, image fusion techniques using 140-kV images and 80-kV images with DECT can provide a way to increase

the CNR [3–6]. Theoretically, if we adequately fuse both low and high voltage images, we can obtain better images that therefore balance the advantages and disadvantages of both low and high voltage images according to the attenuation difference between the lesion or structures of main interest and the background organ. For example, a 0.3 weighting factor means that 30% of the image information is derived from the 80 kV image and 70% from the 140 kV image. As the weighting factor increases, the image looks like more an 80-kV image. These routinely provided fused images are making anatomic structures or pathology differentiation without the benefit of DE processing. Characterized by low image noise, such images create the impression of a 120-kV image [7]. This is because of a dedicated DE convolution kernel that draws 70% of the fused image from the 140-kV image and 30% from the 80-kV image [7]. The aims of this study were to differentiate various body structures even without the presence of contrast media, to differentiate contrast enhanced structures and its (or lesion) vascularity from otherwise dense material in parenchymatous organs and differentiation of contrast-enhanced vessels. Thus, in effect to evaluate the effect of using different weighting factors on differentiation of body tissues/ materials with and without contrast enhancement under a dual energy CT.

6.2.2 MATERIALS AND METHODS

Scanning machine

CT scans obtained by using a recently introduced Second-generation dual-source CT scanner (Somatom Definition Flash; Siemens Healthcare, Forchheim, Germany). This scanner has two X-ray tubes that simultaneously revolve around the patient's body and equipped with two 38.4 mm detectors that each acquire 128 slices of image data. The scanning speed of this scanner is 43 cm/s and a temporal resolution of 75 ms. The tubes can be operated independent of each other with respect to kilovolt (kV) and milliampere (mA) settings. The automatic dose modulation protocol provided by the manufacturer (Care Dose 4D, Siemens Medical Solutions), adjusts tube current in a real-time manner to maintain image noise at the optimal level.

Scan protocol and procedures

Forty consecutive patients were enrolled in this study (29 men and 11 women; mean age 52+/-20 years). Exclusion criteria were contraindication for iodinated contrast medium and age less than 22 years or greater than 80 years. The Neck of the Patients were scanned caudo-cranial direction during a shallow breath from the mid chest to supra orbital margin and all the examinations were carried out with dual energy mode. Tube voltages were set to 80 and 140 kV and the current was almost threefold for the 80-kV over the 140-kV (Sn) tube, i.e., 110 and 290 mA, to compensate for the lower photon output at the lower voltage. The average scan length was 30 cms and the CTDIvol ranged between 9.5 and 10 mGy.

Further, the Field of View (FOV) was 200 mm, the collimation was 2X32 X0.6 mm and the pitch was 0.9. For the contrast scans, all patients received 100 ml Iomeprol contrast medium (CM) containing a standard iodine concentration of 400 mg iodine/ml (Imeron 400 MCT, Bracco Imaging Deutschland GmbH, D-78467 Konstanz, Germany). Using a power injector, contrast medium warmed to 37°C administered intravenously into an antecubital vein via an 18-gauge catheter at a flow rate of 2 ml/s. Application of a saline chaser (25 ml of 0.9% sodium chloride solution) at the same flow rate followed injection of contrast medium. The scanning performed 60 seconds after the injection of contrast medium. All raw data collected by both detectors were reconstructed 2 mm slice thickness using a soft convolution kernel (D30f). Fused images were calculated using different weighting factors: 0.0, 0.3, 0.6, 0.8, and 1.0. A weighting factor of 0.0, for example, results in 100% image information derived from the 140-kVp image, and 0% information taken from the 80-kVp image. A weighting factor of 1.0 leads to the opposite, namely 100% image information from the 80-kVp image and 0% information from the 140-kVp image. The other weighting factors generate fused images between these two extremes.

Quantitative analysis

The mean attenuations measured in the different anatomic structures, including aorta with contrast medium, for all weighted images (weighting factors 0.0, 0.3, 0.6, 0.8 and 1.0) by placing a circular Region of Interest (ROI) at each anatomic site for each patient. The attenuation (HU) assessed in the following regions: thyroid gland, sterno-cleido mastoid muscle of neck, ascending aorta, temporal lobe of brain, bone marrow (odentoid process), spinal cord (at the level of C4), cerebro-spinal fluid and

fat adjacent to the thyroid. Attenuation assessed in three neighboring slices and CT values were average for each region. Corresponding standard deviations were determined. The signal-to-noise ratio (SNR) was then calculated by dividing the mean attenuation number by the corresponding standard deviation, further at all anatomic sites a constant size of the ROI was maintained [8]. The CT scans of the all patients compared in terms of attenuation, noise, SNR and CNR. The contrast-to-noise ratio was defined as the difference between the mean density of the contrast enhanced material/ anatomic structure and the mean density of the surrounding structure, which was divided by image noise [8]. For contrast enhanced brain, brain to cerebro-spinal fluid CNR and other three (contrast enhanced thyroid, muscle and aorta) structures, structure to fat CNRs were calculate for each set of the images.

Qualitative analysis

Three attending radiologists with more than 5 years of clinical experience interpreted differently weighted CT scans (weighting factors: 0.0, 0.3, 0.6, 0.8, and 1.0). The quality of each image based on surrounding artifacts and clarity of structures following contrast enhancement was graded by unaware of the weighting factors used (*Figure 6.1*). Further, the images were randomly reviewed using a 5-point grading system (*table 6.1*) and for a single structure the window width and level made same for all the images. The reviewers were able to alternate the window width and level for different structures.

Statistics

The mean attenuation of the material and image noise of the fused images summarize by the arithmetic mean and the corresponding standard deviation. It is compared graphically the medians, upper extremes, lower extremes, upper quartiles and lower quartiles from box plots of CNR between the different images generated by different weighting factors. Mean SNRs of all the materials under examination showed in table for quality comparison of all the single and weighted images.

All statistical analyses performed in an explorative manner; thus, *P* values of $P \leq 0.05$ presumed to be statistically significant. Paired *t*-tests were use to compare mean attenuation and SNR of images obtained with the different weighting factors. The 2-sided nonparametric-paired Wilcoxon-Wilcox-test was use to compare the results of qualitative grading between these images. The SPSS statistical analysis software package (PASW statistics version 18, Polar engineering and consulting, www.winwrap.com) used for t-test statistical analysis and BIAS Software package (BIAS for windows, epsilon 2008- version 8.4.2) used for Wilcoxon-Wilcox-Test.

6.2.3 RESULTS

Quantitative analysis

Mean CT values increased with increasing weighting factors. The highest CT values were detected for the factor of 1.0 (100% 80 kVp) (*Table 6.2, Fig.6.2*), compared with data sets reconstructed using a weighting factor of 0.0. Compared to 0.0 weighted images the mean CT values generated by a weighting factor of 1.0 were almost twice as high. The SNR showed the highest values for the data sets reconstructed with a weighting factor of 0.6, followed by the factor 0.3 or 0.8 depending on the anatomic site (*Table 6.3, Figure 6.3*). The lowest SNR values detected for the fused data sets with a factor of 0.0 (100% 140 kVp). Differences in mean CT values between the differently weighted data sets were statistically significant at all anatomic sites (P<0.001).

The difference CNR between the weighting factors 0.6 and 0.3 was statistically significant in the contrast enhanced aorta and thyroid gland (*P* =0.012 and *P* =0.016, respectively). The difference in CNR between images made using the weighting factors 0.6 and 1.0 was statistically significant in the muscle or brain (*P* =0.015, *P* =0.026 respectively) (*figure 6.4*). There is no statistically significant differences were found between images weighted with the factors 0.8 and 1.0 for CNRs of aorta, thyroid, muscle and brain (p=0.963, p=0.838, p=0.238, p=0.805)

Qualitative analysis

The highest values for both grading score (*table 6.1*) and CNR (*table 6.3*) of materials detected found with the weighting factor 0.6. Visual assessment of image quality revealed that data sets reconstructed with a weighting factor of 0.6 showed the best image quality (*table 6.4*). *Figure 6.5* shows the relationship between mean visual grading score and mean CNR values of materials or anatomic structures dependent on different weighting factors. The highest mean Visual Grading scores (VG score) noted that for contrast enhanced aorta, thyroid gland, muscle and brain are 4.1, 4, 4 and 4.2 respectively. The differences in grading results seen between the images weighted with the factor 0.6 and those reconstructed with the factors 0.0 and 0.8 were statistically significant ($p < 0.05$). Higher CT values with, correspondingly higher weighting factors, do not lead to increased CNR or to improve grading results.

6.2.4 TABLES AND FIGURES

A) B)

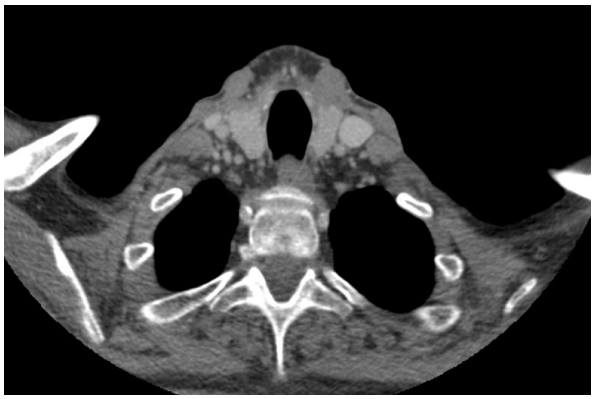

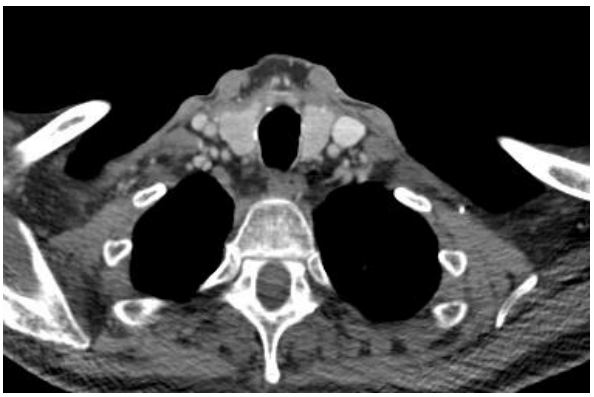

C) D)

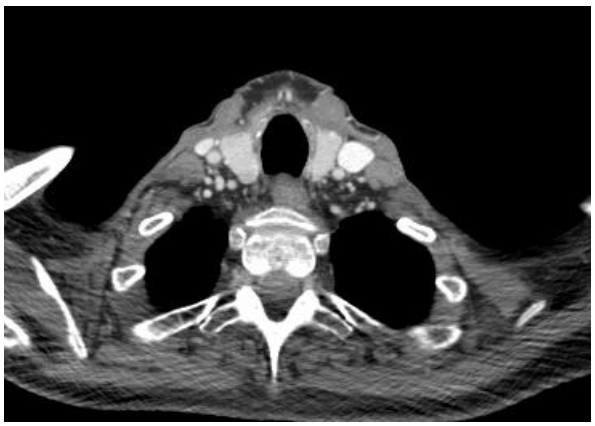

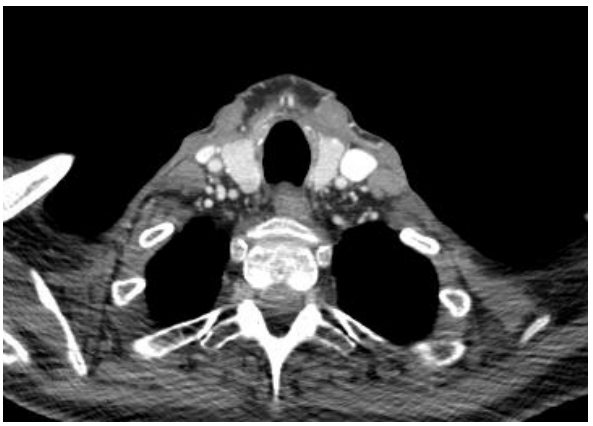

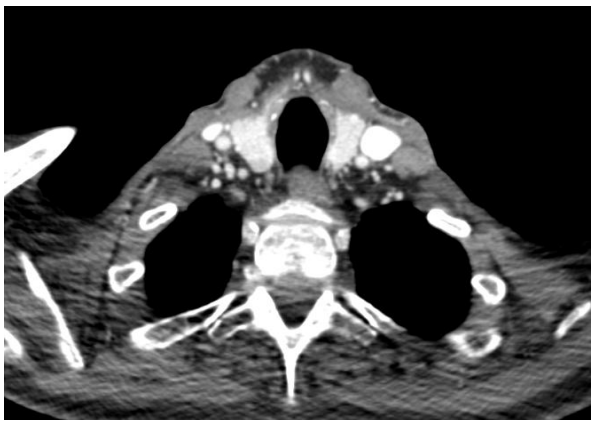

E)

Figure-6.1: Axial dual energy CT images at the level of the thyroid reconstructed with different weighting factors (A) 0.0, (B)0.3, (C)0.6, (D)0.8, and (E)1.0 (window width: 400, window level: 75, for all images).

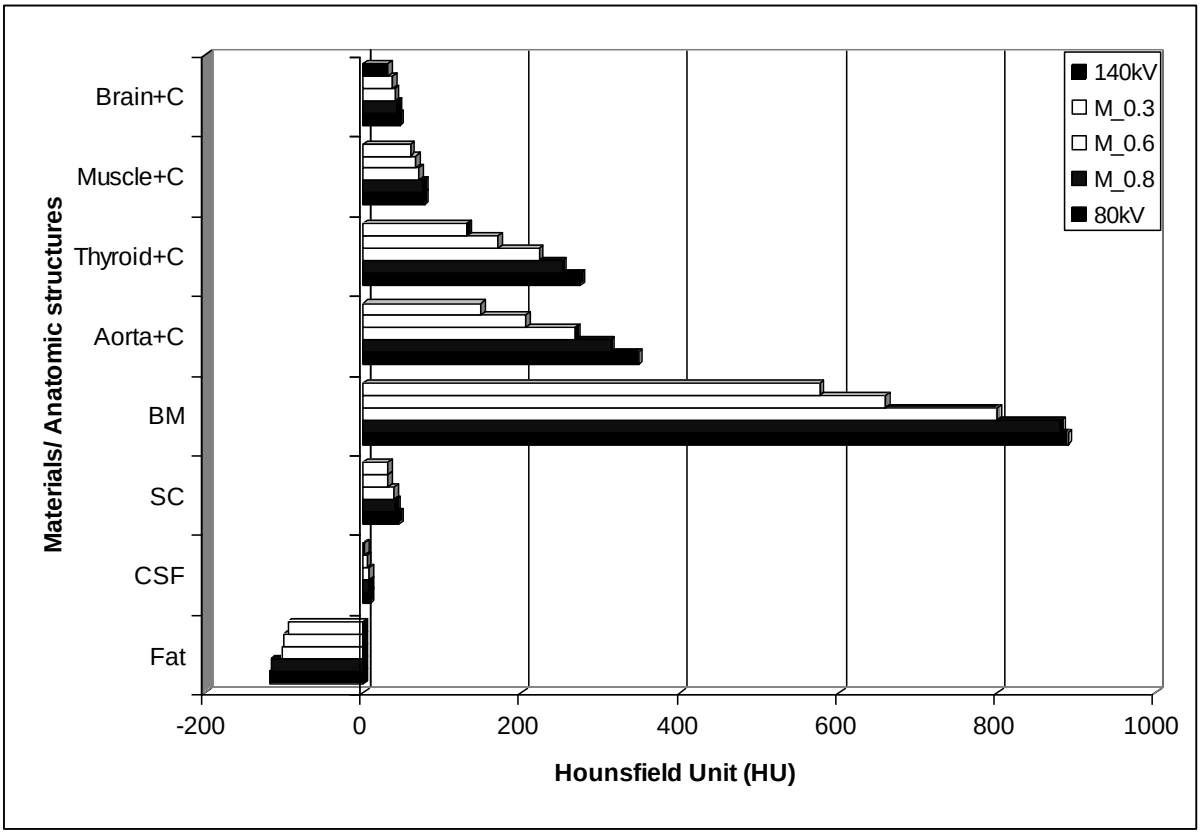

Figure-6.2: Bar diagram of mean Hounsfield Units of the (a) ascending aorta with contrast medium, (b) contrast enhanced thyroid gland, (c) contrast enhanced brain, (d) contrast enhanced neck muscle, (e) bone marrow (f) cerebro-spinal fluid, (g) fat, and (h) spinal cord with image reconstructions using different weighting factors (0.0, 0.3, 0.6, 0.8 and 1.0).

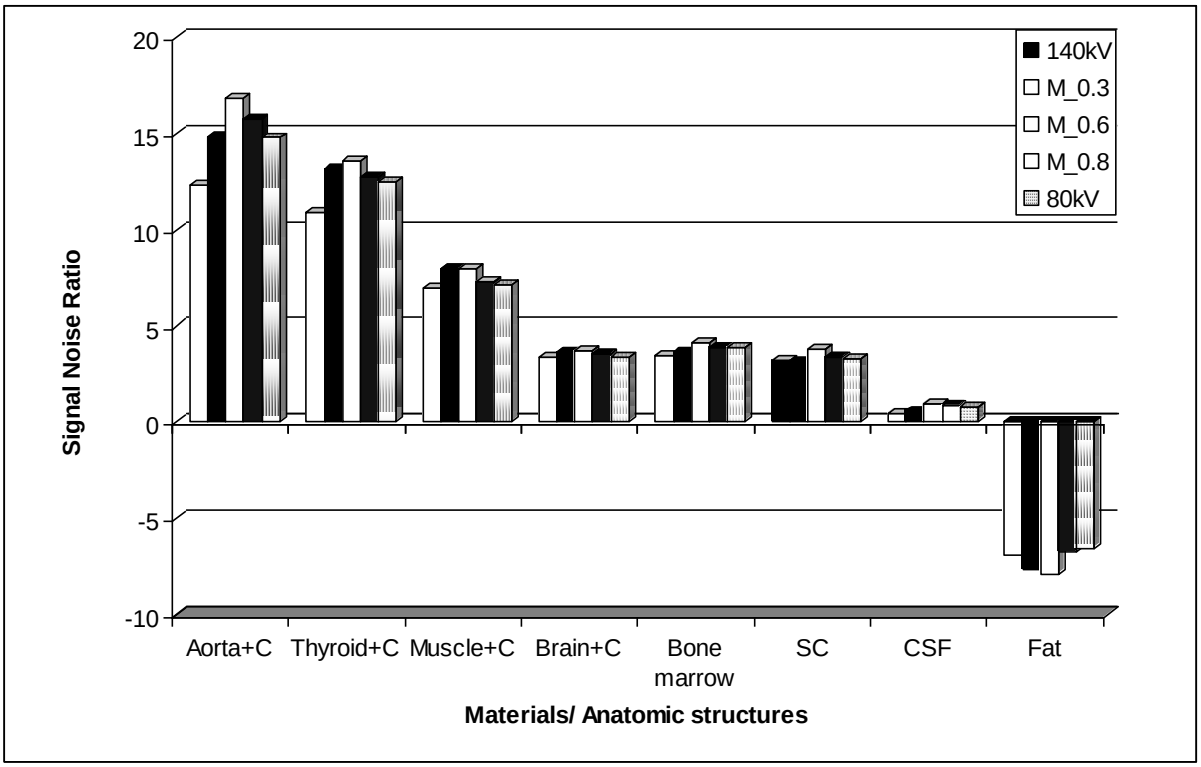

Figure-6.3: Bar diagram shows, mean signal to noise ratio (SNR) of contrast enhanced ascending aorta, thyroid gland, neck muscle, brain and un-enhanced CSF, spinal cord, bone marrow, fat for the different weighting factors (0.0, 0.3, 0.6, and 1.0) used in image fusion.

Figure-6.4: Box plots of CNRs of the ascending aorta with contrast medium (A), contrast enhanced brain (B), contrast enhanced muscle (C), and contrast enhanced thyroid gland (D) based on image reconstructions using different weighting factors (0.0, 0.3, 0.6, 0.8 and 1.0). Upper end of vertical lines, lower end of vertical lines, upper margin of boxes, lower margin of boxes and horizontal lines in boxes represent upper extremes, lower extremes, upper quartiles, lower quartiles and medians of the values, respectively.

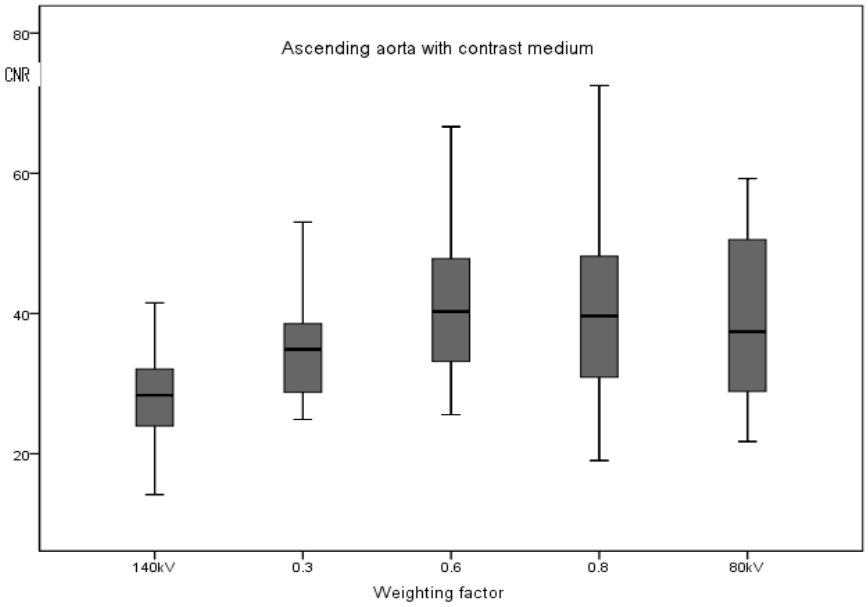

A)

B)

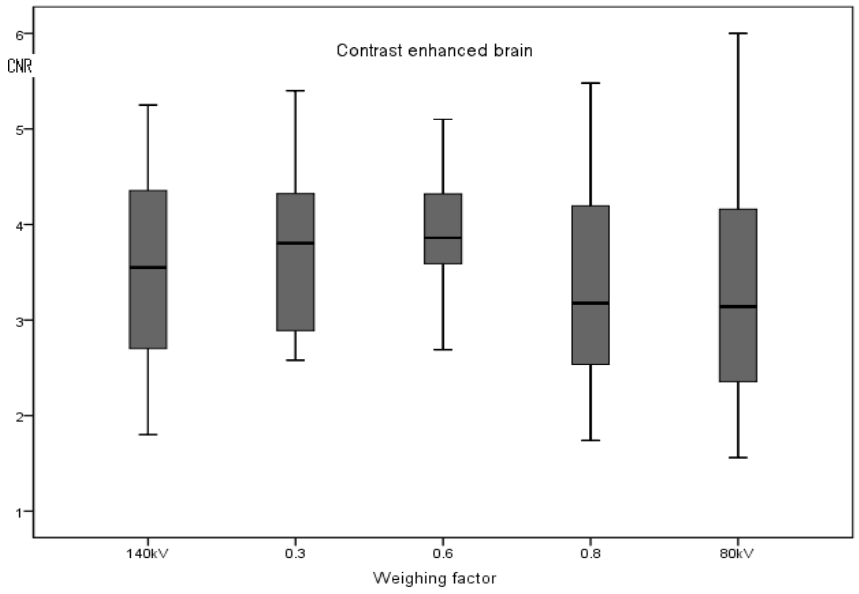

C)

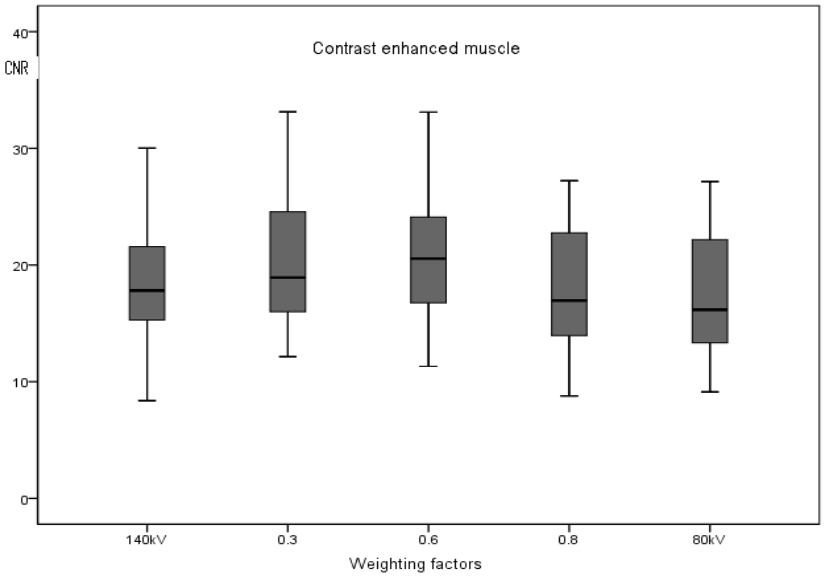
Contrast enhanced muscle
CNR
40
30
20
10
0
140kV
0.3
0.6
0.8
80kV
Weighting factors

D)

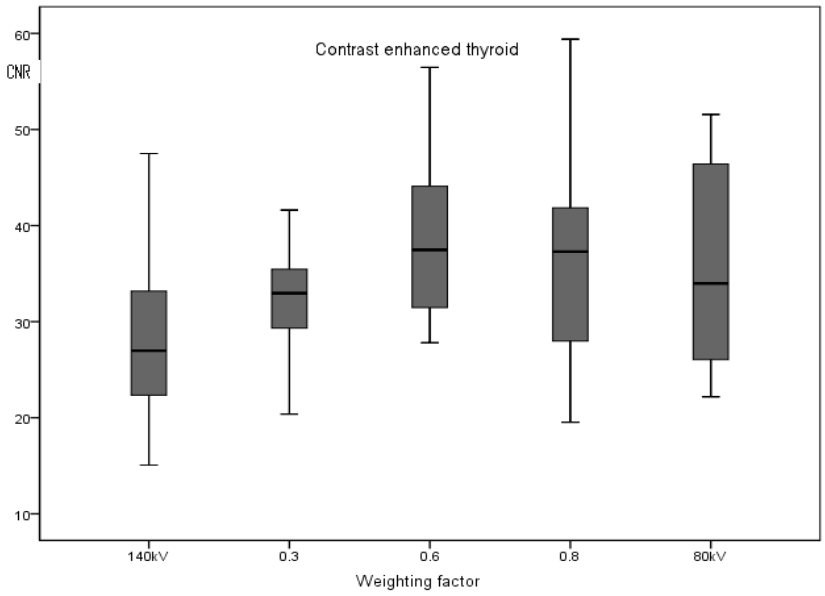
Contrast enhanced thyroid
CNR
60
50
40
30
20
10
140kV
0.3
0.6
0.8
80kV
Weighting factor

Figure-6.5: Line graphs shows the relationship between visual grading score and CNR values for different weighting factors (A) ascending aorta, (B) thyroid, (C) Muscle, and (D) brain. The highest values for the visual grading score and the CNR were obtained with the weighting factor 0.6.

A)

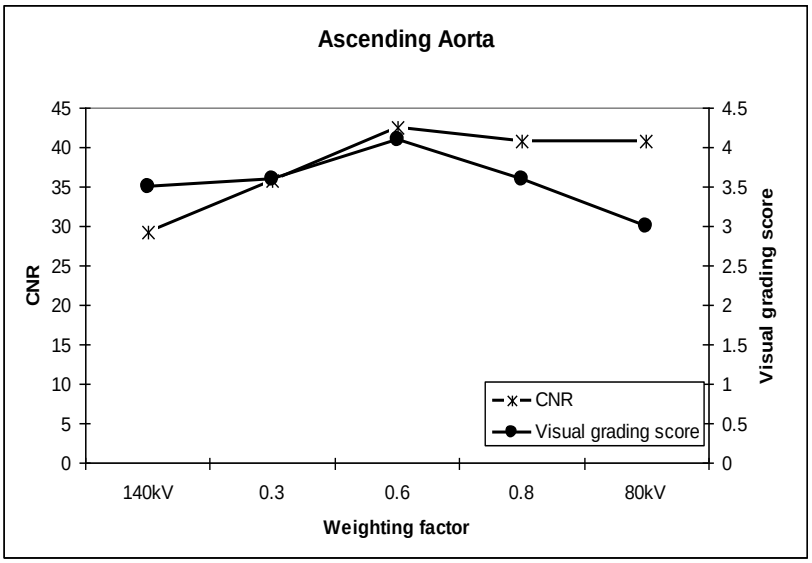

B)

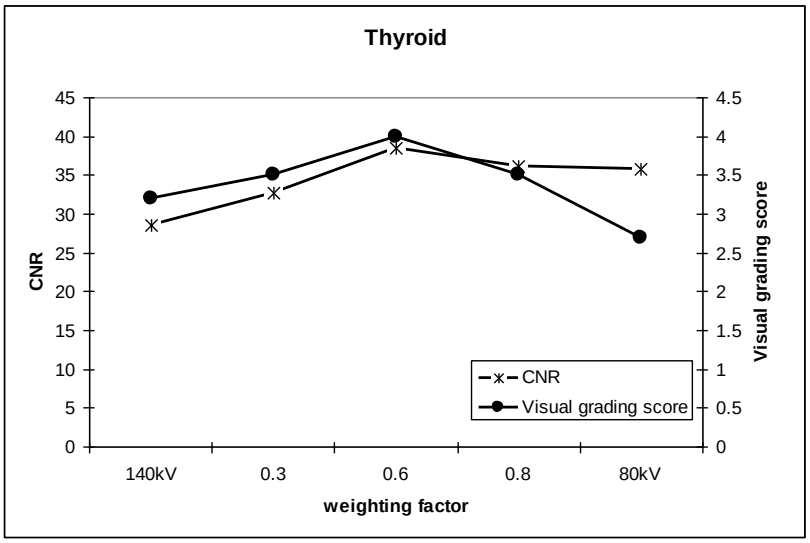

C)

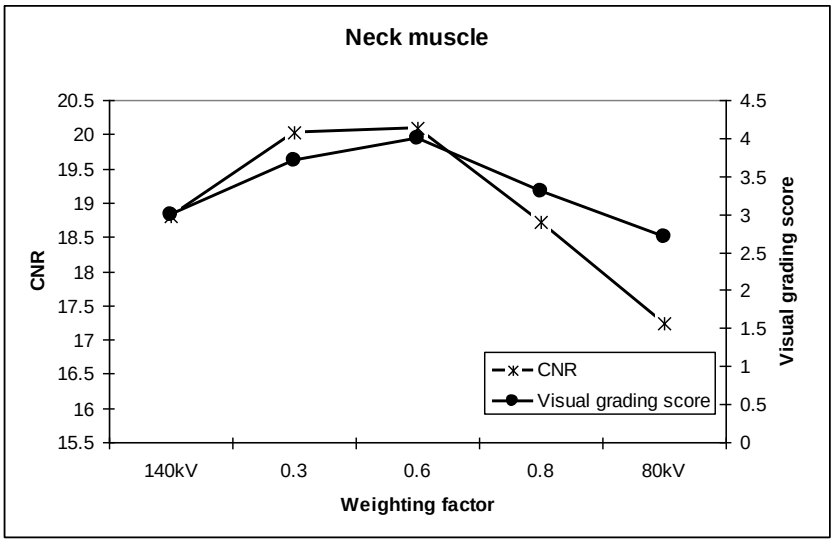
Neck muscle
CNR
Visual grading score
20.5
20
19.5
19
18.5
18
17.5
17
16.5
16
15.5
4.5
4
3.5
3
2.5
2
1.5
1
0.5
0
CNR
Visual grading score
140kV
0.3
0.6
0.8
80kV
Weighting factor

D)

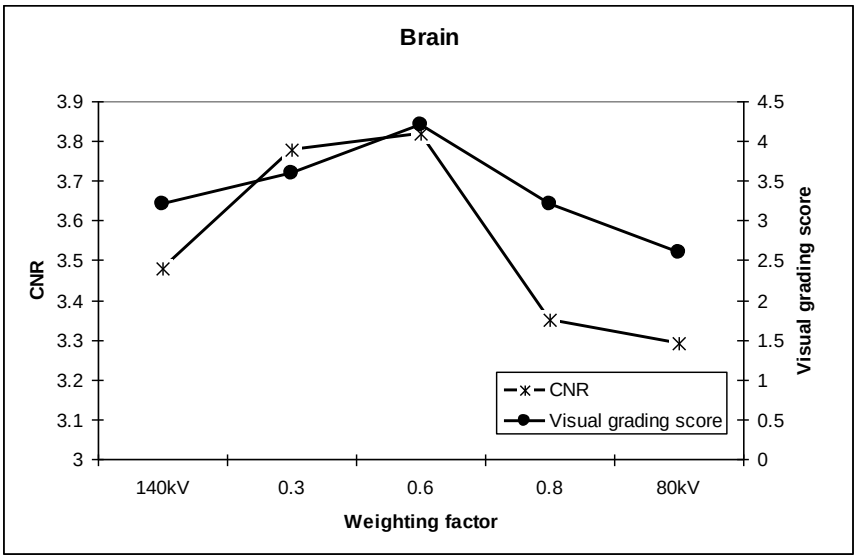
Brain
CNR
Visual grading score
3.9
3.8
3.7
3.6
3.5
3.4
3.3
3.2
3.1
3
4.5
4
3.5
3
2.5
2
1.5
1
0.5
0
CNR
Visual grading score
140kV
0.3
0.6
0.8
80kV
Weighting factor

Tables

Notation	Score	Details
A	1	Very poor structure details (cannot differentiate)
B	2	Structures are not sufficiently detectable
C	3	Fair level of details but some pictures are inadequate for differentiation
D	4	Good level of details but not excellent
E	5	Excellent structure details (well differentiate and possible to evaluate very easy and clear)

Table-6.1: Visual grading scheme for image quality based on the presence of surrounding artifacts and the clarity of structures.

Material / anatomic structure	**Energy / weighting factors** 140kV	M_0.3	M_0.6	M_0.8	80kV
Aorta+C	149.2+/-12.8	204.8+/-14.4	267.5+/-18.6	311.9+/-22.3	347.3+/-24.7
Thyroid+C	130.3+/-12.1	170.3+/-13.5	221.8+/-18.7	251.5+/-22.4	273.9+/-25.3
Muscle+C	59.3+/-9.1	66.9+/-8.9	69.8+/-9.2	76.3+/-11.5	76.9+/-12.3
Brain+C	31.2+/-9.3	37.1+/-10.4	39.8+/-10.7	43.4+/-12.4	45.6+/-13.6
Fat	-95+/-13.8	-101+/-13.7	-103+/-13.4	-117+/-17.7	-118+/-21.3
Spinalcord	30.8+/-10	30.9+/-9.4	39+/-10.9	41.2+/-12.6	44.9+/-14.5
CSF	1.9+/-7.9	4.6+/-7.9	7.3+/-8.4	8+/-10.8	8.6+/-10.9
Bone marrow	576.4+/-162.95	659.1+/-195.98	800.3+/-213.17	880.7+/-241.28	889.3+/-233.42

Table-6.2: Mean contrast enhancements and SD (HU) of the ascending aorta, thyroid gland, neck muscle, brain and un-enhanced CSF, SC, bone marrow, fat for the different weighting factors (0.0, 0.3, 0.6, and 1.0) used in image fusion.

Material/ anatomic structure	**Weighting factors (Part 1-CNR)** 140kV	0.3	0.6	0.8	80Kv
Aorta+C	29.29	35.83	42.52	40.82	40.7
Thyroid+C	28.48	32.79	38.44	36.21	35.72
Muscle+C	18.81	20.03	20.1	18.72	17.23
Brain+C	3.48	3.78	3.82	3.35	3.29
	Weighting factors (Part 2- SNR)				
Aorta+C	12.34	14.85	16.82	15.71	14.78
Thyroid+C	10.87	13.15	13.56	12.75	12.48
Muscle+C	6.98	7.96	8	7.3	7.13
Brain+C	3.38	3.63	3.73	3.52	3.4
Bone m.	3.49	3.65	4.12	3.9	3.85
Spinal cord	3.19	3.12	3.76	3.37	3.32
CSF	0.41	0.57	0.92	0.86	0.79
Fat	-6.95	-7.66	-7.92	-6.77	-6.61

Table-6.3: Part 1 shows the mean CNR (HU) of four different Anatomic regions and part 2 given the mean SNR for the different weighting factors (0.0, 0.3, 0.6, 0.8 and 1.0) used in image fusion.

Fusion/ weighting	**Aorta + cont.**	**Thyroid + cont.**	**Muscle + cont.**	**Brain + cont.**
140kV	3.5	3.2	3	3.2
0.3	3.6	3.5	3.7	3.6
0.6	4.1	4	4	4.2
0.8	3.6	3.5	3.3	3.2
80kV	3	2.7	2.7	2.6

Table-6.4: shows the mean values of visual grading (VG) score for image quality based on the presence of surrounding artifacts and the clarity of structures.

6.2.5 DISCUSSION

The intensity of contrast enhancement is almost double in most of the cases increasing the weighting factor from 0.0 to 1.0 (Table 2). The variability of iodine enhancement explains why it is possible to differentiate iodine from other materials or substances that do not show such attenuation behavior. Two mechanisms, Compton scattering and the photoelectric effect, explain this phenomenon. First, the Compton Effect has little influence on diagnostic CT images so it is not important in this region. The second mechanism, the photo effect is increase at lower tube voltages, especially in materials with a large effective atomic number such as an iodinated contrast material. As a result, reducing the tube voltage setting leads to an increase in the attenuation of iodinated contrast material as the photo effect increases and Compton scattering decreases [9-11].

A previous study [2] demonstrated that a low tube voltage (80 kVp) scan can provide better contrast and conspicuity than a high voltage (140 kVp) scan for the detection of hypervascular liver tumors, as the low tube voltage scan takes advantage of the attenuation property of iodinated contrast material at 80 kVp. However, in a previous study using a liver phantom despite the fact that 80 kVp CT images showed a higher contrast-to-noise ratio (CNR) of simulated hypervascular liver lesions, the low tube voltage scan also showed increased noise compared with the high voltage tube scan. In addition, although increasing tube current is able to decrease noise of the low tube voltage scan, the CT system is not able to provide sufficient radiation dose as desired.

Especially for the neck scan, the shoulder region affects certainly the image quality. Those factors thus limit the widespread use of an 80kVp scan in clinical practice. However, with dual-energy CT (DECT), the noise of the 80 kVp data are offset by the decreased noise of the 140kVp data, and therefore, the difficulty with routine use of low-kVp CT because of increased noise could be minimized with this DECT technique. By dual-energy examination, it is possible to generate fusion-weighted images (this is a part of information obtained from detector A and B according to weighting) with out any additional scanning. This may reduce radiation dose and this technique can be use for further clinical information. Our results show that different weighting of the two data sets has a statistically significant effect on both the contrast enhancement and the visual quality of the fused images. Corresponding to the increasing contribution of the 80-kVp spectrum, contrast enhancement was significantly stronger with increasing weighting factors. This is in accordance to previous studies, which showed that iodine has a higher attenuation at low tube voltage settings [12-14]. Thus, the intensity of contrast enhancement can be tuned by varying the weighting of the fused images. Increasing the weighting factor from 0.0 to 1.0, this doubles the intensity of contrast enhancement (Table 2). This study proves that different fusion ratios affect image quality and the weighting factor 0.6 shows highest CNR or SNR instead of 80 or Sn140kV images.

Based on the presence of surrounding artifacts and the clarity of various structures, different weighting factors resulted in statistically significant differences in image quality. The highest grading score, corresponding with overall high image quality was reach by image reconstructions generated by the weighting factor 0.6.

These fused images derive 60% of their information from the 80-kV image, and 40% from the 140-kV image. In contrast, using a standard DE kernel like the D30 kernel, data sets often reconstructed with a weighting factor of 0.3, which comes closest to the 120-kV spectrums [6]. In our study, however, images fused with the factor 0.3 only received the second best visual score, behind reconstructions made with the weighting factor 0.6. Because of obscured anatomic detail, data sets produced by the high weighting factors 0.8 and 1.0 were often inadequate for material differentiation. One explanation for these results is that lower SNRs lead to poorer visual impression and image quality when compared with reconstructions based on the factor 0.6. Another reason why lower grading scores given to higher weighting factors is the statistically significant increase in contrast enhancement associated with higher weighting factors. Our results suggest that the weighting factor 0.6 should be use for reconstructing fused CT images. When compared with the weighting factor 0.3, the factor 0.6 leads to statistically significant improvements in image quality.

Initial patient studies have confirmed that the technique makes clinically relevant applications of dual energy CT feasible without additional patient dose [3]. The differentiation of iodine in tissue can be of diagnostic value, for example brain and thyroid lesions (hyper-vascular, hypo-vascular or cystic lesions). At present, the depiction of the iodine distribution in the brain raises hope that it may become feasible easily visualize perfusion defects in order to assess the penumbra in acute stroke. DSCT with different weighting is excellent at identifying and characterizing the density of a thyroid lesion, thus defining the presence of calcification, cysts and

hemorrhage accurately. The depiction of pulmonary perfusion may offer new insights comparable to perfusion scintigraphy [15-17]. Imaging of the pulmonary circulation by means of dual-energy CT opens the potential to study pathological changes of circulatory and pulmonary perfusion impairments [18]. This can improve with different weighting fused images. CT demonstrates the precise location of neck mass and its relationships to adjacent muscular and vascular structures. In addition to provide this normal anatomical detail, DSCT is able to characterize the vascularity and internal architecture (solid versus cystic) of a neck mass.

This study has some limitations. First, given that the clinical standard is 120-kV tube potential, a weighting factor of 0.3 is closer to this spectrum than 0.6. This different spectrum could have an impact on the visual evaluation of contrast enhancement or small focal lesions. Second, patient weight affects image quality. Especially in heavy patients, the transmission of 80-kV quanta in dense projections (eg, transversal pelvis/hip or shoulder area) can be so low that a stronger contribution of 140-kV density is necessary.

6.2.6 CONCLUSION

In summary, in a single-phase examination it is possible to differentiate various anatomic structures or lesions more specifically with dual-energy fusion weighted images without any additional scanning (additional scan contribute extra dose). In this study demonstrates that using different weighting factors in DECT causes statistically significant changes in contrast enhancement and image quality of anatomic structures. The differentiation of iodine can be regarded as a most promising and relevant application, our study shows the exact differentiation of anatomic structures possible with dual-energy fusion weighted images with excellent quality, which can be expected to improve the assessment of all types of vascular disease all over the body. Best results obtained using the weighting factor 0.6 and based on these results, we recommend using the weighting factor 0.6 for image fusion in DECT imaging.

6.2.7 REFERENCE

1. Thorsten R. C. Johnson, Bernhard Krauß, Martin Sedlmair, Michael Grasruck, Herbert Bruder, Dominik Morhard, et.al., Material differentiation by dual energy CT: initial experience, Eur Radiol (2007) 17: 1510–1517.

2. Daniele Marin, MD, Rendon C. Nelson, MD, Ehsan Samei, PhD, Erik K. Paulson, MD, Lisa M. Ho, MD, Daniel T. Boll, MD, et al. Hypervascular liver tumors: low tube voltage, high tube current multi-detector row CT for enhanced detection—phantom study. Radiology. 2008;246:125–132.

3. Johnson TR, Krauss B, Sedlmair M, Grasruck M, Bruder H, Morhard D, et.al, Material differentiation by dual energy CT: initial experience, Eur Radiol. 2007 Jun;17(6):1510-7.

4. Holmes DR 3rd, Fletcher JG, Apel A, Huprich JE, Siddiki H, Hough DM, et.al. Evaluation of non-linear blending in dual-energy computed tomography. Eur J Radiol. 2008;68:409–413.

5. Anno Graser, Thorsten R. C. Johnson, Hersh Chandarana and Michael Macari. Dual energy CT: preliminary observations and potential clinical applications in the abdomen. Eur Radiol. 2009;19:13–23.

6. Behrendt FF, Schmidt B, Plumhans C, Keil S, Woodruff SG, Ackermann D, et al. Image fusion in dual energy computed tomography: effect on contrast enhancement, signal-to-noise ratio and image quality in computed tomography angiography. Invest Radiol. 2009;44:1– 6.

7. Kim, Kyung Su BA; Lee, Jeong Min MD; Kim, Seung Ho MD; Kim, Kyung Won MD; Kim, Soo Jin MD; Cho, Seung Hyun MD, et.al, Image Fusion in Dual Energy Computed Tomography for Detection of Hypervascular Liver Hepatocellular Carcinoma: Phantom and Preliminary Studies, Invest Radiol 2010;45: 149–157)

8. Jörg Hausleiter, Tanja Meyer, Martin Hadamitzky, Ester Huber, Maria Zankl, Stefan Martinoff, et.al., Radiation Dose Estimates From Cardiac Multislice Computed Tomography in Daily Practice: Impact of Different Scanning Protocols on Effective Dose Estimates., Circulation 2006;113;1305-1310

9. Yoshiharu Nakayama, MD, Kazuo Awai, MD, Yoshinori Funama, PhD, Masahiro Hatemura, RT, Masanori Imuta, MD, Takeshi Nakaura, MD, et al. Abdominal CT with low tube voltage: preliminary observations about radiation dose, contrast enhancement, image quality, and noise. Radiology. 2005;237:945–951

10. Szucs-Farkas, Zsolt MD; Verdun, Francis R. PhD; von Allmen, Gabriel RT; Mini, Roberto L. PhD; Vock, Peter MD. Effect of X-ray tube parameters, iodine concentration, and patient size on image quality in pulmonary computed tomography angiography: a chest-phantom-study. Invest Radiol. 2008;43:374 –381.

11. Brooks RA. A quantitative theory of the Hounsfield unit and its application to dual energy scanning. J Comput Assist Tomogr. 1977;1:487– 493.

12. Johnson TR, Krauss B, Sedlmair M. Material differentiation by dual energy CT: initial experience. *Eur Radiol*. 2007;17:1510 –1517.

13. Nakayama Y, Awai K, Funama Y., Abdominal CT with low tube voltage: preliminary observations about radiation dose, contrast enhancement, image quality, and noise. *Radiology*. 2005;237:945–951.

14. Mahnken, Andreas H. MD, MBA; Bruners, Philipp MD; Mühlenbruch, Georg MD; Emmerich, Melanie; Hohl, Christian MD; Günther, Rolf W. MD, et al. Low tube voltage improves computed tomography imaging of delayed myocardial contrast enhancement in an experimental acute myocardial infarction model. *Invest Radiol*. 2007; 42:123–129.

15. Winkler SS, Holden JE, Sackett JF, Flemming DC, Alexander SC (1977) Xenon and krypton as radiographic inhalation contrast media with computerized tomography: preliminary note. Invest Radiol 12:19–20

16. Hoffman EA, Chon D (2005) Computed tomography studies of lung ventilation and perfusion. Proc Am Thorac Soc 2:492–498, 506

17. Tajik JK, Chon D, Won C, Tran BQ, Hoffman EA (2002) Subsecond multisection

CT of regional pulmonary ventilation. Acad Radiol 9:130–146.

18. Ferda J, Eva F, Hynek Mírkaa, Jan Baxaa, Alena Bednářováa, Thomas Flohr, et. al. Pulmonary imaging using dual-energy CT, a role of the assessment of iodine and air distribution. Eur J Radiol (2009), doi:10.1016/j.ejrad.2009.08.005.

Chapter: 7

Conclusion

7.1 CONCLUSION

In conclusion, the use of organ-based dose estimates in place of DLP-based estimates with a fixed k coefficient of 0.014 mSv/mGycm will result in an increased effective patient dose for chest CT examinations for the evaluated dual-source CT scanner and protocols by 4.5-16.56% when using ICRP 60 and by 5.2-15.8% when using ICRP 103 tissue weighting factors. These results are essentially independent of tube potential, suggesting that estimates of effective dose based on DLP work equally well for single-energy and dual-energy CT examinations. Only for the dual-source high-pitch mode, a substantial difference observed and a conversion coefficient of 0.0166 mSv/mGycm should used for DLP-based calculation of E. Further, effective dose estimations by ICRP 103 and 60 for both single-energy and dual-energy examinations did not differ by more than 0.04 mSv.

Dose parameters and image noise are significantly lower in NECT than CECT in all investigated CT scanners with AEC. Again, with AEC patient dose will be significantly different between NECT and CECT chest examinations for three generations of CT machines. However, technological developments lead to a significant reduction of dose and image noise with the latest CT generation.

The clinical protocol, reconstruction kernel, slice thickness and phantom diameter or the density of material it contains directly affects the image quality. Appropriate choices of scan technique, reconstruction algorithm and patient (phantom) size as well as use of image averaging and digital image filtering can dramatically reduce image noise. Dual Energy protocol shows the lowest DLP compared to all other protocols examined.

Dual-energy Sn140kV and 100kV shows higher noise compared with other single-or high-pitch protocols examined. Even though the image noise is higher for Sn140kV and 100kV dual energy image sets, the fused images show excellent image quality and the noise is same as single or high-pitch mode protocol images. Advanced CT technology improves image quality and considerably reduce radiation dose.

In a single-phase examination it is possible to differentiate various anatomic structures or lesions more specifically with dual-energy fusion weighted images without any additional scanning (additional scan contribute extra dose). In this study demonstrates that using different weighting factors in DECT causes statistically significant changes in contrast enhancement and image quality of anatomic structures. The differentiation of iodine can be regarded as a most promising and relevant application, our study shows the exact differentiation of anatomic structures possible with dual-energy fusion weighted images with excellent quality, which can be expected to improve the assessment of all types of vascular disease all over the body. Best results obtained using the weighting factor 0.6 and based on these results, we recommend using the weighting factor 0.6 for image fusion in DECT imaging.

CURRICULUM VITAE

Jijo Paul

Personnel Details

Sex	:	Male
Age / Date of Birth	:	30 Years, 17 November 1980.
Place of Birth	:	Rajakumari south, India
Marital status	:	Single
Nationality	:	Indian
E-mail	:	jijopaul1980@gmail.com

University Education

1. Goethe University- Frankfurt am Main, Germany.

   PhD in Medical Physics, (started from 2009- to till date)

2. Vinayaka Missions University, Salem, India

   M.Phil in Physics, (2 semesters/ 1 year, 2008-2009)

3. Manipal University, Manipal, India

   M.Sc Medical Radiation Physics, (4 semesters / 2 years, 2005-2007)

4. National Institute of Business Management, Chennai, India (1 year, 2007)

   Executive Master of Business Administration [E.MBA] in HRM

5. Mahatma Gandhi University, Kottayam, India

   B.Sc in Medical Radiological Technology, (8 semesters/ 4 years, 1998-2003)

Certification

Bhabha Atomic Research Center (Radiological Physics and Advisory Division), Mumbai

Radiation Safety Officer Certification. (RSO- Level-3)- By examination- 2007

Preliminary Education

Vocational Higher Secondary Education board, Government of Kerala, India

Higher secondary (12th class), 1998

Board of Public Examinations, Government of Kerala, India

Secondary School Leaving Certificate (S.S.L.C/ 10thclass), 1996

Academic tutors

Prof.Dr. Werner Maentele PhD, Prof.Dr. Thomas J.Vogl MD

Goethe University- Frankfurt am Main, Germany.

Work Experience

I. Worked as full time Medical Physicist (42 hrs/week) and Lecturer (6 hrs/week) at Indo-American Cancer Institute and Research Centre, Hyderabad, India (From 27-11-2007 to 16.05.2009)

II. Worked as full time Medical Physicist cum Radiation safety Officer (42 hrs/week) and Lecturer (6 hrs/ week) at Jubilee Mission Medical College and Research Institute, Thrissur, India (From 15.07.2007 to 12.11.2007)

III. Worked as Radiation Technologist (24 hrs/week) and Lecturer (18 hrs/week) at Jubilee Mission Medical College and Research Institute, Thrissur, India (From 5.06.2003 to 29.08.2005)

Membership

American Association of Physicists in Medicine (AAPM); Corresponding member- 51528

Institute of Physics and Engineering in Medicine (IPEM), United Kingdom; Overseas Affiliate Europe membership- 3503

Association of Medical Physicists of India (AMPI); Life membership- 1809

Indian Association of Radiological Technologists (IART); Life membership- 1354)
Association of Radiation Therapy Technologists of India (ARTTI); Life membership – 480/08

Indian Red Cross Society (IRCS): Life membership- L 00491

Dissertation

PhD Medical Physics: Image Quality and Dosimetry of a Dual Source Computed Tomography Scanner with Special Emphasis on Radiation Dose of Lung in a Chest Examination

M.Phil Physics: Quality Assurance of the X-Ray Volume Imaging (XVI) System of an Image Guided Radiotherapy (IGRT) Capable Linear Accelerator

M.Sc. Medical Radiation Physics: Verification of Dose Calculations in External Beam Therapy using Plato Treatment Planning System

B.Sc. Medical Radiological Technology: Importance of Ultrasound in the Imaging of Thyroid

Scientific Publication

1. *Paul J, M.Sc(MRP), M.Phil, Banckwitz R, PhD, Krauss B, PhD, Vogl TJ, MD, Maentele W, PhD, Bauer RW, MD*- Estimation and Comparison of Effective Dose (E) in Standard Chest CT by Organ Dose Measurements and Dose-Length-Product Methods and Assessment of the Influence of CT Tube Potential (Energy Dependency) on Effective Dose in a Dual-Source CT. *(doi:10.1016/j.ejrad.2011.06.006) European Journal of Radiology*

2. *Paul J M.Sc(MRP), M.Phil, Krauss B, PhD, Banckwitz R, PhD, Maentele W, PhD, Bauer RW, MD, Vogl TJ, MD*- Relationships of Clinical Protocols and Reconstruction Kernels with Image Quality and Radiation Dose in a 128-slice CT scanner: Study with an Anthropomorphic and Water Phantom. *(doi:10.1016/j.ejrad.2011.01.078),* European Journal of Radiology

3. *Paul J M.Sc(MRP), M.Phil, Bauer RW, MD, Maentele W, PhD, Vogl TJ, MD*- Image Fusion in Dual Energy Computed Tomography for Detection of Various Anatomic Structures - Effect on Contrast Enhancement, Contrast-to-Noise Ratio, Signal-to-Noise Ratio and Image Quality. *(doi:10.1016/j.ejrad.2011.02.023) European Journal of Radiology*.

4. *Paul J, MSc, MPhil, Kerl JM, MD, Schell B, MD, Vogl TJ, MD, Bauer RW, MD*- Effect of Contrast Medium on Image Noise and Radiation Dose in Adult Chest Computed Tomography using Automatic Exposure Control: A Comparative Study between 16-, 64- and 128-slice CT. *(doi:10.1016/j.ejrad.2011.05.012) European Journal of Radiology*.

Scientific Papers Presented

1. Scientific paper entitled “Effect of Contrast Medium on Image Noise Level and Radiation Dose using Automatic Exposure Control in Adult Chest CT: A Comparative Study with Different Generation CT Scanners” has accepted for presentation” (Abstract No: E-80605) – ESTRO 2011 March PREVENT Conference, Brussels, Belgium.

2. Scientific paper entitled “Estimation and Comparison of Organ and Effective Dose (E) Values for Chest CT Examinations using Different Approaches and Assessment of the Influence of CT Tube Potential (Energy Dependents) on Effective Dose” (Abstract No: 63P) has been accepted for presentation during the European Multidisciplinary Conference in Thoracic Oncology (EMCTO), February 2011, Lugano, Switzerland.

3. Scientific paper entitled **“**Accuracy and Reproducibility of Pulmonary Nodule at Dual Source CT: Volumetric Measurements with Comparison of Manual, RECIST and Lung care Software Methods: A Phantom Study” (Abstract No: 1412) has accepted for Oral presentation- European Congress of Radiology (ECR) 2011 March, Vienna, Austria.

4. Scientific paper entitled “Relationships of Clinical Protocols and Reconstruction Kernels with Image Quality in a Dual Source Computed Tomography Scanner (DSCT): Study with an Anthropomorphic and Water Phantom” (Abstract No: 1481), has accepted for European Congress of Radiology (ECR) 2011 March, Vienna, Austria.

5. Scientific paper entitled “Estimation and Comparison of Organ and Effective Dose (E) Values for Chest CT Examinations using Different Approaches and Assessment of the Influence of CT Tube Potential (Energy Dependents) on Effective Dose.” (Abstract No: 1398), has accepted for European Congress of Radiology (ECR) 2011 March, Vienna, Austria.

6. Presented a paper “Image Quality Tests Performance of a Dedicated 85 cm Big Bore CT Simulator”, International Conference on Medical Physics (ICMP), Mumbai, India on November 2008.

7. presented a paper as a co-author, entitled “Test Performance of Simulation Process using 85 cm Big Bore CT Simulator”, International Conference on Medical Physics (ICMP), Mumbai, India on November 2008.

8. Presented a paper “Dose Evaluation Methods in HDR Brachy therapy”, National workshop on HDR Brachy therapy 2008, organized by Indo-American Cancer Institute and Research Center (National level conference), Hyderabad on 2008 May.

9. Presented a paper “Basic Principles and Recent Advances of CT Scanner”, Advances in Biomedical Engineering and Symposium on Clinical Engineering (State Level Conference), Kerala, India on July 2004.

Education Programs and Conferences Attended

1. Participated “Frankfurt Interdisciplinary Symposium for Innovative Diagnostics and Therapy” conducted by Johann Wolfgang Goethe- University hospital Frankfurt am Main, Germany on September 2010.
2. Participated “National Conference on Medical Physics and Radiation Safety” conducted by Indo-American Cancer Institute and Research Center, Hyderabad on March 2006.
3. Participated “Peaceful Application of Radioisotopes” Seminar conducted by Mangalore University and NAARI (National Association for Applications of Radioisotopes and Radiation in industry) on Nov. 2006.
4. Continuing Medical Education (CME) program “Diagnosis in Nuclear-imaging”, conducted by Kasturba Medical College hospital, Manipal, on 04 November 2006.
5. Participated “Education program” conducted by AGFA India Pvt. Ltd on 19 may 2002.
6. Participated “Continuing Medical Education program in Radiology”, conducted by Jubilee Mission Hospital, Thrissur, Kerala, India on February 2001.
7. “Continuing Medical Education program in Ultrasound anatomy” conducted by Government Medical College Kottayam, Kerala, on October 2000

Declaration

I here by declare that all the statements made in this application are true, complete and correct to the best of my knowledge and belief.

Frankfurt am Main

Germany ***JIJO PAUL***